Technical Report

TR-99-03

Calculation of displacements on fractures intersecting canisters induced by earthquakes:

Aberg, Beberg and Ceberg examples

Paul R LaPointe, T Cladouhos
Golder Associates, Inc.

Sven Follin
Golder Grundteknik KB

January 1999

Svensk Kärnbränslehantering AB
Swedish Nuclear Fuel
and Waste Management Co
Box 5864
SE-102 40 Stockholm Sweden
Tel 08-459 84 00
+46 8 459 84 00
Fax 08-661 57 19
+46 8 661 57 19

Calculation of displacements on fractures intersecting canisters induced by earthquakes:

Aberg, Beberg and Ceberg examples

Paul R LaPointe, T Cladouhos
Golder Associates, Inc.

Sven Follin
Golder Grundteknik KB

January 1999

Keywords: Earthquake, Fracture Displacement, Canister

ABSTRACT

This study shows how the method developed in La Pointe and others (1997) can be applied to assess the safety of canisters (Figure 1-1) due to secondary slippage of fractures intersecting those canisters in the event of an earthquake. The method is applied to the three generic sites Aberg, Beberg and Ceberg (Figure 1-2). Estimation of secondary slippage or displacement is a four-stage process. The first stage is the analysis of lineament trace data in order to quantify the scaling properties of the fractures. This is necessary to insure that all scales of fracturing are properly represented in the numerical simulations. The second stage consists of creating stochastic discrete fracture network (DFN) models for jointing and small faulting at each of the generic sites. The third stage is to combine the stochastic DFN model with mapped lineament data at larger scales into data sets for the displacement calculations. The final stage is to carry out the displacement calculations for all of the earthquakes that might occur during the next 100,000 years. Large earthquakes are located along any lineaments in the vicinity of the site that are of sufficient size to accommodate an earthquake of the specified magnitude. These lineaments are assumed to represent vertical faults. Smaller earthquakes are located at random. The magnitude of the earthquake that any fault could generate is based upon the mapped surface trace length of the lineaments, and is calculated from regression relations discussed in La Pointe and others (1997). Recurrence rates for a given magnitude of earthquake are based upon published studies for Sweden.

A major assumption in this study is that future earthquakes will be similar in magnitude, location and orientation as earthquakes in the geological and historical records of Sweden. Another important assumption is that the displacement calculations based upon linear elasticity and linear elastic fracture mechanics provides a conservative (over-) estimate of possible displacements. This assumption is discussed in La Pointe and others (1997). A third assumption is that the world-wide earthquake source parameter database upon which the relations between surface rupture length, subsurface fault displacement and fault width (depth for vertical faults) is representative of Swedish earthquakes. This assumption has also been discussed in La Pointe and others (1997).

Results of the calculations are presented in several ways. A canister is considered to be damaged or to have failed if a fracture intersecting the canister has an instantaneous or cumulative slip greater than 0.1m. Canisters may fail during a single earthquake, or due to the cumulative effects of multiple smaller earthquakes. Failure percentages for single earthquakes for a 100,000-year period range from a high of 0.59% for Aberg to a low of 0.03% for Ceberg. Failure for cumulative effects only vary from 0.056% for Aberg to 0.004% for Ceberg. For combined cumulative and single failures, canister failure percentages show a high of 0.59% for Aberg

to a low of 0.03% for Ceberg. Results for Beberg are intermediate, but typically closer to the lower failure percentages of Ceberg. Additional considerations of the magnitude/frequency relations for southern Sweden, which partially compensates for the higher seismic risk in the Lake Vänern region, may reduce the failure percentages for Aberg to be comparable with those at Beberg and Ceberg.

Additional investigation of the single earthquakes that cause unacceptable slippage suggests that their probability of occurrence over a 100,000 year time period is very low, but that their consequences are more severe in that they tend to damage multiple canisters. The probability of an earthquake occurring that damages one or more canisters varies from 0.32 for Aberg to a low of 0.07 for Ceberg. Once again, compensation for the higher seismic activity in the Lake Vänern region in southern Sweden may reduce the probability for Aberg to a value near 0.05.

When a damaging earthquake occurs, an average of from 0.4% to 1.8% of the canisters experience induced slips greater than 0.1m, the higher number representative of Aberg, and the lower value representative of Ceberg. Compensation for the higher seismic activity in the Lake Vänern region in southern Sweden may reduce the mean failure percentage for Aberg to a value near 0.6%, making it comparable to Beberg and Ceberg.

Although earthquakes were simulated at distances over 100 km from the canister positions, single earthquakes that produced displacements greater than 0.1 m were confined to the immediate vicinity of the repository. A plot for the Ceberg simulations shows that over 95% of the single, damaging earthquakes are within 1 km of the canister that they damage, and 99% are within 2.5 km. The maximum distance for the simulations was approximately 31 km. This suggests that the vast majority of faults that might potentially produce damaging earthquakes lie with a few kilometers of the repository. The simulations suggest that faults tens or hundreds of kilometers distant from the canisters are very unlikely to produce damage due to single earthquake events.

SAMMANFATTNING

Föreliggande studie behandlar risken för kapselskada till följd av jordbävningar i Aberg, Beberg och Ceberg under de kommande 100 000 åren. Den använda beräkningsmetoden (LaPointe m fl, 1997) bygger på en uppskattning av spricknätverksförskjutningar (sekundära skjutrörelser) till följd av en jordbävning i en närbelägen större sprickzon (primär skjuvrörelse). Beräkningsmetodens består av fyra arbetsmoment: (i) statistisk analys av strukturgeologiska/geofysiska lineament, (ii) generering av stokastiska realiseringar av bergmassans sprickighet (spricknätverk), (iii) överlagring av deterministiska (stora) strukturer, samt (iv) simulering av primära och sekundära förskjutningar. Magnituden hos de jordbävningar som simuleras i denna rapport bestäms dels av historiska jordbävningsdata för Sverige, dels av det regressionssamband mellan magnitud och lineamentstorlek som diskuteras i LaPointe m fl (1997).

I studien görs tre viktiga förenklingar/antaganden: (i) att återkomstfrekvens och epicentrum för framtida jordbävningar i Sverige kan predikteras (simuleras) med ledning av statistisk bearbetning av geologiska och historiska data, (ii) att den elastiska modellen som används för att simulera deformationer är konservativ, dvs överskattar deformationerna, samt (iii) att den världsomfattande databasen för jordbävningar (med tillhörande regressionssamband mellan olika parametrar) är tillämpbar på svenska förhållanden. Det senare antagandet diskuteras närmare i La Pointe m fl (1997).

Med kapselskada menas i denna studie att en spricka, som skär in i ett kapselhål, förskjuts minst 0,1 m till följd av en eller flera jordbävningar under de kommande 100 000 åren. I studien beräknas både risken för att en enskild, större, jordbävning kan orsaka förskjutningsbelopp större än 0,1 m, respektive risken för att två eller flera, mindre, jordbävningar kan orsaka förskjutningsbelopp större än 0,1 m. Kapselskaderisken till följd av en enskild, större, jordbävning varierar i denna studie mellan 0,59% i Aberg till 0,03% i Ceberg. Motsvarande risker till följd av två eller flera jordbävningar varierar mellan 0,056% i Aberg till 0,004% for Ceberg. Om man kombinerar de två fallen erhålls en risk för kapselskada till följd av en eller flera jordbävningar på 0,59% i Aberg och 0,03% i Ceberg. För Beberg ligger samtliga beräkningsresultat mellan de ovan angivna värdena för Aberg och Ceberg, med en viss tonvikt mot värdena för Ceberg. Om man beaktar att det finns geografiska skillnader i såväl magnitud som återkomstfrekvens hos historiska jordbävningsdata för södra Sverige, bedömer vi att risken för kapselskador i samband med jordbävningar förmodligen är densamma i Aberg som i Beberg och Ceberg.

Även om enskilda, större, jordbävningar har mycket låg återkomstfrekvens, ger de upphov till jämförelsevis stora konsekvenser om de inträffar

beroende på att förekommande sprickor inte sällan skär över flera kapselpositioner. Sannolikheten för att minst en större enskild jordbävning med oönskade förskjutningar i de sprickor som skär kapselpositionerna skall inträffa i Aberg under de kommande 100 000 åren är 0,32. Om man tar hänsyn till de geografiska skillnaderna i såväl magnitud som återkomstfrekvens hos jordbävningsdata för södra Sverige, bedöms dock sannolikheten i Aberg inte vara större än ca 0,05. Motvarande värde i Ceberg är 0,07.

De jordbävningar som simuleras i denna studie påverkar i medeltal som lägst 0,4% (Ceberg) och som högst 1,8% (Aberg) av kapslarna med sprickförskjutningar som är större än 0,1m. Om man återigen beaktar de geografiska skillnaderna hos jordbävningsdata för södra Sverige, uppskattas kapselskaderisken i Aberg till högst ca 0,6%, vilket överensstämmer med värdena i Beberg and Ceberg.

I denna studie har jordbävningar simulerats inom en radie av 100 km från de studerade kapselpostionerna. Resultatet från de genomförda simuleringarna visar att det är huvudsakligen närbelägna jordbävningar som orsakar förskjutningar större än 0,1 m. Som exempel kan nämnas att 95% av de enskilda jordbävningar som orsakade oönskade förskjutningar i kapselskala i Ceberg inträffade inom en radie av 1 km. 99% inträffade inom en radie av 2,5 km. Det maximala avståndet för en skadlig jordbävning i Ceberg var ca 31 km. Beräkningarna i denna studie indikerar med andra ord att flertalet av de deformationszoner som kan tänkas vara potentiella kandidater för att utlösa jordbävningar med oönskade förskjutningar ligger högst inom ett par kilometers radie från förvaret. Deformationszoner som ligger på tio- till hudratalstals kilometer bedöms inte som potentiella kandidater för att enskilda jordbävningar skall orsaka oönskade förskjutningar i kapselskala.

TABLE OF CONTENTS

LIST OF FIGURES

LIST OF TABLES

1. INTRODUCTION

High-level nuclear waste repository performance assessment must consider the impact of many potential events during the repository's performance period. One of these events is the impact that an earthquake might have on the integrity of the canisters. Relatively small earthquakes occur in Sweden at present. During Sweden's most recent deglaciation, much larger earthquakes may have occurred as stresses that accumulated under the ice loading were released as the ice retreated. Thus, earthquakes due to tectonics or a combination of tectonics and deglaciation are likely to occur in the future during the time period when nuclear waste needs to be contained safely in an underground repository.

The earthquake need not occur on a fracture intersecting the repository or a canister hole for it to affect repository performance. Earthquakes can cause other fractures to slip. This slippage is not limited to fractures immediately adjacent to the fault. Thus, an earthquake located on a fault kilometers distant from a repository may cause fractures intersecting canister holes to slip. This slippage, if it were large enough, might adversely impact the integrity of the canisters. Unacceptable slippage might also occur through the cumulative displacements induced by a series of earthquakes over the performance period.

This study demonstrates a methodology to make conservative estimates of the amount of slippage on fractures intersecting canister holes produced by earthquakes on faults not directly intersecting the canisters (Figure 1-1). It also provides an estimate of the minimum size fracture that could exceed a displacement threshold were an earthquake to occur on it due to post-glacial faulting. Three generic sites, Aberg, Beberg and Ceberg are evaluated (Figure 1-2). As described in La Pointe and others (1997), the method to assess this risk simplifies the dynamic mechanical processes that actually take place during an earthquake. The simplification produces conservative estimates and thus is useful for stochastic performance assessment calculations. The method assumes that future earthquakes will be similar to earthquakes that have occurred in Sweden's historic and geologic past.

The approach consists of several steps, as listed below:

1) Analyze fracture geometry to determine the number of sets, their sizes, orientations and intensity.

2) Use this information to generate 3D Discrete Fracture Network (DFN) models.

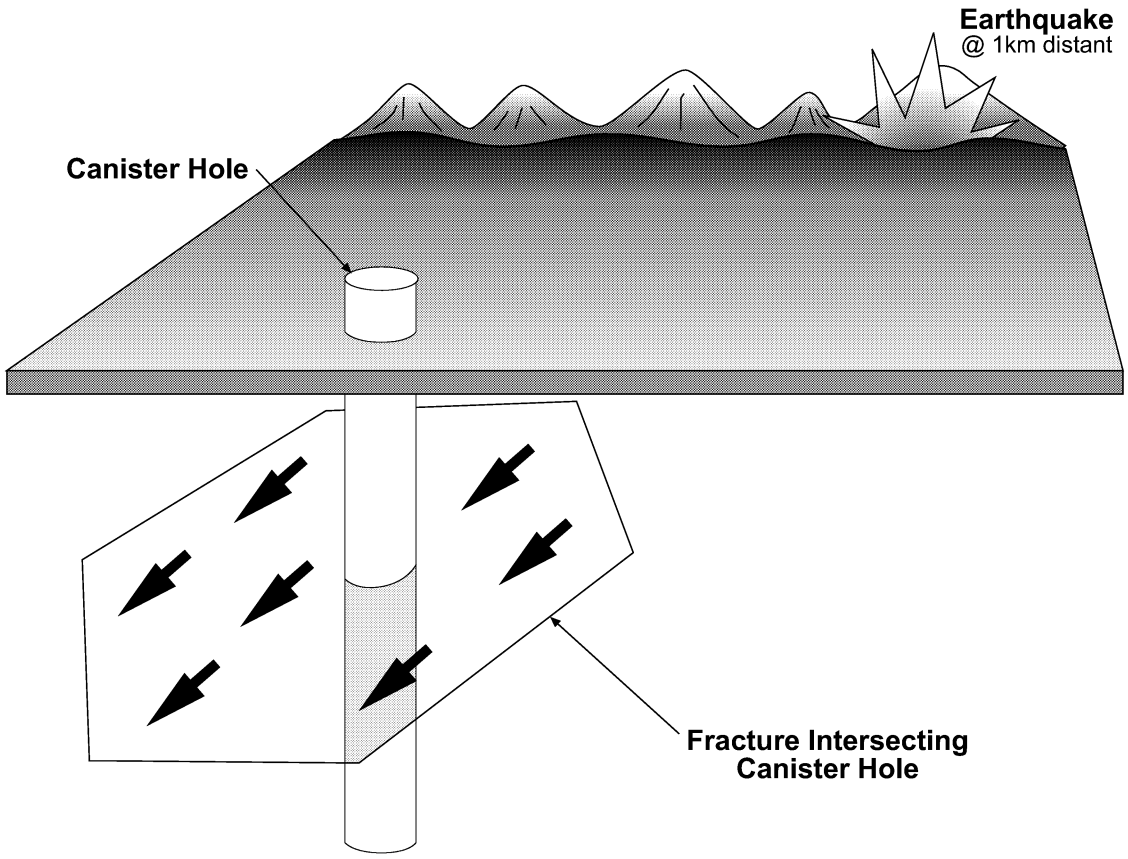

FIGURE **1-1**
FRACTURE SLIPPAGE DUE TO AN EARTHQUAKE
SKB/EARTHQUAKES

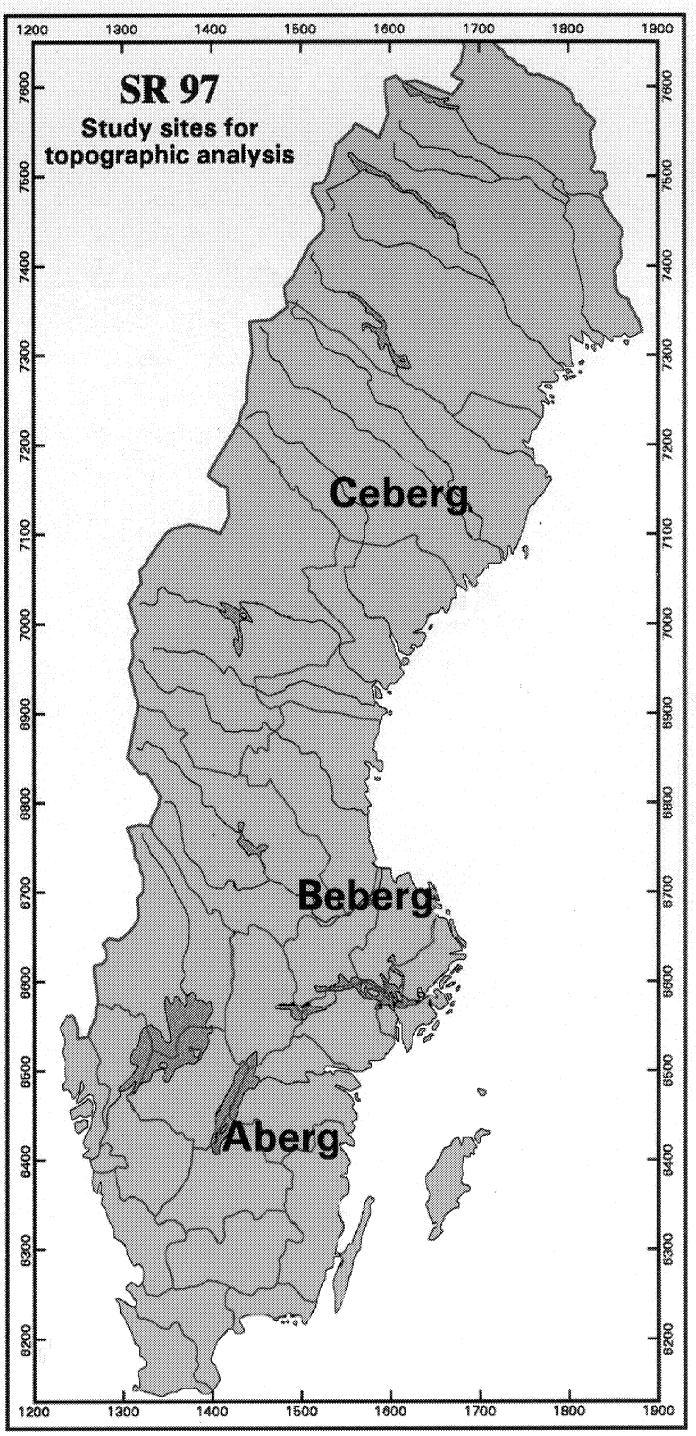

FIGURE **1-2**
SITE INDEX MAP

3) Combine each stochastic realization of the DFN model with a proposed canister hole layout to determine which fractures intersect canister holes (Figure 1-4).

4) Establish relations between earthquake parameters that will be used for modeling. These include earthquake magnitude, subsurface displacement, surface rupture length, and rupture width (depth).

5) Determine local earthquake magnitude and frequency statistics.

6) Use the information in (4) and (5) to determine spatial and temporal boundary conditions for a series of numerical simulations to determine possible cumulative displacements induced on the fractures in (3) that were found to intersect canister holes.

7) Evaluate numerical modeling results.

These detailed steps can be combined into four stages (Figure 1-3):

Stage 1 – Analysis of fracture trace data

Stage 2 – DFN model generation

Stage 3 – Determination and specification of seismic boundary conditions

Stage 4 – Numerical earthquake simulation

The first stage is to analyze the existing fracture data on a wide range of scales in order to construct DFN models for the site that are geologically realistic (Figure 1-3). Section 2 describes this data analysis for Aberg, Beberg and Ceberg. The second stage consists of generating multiple stochastic realizations of these models, as described in Section 3. Section 4 describes the third stage, which consists of the relation between earthquake magnitude, displacement and geometry, as well as how the number and magnitude of earthquakes were estimated for the next 100,000 years based upon the earthquake catalog for Sweden. In the fourth stage, the numerical code POLY3D (Thomas, 1993) is used to compute slip on fractures intersecting canister holes due to an earthquake in the repository vicinity. Section 5 discusses the results obtained. The final Section (Section 6) summarizes the most important results from the studies at Aberg, Beberg and Ceberg in terms of earthquake risk assessment.

This study considered three issues in applying the methodology to the three generic sites as well as to other sites:

Stage 1: Analyze Trace Data

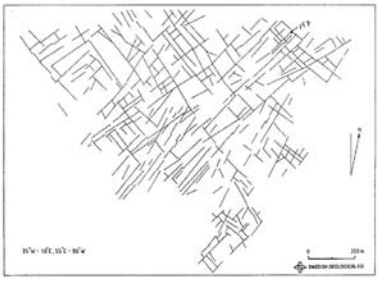

FracMan

Stage 2: DFN Model Generation

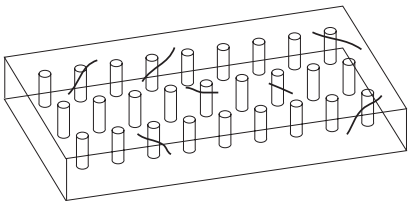

Monte Carlo Simulation

Stage 3: Select a Fault Lineament and Assign Fault Width and Displacements from Regression Relations

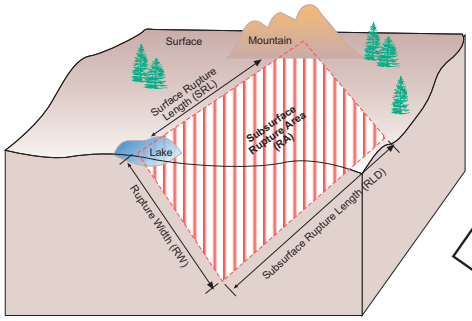

Poly 3D

Stage 4: Simulate Earthquakes using Poly 3D

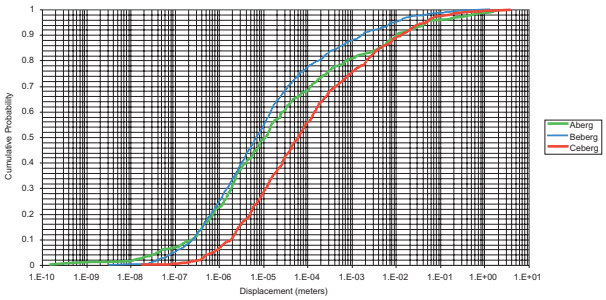

FIGURE **1-3**
FOUR-STAGE PROCESS FOR ESTIMATING EARTHQUAKE-INDUCED DISPLACEMENTS

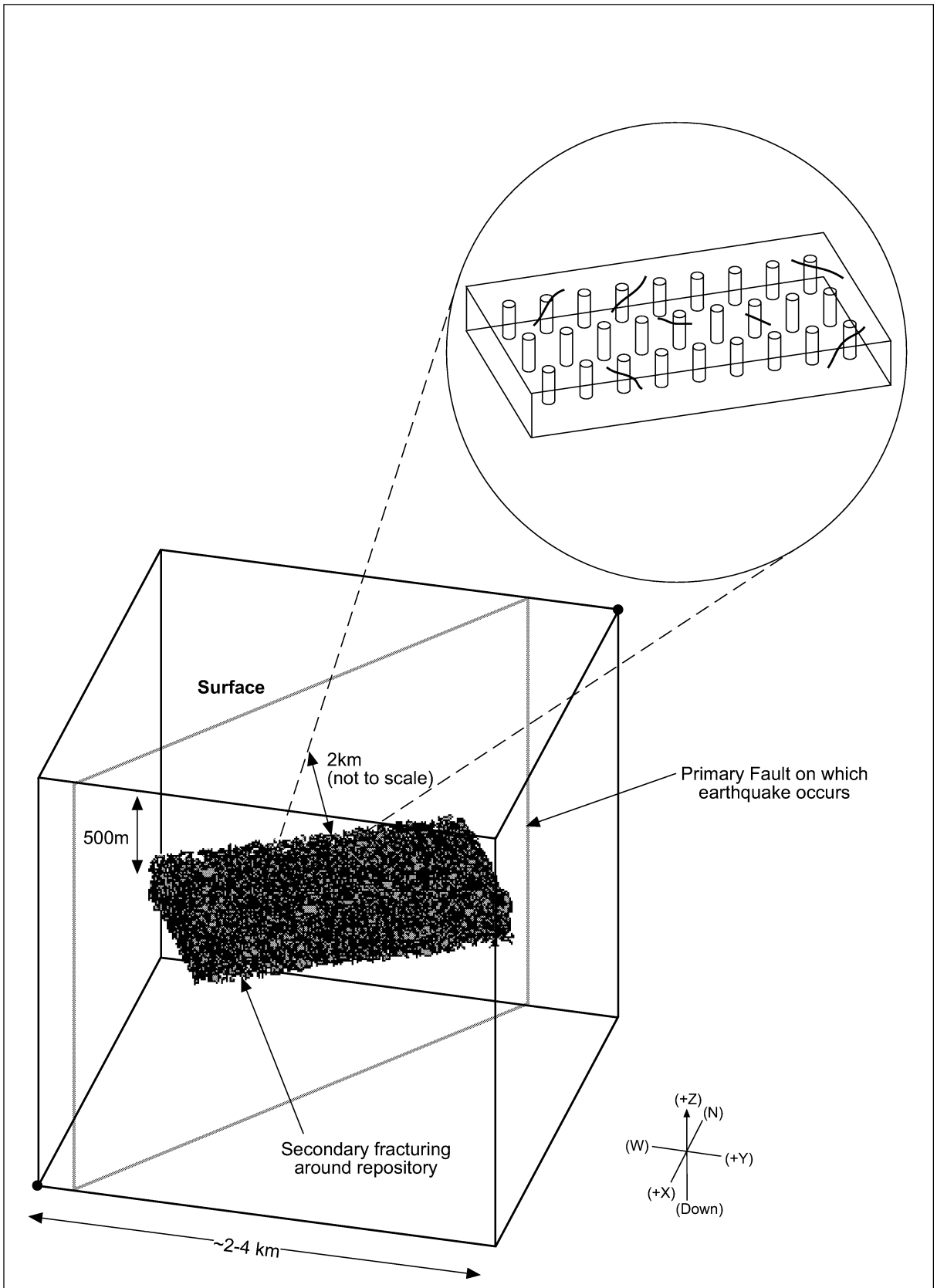

FIGURE **1-4**
POLY 3-D FRACTURE MODEL

- *The need to take into account fractures at many different scales*. This includes the small scale fracturing which intersects canister holes, as well as very large plate-scale faults that may be hundreds of kilometers distant from a repository but might be important should a large earthquake occur on them.
- *The appropriate way to reconcile a hierarchical classification of fractures (for example, Class 1, Class 2) that are defined as a basis for laying out and constructing the repository, with fracture sizes and properties*. The hierarchical classes are not defined in terms of their size or mechanical properties. In other words, a Class 1 or Class 2 feature is not allowed to intersect a canister hole, but how does this relate to some measurable fracture parameter such as size?
- *Determining the distance from a repository that an earthquake can still have an effect*. Is an earthquake 100 km distant from the repository important to model, and if so, does all of the fracturing within 100 km in every direction of the site have to be characterized and explicitly modeled in the DFN models?

These issues are addressed in the modeling effort, as described in Sections 2 and 3.

2. SCALING PROPERTIES OF FRACTURE DATA

2.1 Objectives

Determination of the scaling properties of fractures addresses the first two issues described above in Section 1: *The need to take into account fractures at many different scales; and The appropriate way to reconcile a hierarchical classification of fracturing with measurable fracture parameters.*

While fractures on the order of meters or tens of meters in diameter will not produce large earthquakes, fractures at this scale could be important if they intersect canisters since they could slip and damage canister integrity during a larger earthquake. Faults that are tens or hundreds of kilometers in scale will be important because these are the faults on which large earthquakes can occur. This suggests that an earthquake risk study must incorporate five or more orders of magnitude of fracture size. This presents two problems.

1. How is it possible to characterize the size of fractures at scales where there are no measurements?
2. And, how can this information be incorporated into a numerical model that does not overwhelm the computational capabilities of modern computers?

Analysis of the scaling properties of the fractures provides the answer.

The DFN models required for earthquake studies differ from the DFN models used for fluid flow modeling. The fluid flow modeling undertaken to address questions concerning possible radionuclide releases considers only the fractures that play a substantive role in fluid flow movement at the scale of interest. Studies in Sweden at Stripa, Finnsjön and Äspö, and indeed throughout the world have repeatedly demonstrated that a small subset of fractures typically dominate fluid movement at any particular scale. Field studies have shown that only one in ten fractures may have any conductive significance. Thus, the statistics that underlie the DFN models used for flow or transport calculations are only a subset of those that need to be considered for earthquake analyses. This first problem is that existing fluid flow studies are focused on a subset of fractures which excludes many that are important for earthquake calculations.

A second problem concerns scale. Although flow and transport have been the focus of much DFN modeling, some DFN models have been prepared for mechanical or geotechnical purposes (for example, Follin and Hermanson, 1996). These models are more representative of all of the

fractures, not just those important for flow. However, they were designed to address problems at a particular scale, typically a scale not much bigger than a few tens of meters. In this sense they are scale-limited. Available data on fracturing at larger scales typically comes from lineament maps. Such maps usually omit features smaller than some threshold, and may also miss some of the very large-scale features that are not numerous, but may be very important. Hence, a significant number of fractures may be poorly sampled by lineament maps or underground exposures that are nonetheless important for earthquake modeling. Determination of the scaling properties of the fracture network may make it possible to properly model fractures at scales that are poorly represented in existing data sets.

A knowledge of the scaling properties of the fracturing for each generic site makes it possible to "fill in" the data between the different measurement scales at which fracture data has been or can be collected. Thus, scaling studies address the first question.

The second question is resolved by considering *all* of the fractures, without regards to their size or any other property. In the modeling, fractures are not excluded from intersecting canister holes based upon their size. In theory, fractures hundreds of kilometers in length could intersect a canister hole, although such large fractures do not intersect canisters in any of the three generic sites. Somewhat smaller fractures can and do intersect the canister holes in the models. Since the numerical simulations described in this report did not preclude large fractures that might be identified during repository construction from intersecting canister holes, the predicted risk of canister failure could be reduced if some of these larger fractures can be identified and avoided during construction. The modeling results can be analyzed to determine if there is a minimum-sized fracture that is likely to be of concern. This issue is discussed in Section 5.

For these reasons, it is necessary to compute the scaling properties of the natural fracture systems for Aberg, Beberg and Ceberg and in the regions surrounding them, in order to have a more realistic DFN model for earthquake calculations. Section 2.2 describes how the scaling studies were carried out.

2.2 Methodology

The methods devised by the practitioners of fractal geometry (Mandelbrot, 1983) to study the scaling properties of natural fracture systems (Barton and La Pointe, 1995) provide an appropriate way of quantifying the scaling properties of fracture intensity, size/frequency and location. These tools do not require that the fracture systems be fractal. The mathematical tools are generic, and will reveal whether a system is fractal or follows some other type of scaling behavior. In fact, application of these tools to fault data might show that the system scales in non-fractal ways, as concluded by Castaing and others (1996). A system that scales in a fractal manner has some particularly nice mathematical properties, and many mechanical arguments have been put forth to show how fractal properties can arise from

various mechanical processes that occur during brittle fracture and earthquakes (for example Turcotte, 1992; Bak and Chen, 1995; Scholz, 1995). However, it is also possible that the fracture patterns relevant to Aberg, Beberg or Ceberg may scale in a different manner. Thus the scaling properties at each site were evaluated in both local and regional contexts. There are several aspects to quantifying the scaling of fracture patterns. These include the size of the fractures and their spatial pattern. Section 2.2.1 describes the analytical approach for studying the size-scaling of the fractures; section 2.2.2 describes the approach for studying the scaling properties of the spatial pattern of fracturing and fracture intensity.

2.2.1 Size/Frequency Scaling

Computation of size/frequency scaling relations is relatively straightforward, although there are some serious pitfalls to be avoided that have not always been taken into account in the published literature. These are discussed at the end of this section.

The basic approach for studying the scaling properties of fracture size is to compute the complementary cumulative density function (CCDF) for trace lengths in each fracture set. The probability that the trace length, X, is greater than x, P(X > x), is given by:

$$P(X > x) = G(x) = 1 - F(x) = \left(\frac{x_o}{x} \right)^D \qquad 2\text{-}1$$

where

G(x) is the complementary cumulative density function (CCDF),
F(x) is the cumulative density function (CDF),
x_o is the minimum size,
x is the size, and
D is the fractal dimension.

There are two unknown parameters in this equation, D and x_o. D is equal to the slope of the line when G(x) and x are plotted on log-log axes. x_o is equal to $xG(x)^{1/D}$ where x and G(x) are the coordinates of any point on the line, and should be no greater than the smallest mapped trace length.

Other types of distributions have very distinctive CCDF's (Figure 2-1) when plotted on logarithmic axes. Note that the power law is the only distribution that plots as a straight line over a large range of scales. The approximately linear portions of other distributions occur for much narrower scale ranges. Moreover, the approximately linear portions of these other distributions occur where the function is either very flat or very steep. Thus, a log-log plot of CCDF that appears linear and has slope that is not close to vertical or horizontal is good evidence of power law scaling, even for a narrow range of scales.

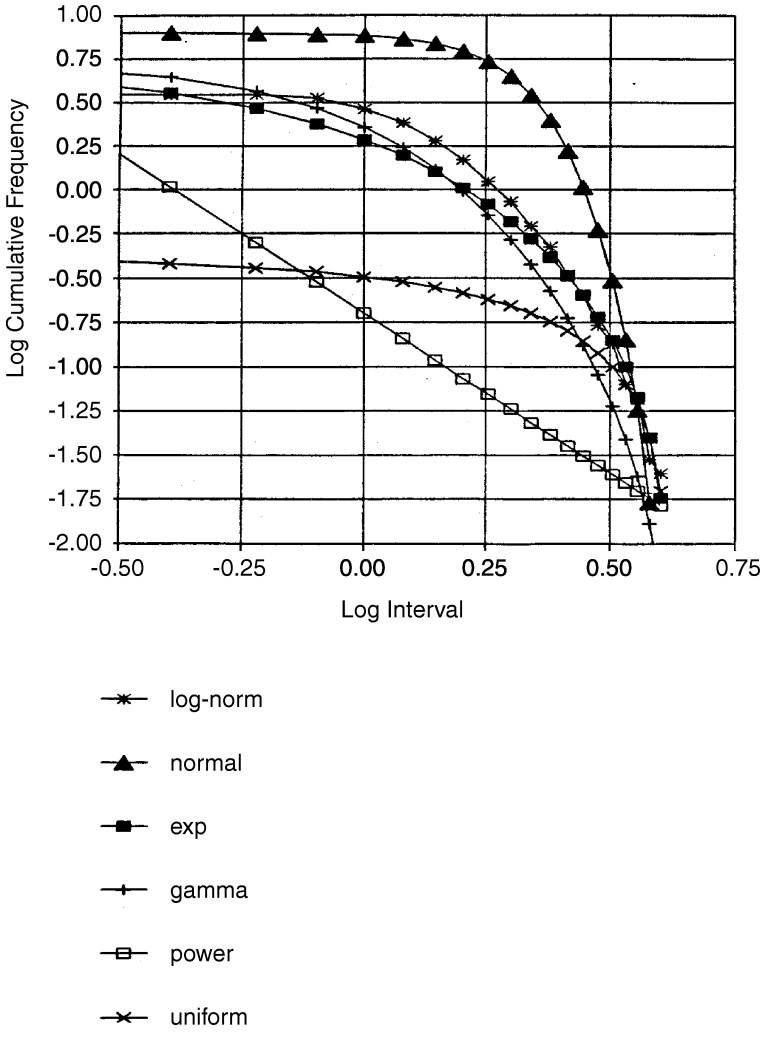

FIGURE **2-1**
CHARACTERISTIC CCDF'S FOR COMMON DISTRIBUTIONS

While this calculation might seem straightforward, it can produce incorrect results if certain pitfalls are not avoided.

2.2.1.1 Pitfall 1 - Trace Length Censoring

There are pitfalls for carrying out size/frequency scaling analyses that have not always been taken into account in published studies, and these pitfalls may have led the authors to conclude incorrectly that fractures did not have power-law scaling properties. It is worthwhile to discuss these pitfalls both to strengthen confidence in the current study and to improve future studies on fracture size distributions.

There are a number of published studies attempting to quantify the scaling properties of fault trace lengths, spacings and displacements. Some of these studies have concluded that aspects of fault patterns scale in a fractal manner, while others have reached an opposite conclusion (e.g. Castaing and others, 1996; Ouillon and others, 1996). Many of the studies that have concluded that fracture trace length do not scale as power laws may be more due to an error in the way that the data was analyzed.

Castaing and others (1996) computed the length-frequency statistics of fault traces at a number of different scales. Their procedure was to start with a large-scale map of fault traces, analyze the trace length distribution, and then to take out successively smaller windows of the data and analyze the distribution for each window. They concluded that the histogram for each window was not a power law, but rather could be reasonably well approximated by a lognormal distribution.

While fault trace lengths in some locations may truly conform to a lognormal distribution, the manner in which they have been analyzed may have distorted the results. This distortion occurs when data are sampled in a window.

Selecting traces within a window alters the trace length distribution, because some fault traces are truncated against the window boundaries. This produces a number of smaller trace lengths. While this might not be a problem for some types of statistical distributions, it is a problem for power law (fractal) distributions. The problem arises because a power law distribution is always defined in terms of some minimum cut-off size (see Equation 2-1).

To illustrate how the truncation of trace lengths by the edges of the window affects the results, consider the following simple illustration. A series of fault traces has been generated according to a power law distribution with $x_o = 10$ m, and $D = 2.4$ (Figure 2-2). The mean trace length is approximately 16.7 m. These fault traces have been generated within a 100 m by 100 m square. The CCDF of the parent trace length distribution are shown in Figure 2-2. The CCDF plots as a straight line with slope equal to -2.40. The non-linear regression line is shown superimposed on the data in the figure.

Next, a smaller window is cut out of the data. This window, shown at the top of Figure 2-2, measures 40 m by 40 m, and is centered within the larger area.

Figure 2-3 shows the results of analyzing all of the trace lengths within the window. Because some of the traces are truncated against the window, there are now some trace lengths *smaller* than the original minimum size (x_o = 10 m). As a result, the histogram now contains a mode near to the value of the original minimum size. The CCDF shows two departures from linearity. The first, and most noticeable, is for the small trace lengths, which is due to the aforementioned affect. There is also a truncation at large sizes that becomes noticeable at about 20 m. This steepening of the CCDF is due to the fact that the window is truncating large traces. The dashed line on the figure is a lognormal fit to the data with mean equal to 2.45 and standard deviation of 0.5. The lognormal fit passes a Kolmogorov-Smirnoff test at 90%. It is interesting to note that the lognormal distribution fit to the data visually appears to be about as good as many of the distributions shown by Castaing and others (1996).

This example illustrates how important it is to avoid biases introduced by sampling trace length distributions from within a window. Fortunately, these problems can easily be overcome by not including in the CCDF traces that intersect the boundaries of the sampling window. This will eliminate the censoring effects that occur at the scale of the sampling window for the very large fractures, and also for those small traces that are below the minimum size. The data corrected for censoring and truncation, shown as the red triangles in Figure 2-3 plot as a power law with approximately the same slope as the parent uncensored population up to about the 20 m scale. Non-linear regression of all of the data still yields a power law distribution with a slope (fractal dimension) of -2.44 and a minimum size of 9.9. This is essentially the correct value for the parent population. It is worth noting that the linear portion of the CCDF for the uncorrected, windowed trace lengths over the scale ranges of 10 m to 20 m has the same slope as the parent population. This suggests that it should be possible to obtain a representative fractal dimension by fitting only this linear portion even if the data has not been corrected for the windowing effect, which is not always possible. Nonlinear regression of the portion of the uncorrected data lying between 10 m and 20 m yielded a slope of -2.35 and a minimum size of 8.4.

The implication for the present study is two-fold. First, existing studies that conclude that fracture patterns do not scale in a fractal manner may be flawed due to their analytical methodology. Secondly, the results of Section 3 are more credible since the problems that could lead to incorrect results were recognized and avoided.

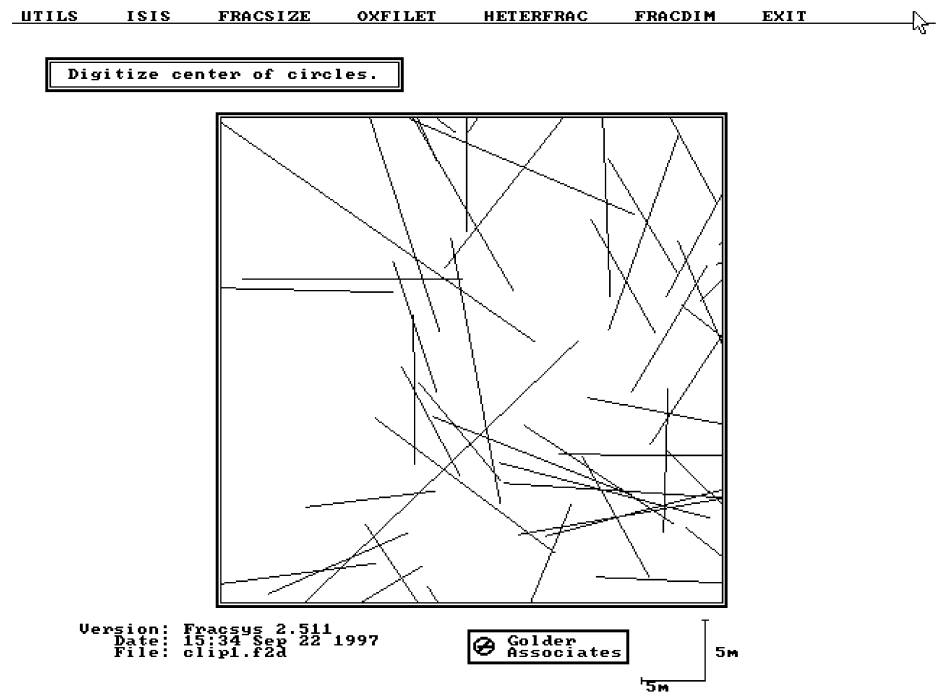

a. Simulated Traces in Window Area

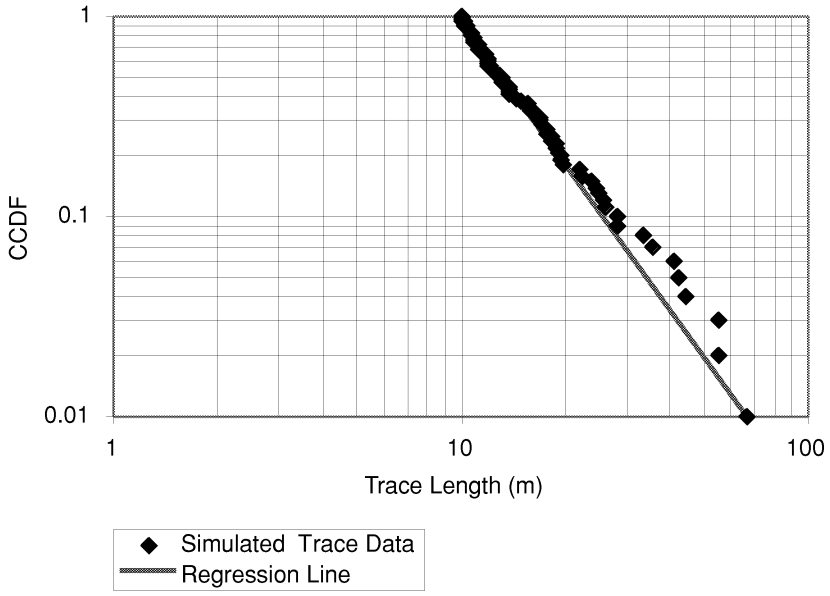

b. Parent Trace Population Power Law Distribution

FIGURE **2-2**
WINDOW SAMPLING PROBLEMS

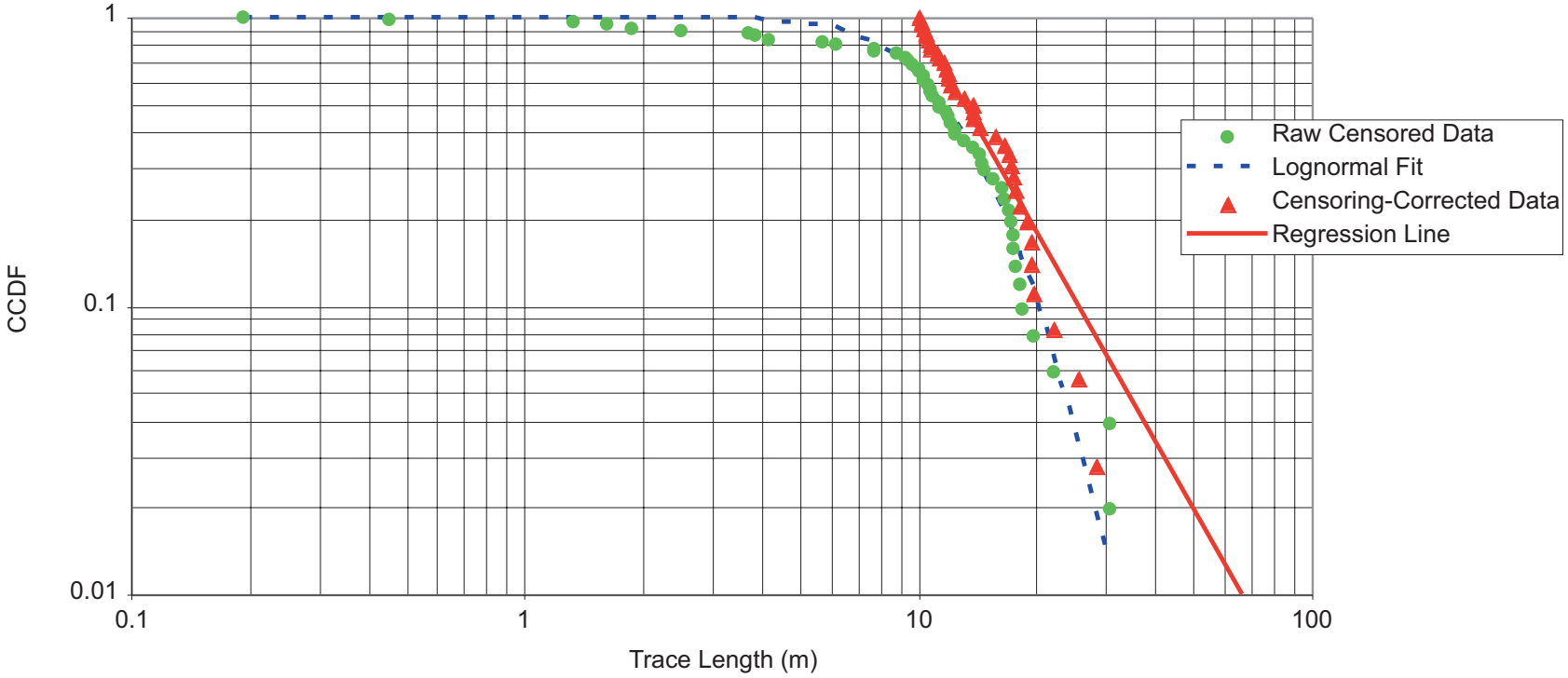

FIGURE **2-3**
TRACE LENGTHS AND TRACE LENGTH STATISTICS FOR WINDOWED REGION

2.2.1.2 Pitfall 2 - What Constitutes a Single Trace?

In order to obtain a meaningful CCDF of trace lengths from a lineament, outcrop or subsurface maps underground, it is necessary to identify which portion of a trace represents a single earthquake or fault rupture event. This is important for the current study since the surface rupture length (SRL) is used to estimate the size of earthquakes that might occur along them in the future. It is usually not difficult to distinguish individual fractures in outcrop or underground, since the trained geologist can usually make detailed observations of the fractures of such diagnostic surface morphological features as plumose markings. However, this level of observational detail is generally impossible for lineament trace maps. Geologists who interpret lineament or large-scale fault trace maps for seismological studies in the United States have adopted some working guidelines to separate lineaments into individual fault rupture events. Knuepfer (1989), who studied strike-slip faults, suggests that the following criteria can be used to define the endpoints of a single rupture:

- Geometric properties, such as fault bends; release structures (double bends, step-overs, splays); and fault trace gaps, discontinuities or steps
- Structural features, such as branches and intersections with faults and folds; and terminations of faults against other cross-cutting structures
- Geological features, such as basin margins; and changes in bedrock geology relating to changes in rock rheology
- Behavioral changes, such as changes in complexity of fault traces; change in sense of slip; change in the mechanics of slip; the recency of prior ruptures on the same segment; and in the die-out of fault traces

In digitizing the lineament maps, these factors were used qualitatively to try to insure that each trace length corresponded to an individual rupture or fault. When there was doubt, the decision was to aggregate fault trace segments into as few a number of faults as possible. This will tend to maximize the individual fault trace length, which will be conservative from the standpoint of calculated earthquake effects. It is a conservative alternative because the amount of slip or energy released during an earthquake is proportional to the mapped trace length (Wells and Coppersmith, 1994), and the induced slip on other fractures is also proportional to fracture area (Pollard and Segall, 1987).

2.2.1.3 Pitfall 3 - What is the Relation of a Trace Length Distribution to a Fracture Area Distribution?

DFN models generate fractures as polygons, and so it is necessary to specify a proper fracture area distribution. Wells and Coppersmith (1994) have compiled a worldwide database of earthquake source parameters that provide statistically significant relations between surface rupture length, subsurface rupture length and rupture width (depth) for earthquakes greater than about moment magnitude 4.5. Recent work by Nadeau and McEvilly (1997) suggests that these relations may extend to faults with subsurface rupture lengths on the order of 10 m. Using these relations, it is possible to

assign a subsurface length and width to each fault represented in the larger scale lineament maps. The derivation of these and other relations are described in Section 4.

2.2.2 Spatial Scaling

Spatial scaling can be quantified in several ways. A common way to examine the scaling characteristics of fracture patterns is to compute the box dimension (Barton, 1995). Box fractal dimensions of random fractals can be computed from 1D (borehole, scanline), 2D (outcrop, lineament map, drift map) or 3D data and easily compared. The fractal Box dimension describes how "space-filling" the fracture pattern is. For a lineament or outcrop map, the dimension varies between 1.0 and 2.0. A dimension of 1.0 implies that traces are tightly grouped and aligned, occupying very little space. A dimension of 2.0 implies that the traces are evenly dispersed throughout the area under study.

A fracture pattern that is well modeled by a Box fractal dimension contains no inherent scale. In other words, the fracture pattern at one scale looks like the pattern at other scales. Fracture patterns that exhibit fractal scaling laws in one aspect, such as trace lengths, often exhibit fractal scaling in many other aspects. If rock fracturing is in fact an expression of a self-organized critical system, as postulated by Bak and Chen (1995), then the patterns would be expected to exhibit fractal scaling behavior in many aspects of their geometry.

Each trace map for the three sites was analyzed to compute its Box fractal dimension. If the trace map did not conform to a fractal model, other models were evaluated.

2.2.3 Summary

There are several pitfalls to be avoided in computing the scaling properties of fracture patterns. The present study has taken these into account in order to insure that fractures at all of the orders of magnitude that are important are properly included in the numerical simulations.

3. GENERATION OF STOCHASTIC DISCRETE FRACTURE MODELS

3.1 Aberg

3.1.1 Trace Length Analyses

Trace length maps at four scales were analyzed. These maps are shown in Figure 3-1. The map scales vary from 1:1,000,000 for southern Sweden (Tirén and Beckholmen, 1990) to 1:10,000 for Äspö (Nisca and Triumf, 1989). Two intermediate scale maps for the Simpevarp-Oskarshamn region (Tirèn and others, 1987) were also analyzed. Data sources used are summarized in Table 3-1.

Table 3-1. Aberg (Äspö) Data Sources

Source	Fig. #	Scale
Tirén and Beckholmen, 1990	3-1a	1:1,000,000
SKB PR 25-87-21 (Tirén and others, 1987)	3-1b	1:250,000
SKB PR 25-87-21 (Tirén and others, 1987)	3-1c	1:150,000
SKB PR 25-89-01 (Nisca and Triumf, 1989)	3-1d	1:7,000

There are many different ways to interpret lineaments from topographic or other data. The maps reproduced in Figure 3-1 were derived using different criteria for defining lineaments. A discussion of each map is beyond the scope of the present study. These four maps were selected for analysis because:

- They represented fracturing at different scales
- They were based on topography
- They contained a lot of data, and the traces were generally shown as continuous lines or as dashed traces that could easily be recognized as portions of a single fault.

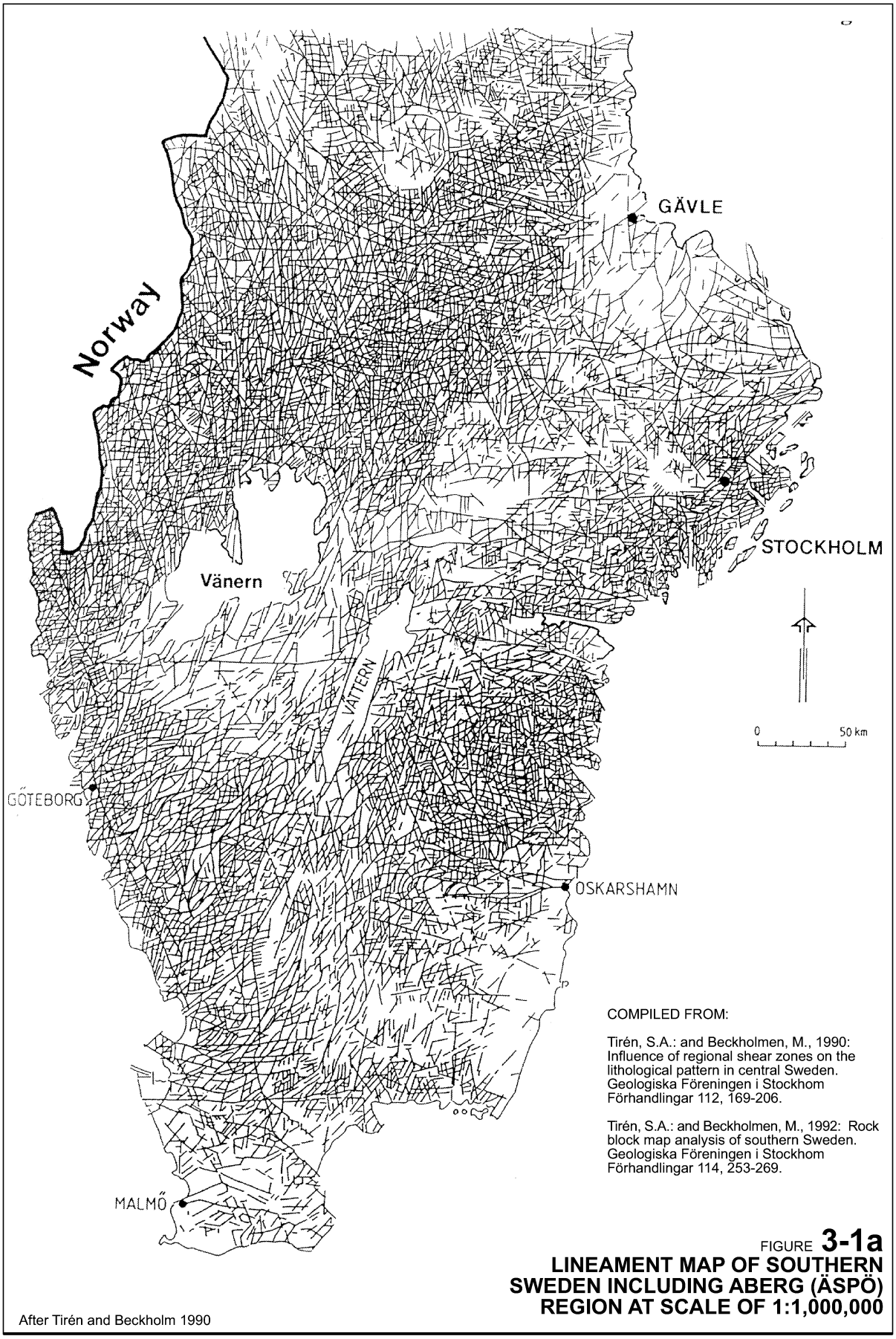

COMPILED FROM:

Tirén, S.A.: and Beckholmen, M., 1990: Influence of regional shear zones on the lithological pattern in central Sweden. Geologiska Föreningen i Stockhom Förhandlingar 112, 169-206.

Tirén, S.A.: and Beckholmen, M., 1992: Rock block map analysis of southern Sweden. Geologiska Föreningen i Stockhom Förhandlingar 114, 253-269.

FIGURE **3-1a**
LINEAMENT MAP OF SOUTHERN SWEDEN INCLUDING ABERG (ÄSPÖ) REGION AT SCALE OF 1:1,000,000

After Tirén and Beckholm 1990

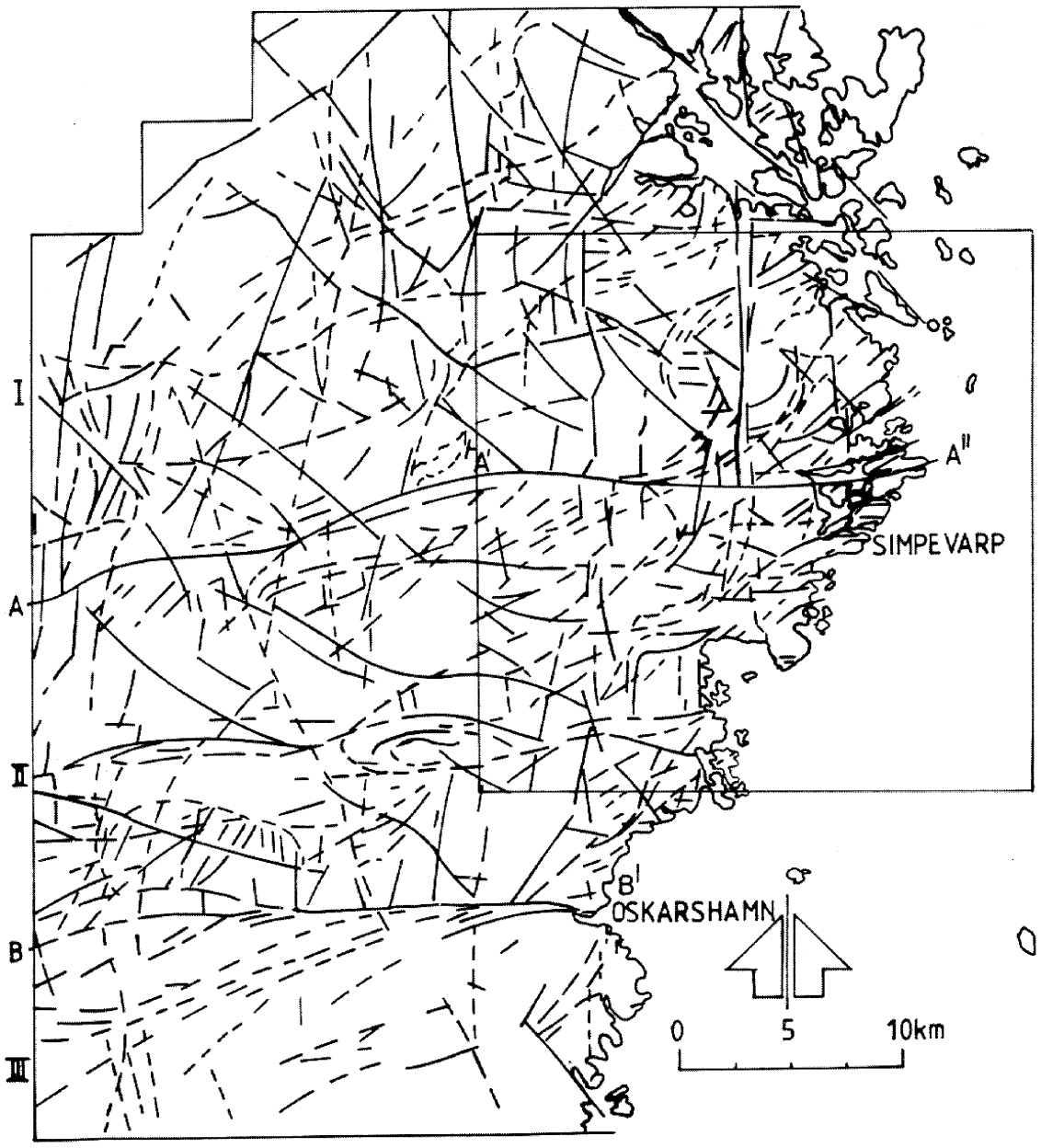

* Reduced to 90% for this figure

FIGURE **3-1b**
LINEAMENT MAP DERIVED FROM RELIEF MAP MAP AT ABERG (ÄSPÖ), SCALE 1:250,000*

After SKB PR 25-87-21 (Tirén et al., 1987)

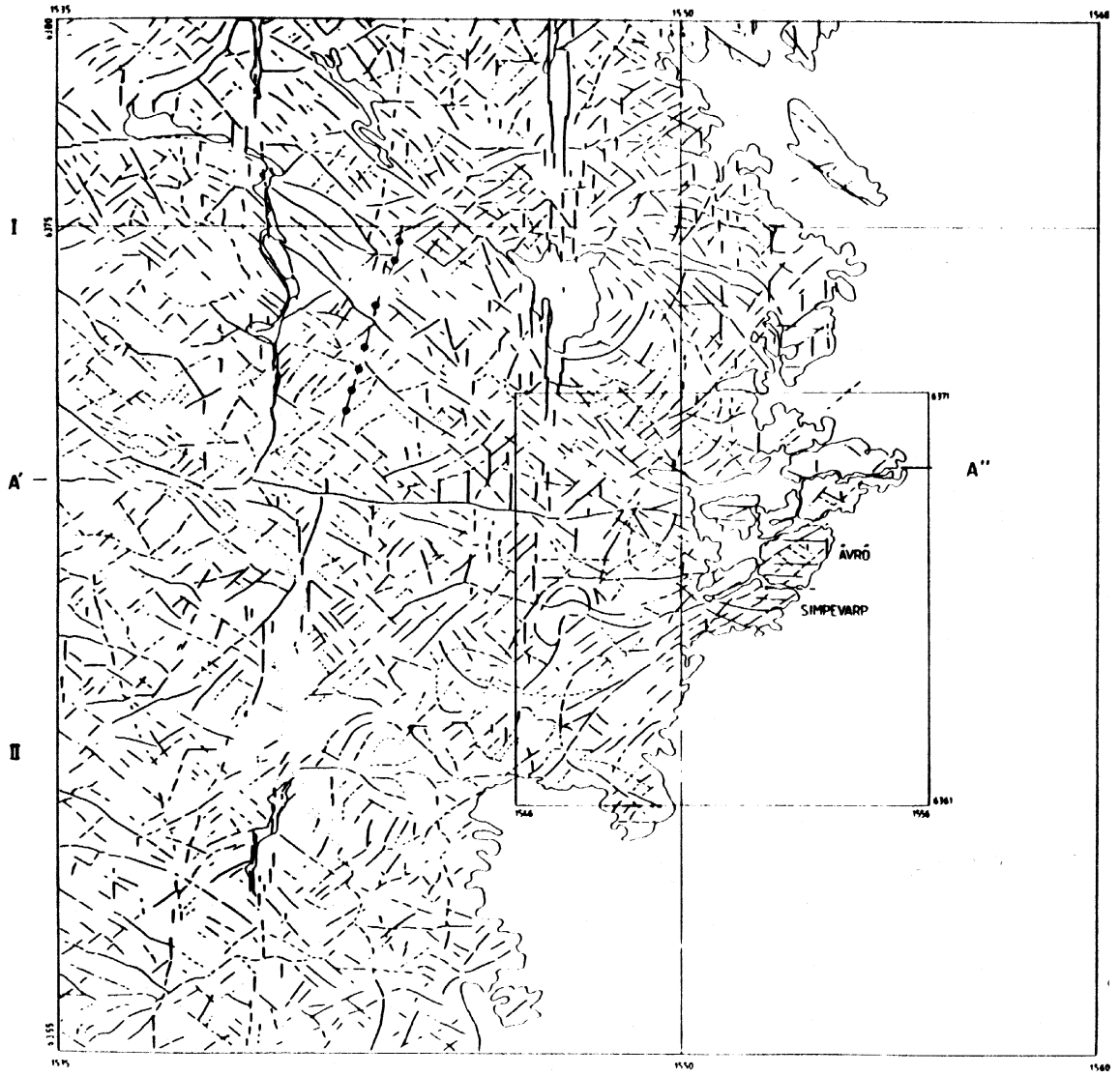

SIMPEVARP AREA
MAP SHEET 6G SE, NE and 6H SW, NW

— Lineament

—●— Lineament, ridge

Esker

Åvrö-Simpevarp Area

N

0 5

SCALE IN KILOMETRES

FIGURE **3-1c**
LINEAMENT MAP OF SIMPEVARP AREA INCLUDING ABERG (ÄSPÖ) SCALE OF 1:150,000

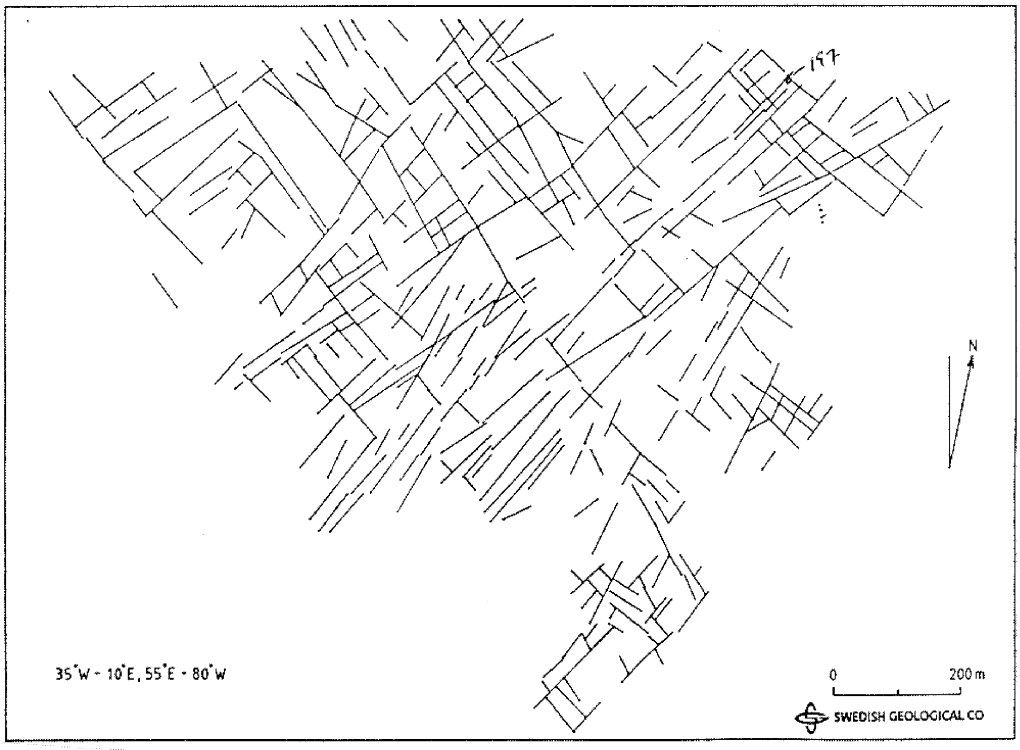

* Reduced to 90% for this figure.

FIGURE **3-1d**
LINEAMENT MAPS OF ÄSPÖ ISLAND (ABERG) AT A SCALE OF 1: 7,000*

After SKB PR 25-89-01 (Nisca and Triumf 1989)

Traces were divided into sets for each map (Table 3-2). Division was based upon the rosettes shown in Figure 3-2. The trace length CCDF was calculated for each set separately. The results are shown in Figure 3-3. This graph shows that the CCDF's for all four data sets have approximately linear portions that extend over a wide range of scales. The slopes of these linear portions do not show marked differences among the different fracture sets at each scale. This implies that all of the sets scale in approximately the same way at a given scale of observation. Even though the curves may have nearly the same slope, they do not always overlap. An offset among the curves representing different sets for a given dataset implies that each trace set has a different mean size. A summary of the trace length scaling parameters is given in Table 3-3.

Because trace lengths scale over all of the sizes of interest for earthquake modeling, a single power-law size model can be used for each fracture set for the Aberg study.

Figure 3-3 shows that the trace data for Äspö Island departs from linearity at a scale around 50 m. For scale larger than 50 m, the CCDF for trace lengths is linear and has a slope (fractal dimension) equal to 1.6. The linear portion of next smaller scale of measurements, made underground in the HRL by Hermanson and others (1997) shows a similar, though slightly shallower, slope. The slope is approximately 1.45. These two sets of data define the scales of the stochastic fracturing. Fractures larger than 50 m will be simulated deterministically, while those much smaller than 1 meter are ignored since they have little potential for causing canister damage during an earthquake. The previous work by La Pointe and others (1997) showed that the amount of slip increased with fracture size. Thus the safety is most influenced by the larger fractures. For this reason, the slope for the Äspö Island traces, 1.6, was used to define the scaling properties of the stochastic fractures in the DFN model. The same scaling exponent was used for all sets, since the slope is nearly identical for all three sets (Figure 3-4).

3.1.2 Box Dimension Calculations

The fact that fracture traces may exhibit fractal scaling does not imply that fracture locations or intensity scale in a fractal manner. The dimensions for the four sets of traces mapped on Äspö Island show consistent box fractal dimensions (Figure 3-5). Each curve plotted in the figure can be broken into two linear segments. The more shallowly-dipping portion has a slope of approximately 1.0, and is an artifact of allowing box sizes to become too small (Barton, 1995). The steeper portion of each curve is not biased by box size and represents the true box dimension of the data. Nonlinear regression of this more steeply-dipping portion of each curve yields box dimensions varying from 1.49 to 1.62, with an average value of 1.58. Similar values have been found for other fracture patterns over the same scale range outside of Sweden (Barton, 1995). Table 3-3 summarizes mean box dimensions for the trace maps.

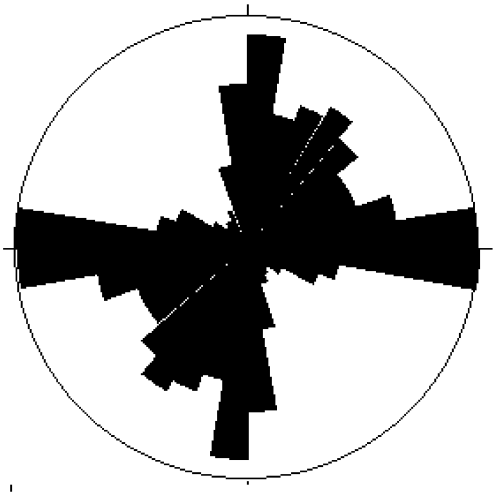

a. Southern Sweden, 1:2,000,000 Map

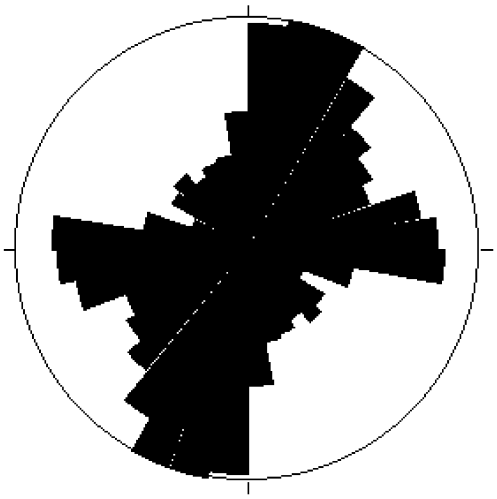

b. Oskarshamn Region, 1:250,000 Map

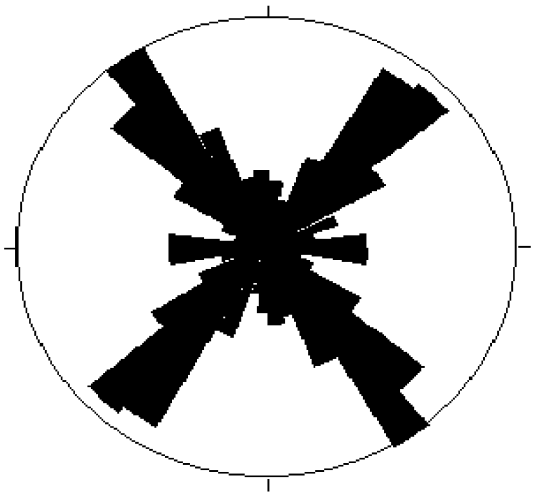

c. SimpevarpArea, 1:150,000 Map

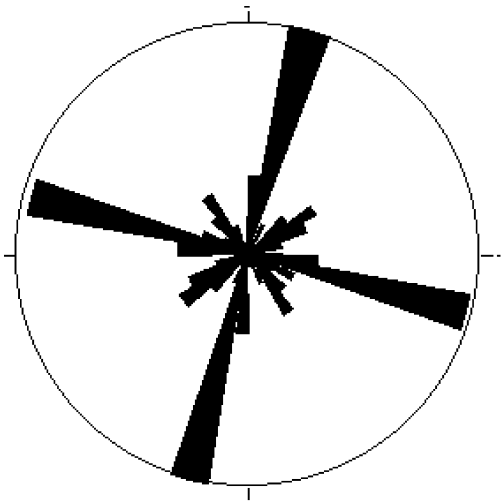

d. Äspö Island, 1:7,000 Map

FIGURE **3-2**
ORIENTATION ROSETTES FOR ABERG AND ABERG REGION

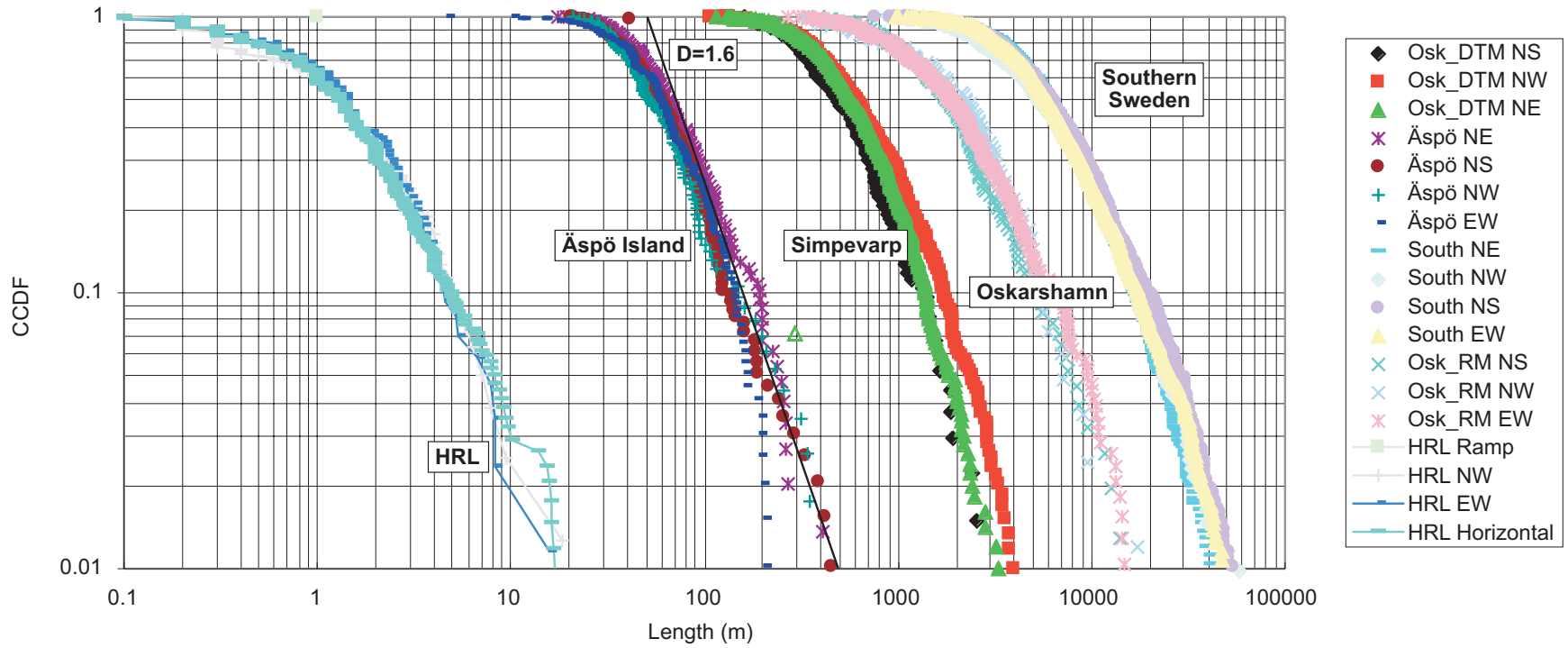

FIGURE **3-3**
TRACE LENGTH CCDF FOR ABERG AND SURROUNDING REGION

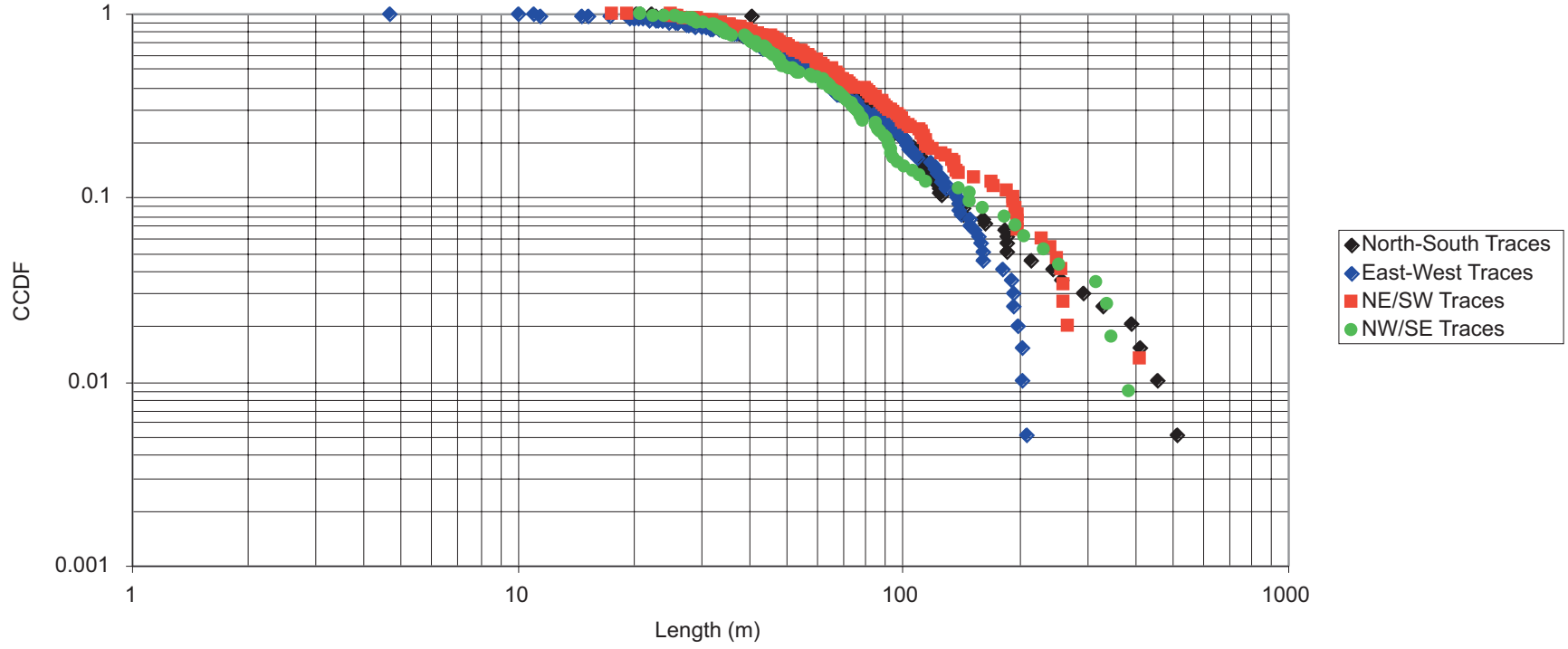

FIGURE **3-4**
COMPOSITE TRACE LENGTH CCDF FOR ABERG DFN MODEL

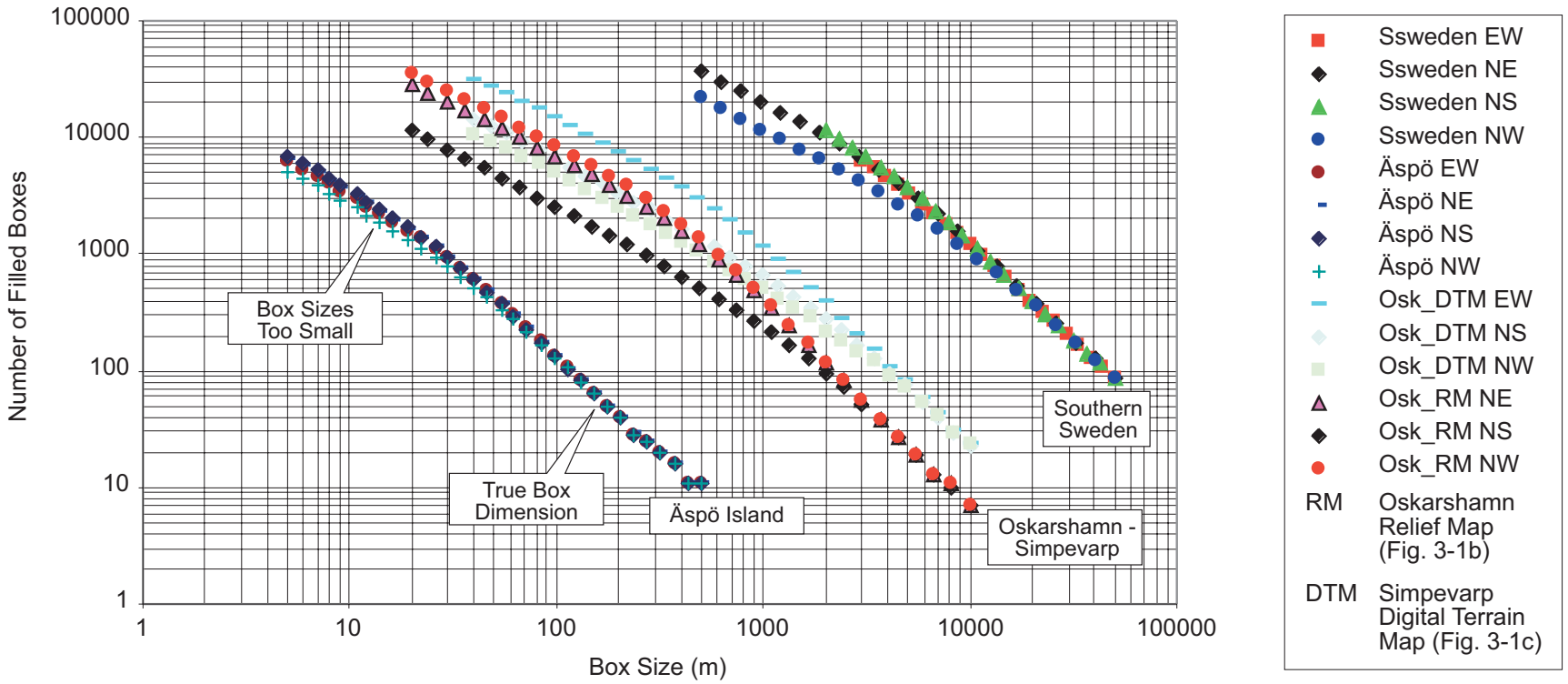

FIGURE **3-5**
BOX DIMENSIONS FOR SOUTHERN SWEDEN – ABERG SITE

Table 3-2. Trace Set Definitions for Aberg

Map Scale	Set Name	Azimuthal Range
1:2,000,000	South NE	35-70º
1:2,000,000	South NW	315-355º
1:2,000,000	South NS	175-215º
1:2,000,000	South EW	70-135º
1:250,000	OSK_RM NS	165-205º
1:250,000	OSK_RM NW	305-345º
1:250,000	OSK_RM EW	25-125º
1:150,000	OSK_DTM NS	165-195º
1:150,000	OSK_DTM NW	250-345º
1:150,000	OSK_DTM NE	15-70º
1:7,000	Äspö NE	10-55º
1:7,000	Äspö NS	145-190º
1:7,000	Äspö NW	280-325º
1:7,000	Äspö EW	55-100º

Table 3-3. Aberg Results

Map	# Sets	Set Orients	D, tracelength	D, box
1:2,000,000	4	EW, NE, NS, NW	D = 1.66	D_b = 1.60
1:250,000	3	NS, NW, EW	D = 1.56	D_b = 1.59
1:150,000	3	NS, NW, NE	D = 1.52	D_b = 1.71
1:7,000	4	NS, NE, NW, EW	D = 1.60	D_b = 1.61

A dimension of 1.58 suggests that the fracture pattern is somewhat clustered, dividing the rock mass into blocks of non-uniform size. The various trace maps shown in Figure 3-1 show blocks (in 2 dimensions) of various sizes as well, and thus are consistent with a dimension of 1.58. A dimension approaching 2.0 would lead to a densely fractured rock mass with many blocks of nearly the same size (Figure 3-6). A pattern with dimension close to 1.0 would consist of many fewer blocks, with a few of them being very large.

The consequence of the box dimension analysis is that it supports a DFN model that scales over a large scale range in a predictable manner. The analyses suggest that a box fractal model with dimension 1.58 (or 2.58 in three-dimensions) is appropriate for generating the stochastic component of the DFN model for Aberg.

More detailed studies of fracturing in the HRL (La Pointe and others, 1995), however, have shown that traces mapped underground on the roof and walls are best modeled by a Poissonian pattern, which has a Box dimension of 2.0. The reason for this discrepancy is not known. It is probably related to the "missing" smaller scale fractures in the trace map of Äspö Island. The trace maps shown in Fig. 3-1d have almost certainly missed many smaller-scale fractures. Were these fractures included in the Box dimension calculations, the resulting Box dimension would be much higher. For this reason, a

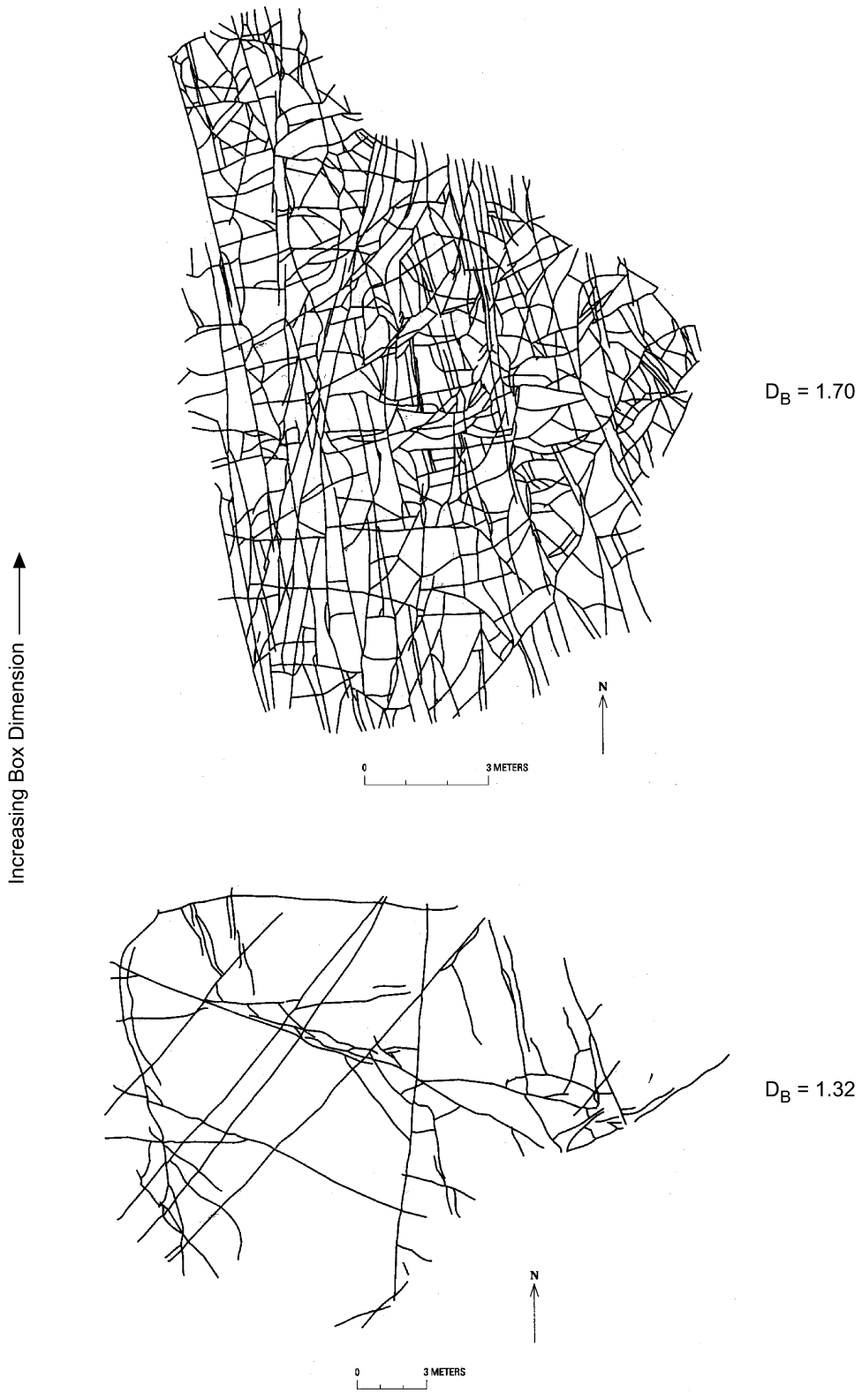

From Barton (1995)

FIGURE **3-6**
RELATION OF BOX DIMENSION AND "BLOCKINESS"

Poissonian model was adopted for the stochastic fracturing. Moreover, it is unlikely that the spatial pattern of the fracturing plays as important a role in earthquake performance assessment as it does in flow and transport studies. This is because fracture connectivity controls regional flow; connectivity probably plays little role in the induced slippage during an earthquake, and plays no role in the numerical modeling.

It may well be that the slopes around 1.6 that the larger scale fracture patterns exhibit is also due to the absence of smaller scale traces. What is important to note from the Box dimension calculations of the larger scale patterns is that they appear to be reasonably consistent in their dimensions. This suggests that the rock breakage due to tectonic forces, uplift or glacial unloading produced fracturing over a large range of scales; thus knowledge of fracturing at one scale is a useful predictor of fracturing geometry at other scales. It implies that it is not unreasonable to assume that a single scaling model applies to traces ranging from 1 meter to 50 meters; there is not evidence of a discontinuity in the fracturing over the scales at which stochastic fractures are generated.

3.1.3 DFN Model Parameters

The calculation of fracture intensity for these models can be somewhat complicated. Fracture intensity is defined as the surface area of fractures divided by the volume of rock containing the fractures. This parameter is denoted P_{32}, and has units of m^2/m^3 or m^{-1}. A related parameter is P_{21}, which is the total trace length of all fractures traces divided by the surface area on which the traces have been mapped. P_{21} has units of m/m^2, or m^{-1} (Figure 3-7). Dershowitz and Herda (1992) have shown that P_{21} is linearly correlated to P_{32} according to the equation:

$$P_{32} = C * P_{21} \qquad 3\text{-}1$$

where C is an unknown constant of proportionality. This constant depends only upon the orientation and size distribution of the fractures in the rock mass, and the orientation of the surface on which fracture traces have been mapped.

The strategy for estimating P_{32} for Aberg is to compute the P_{21} for the traces mapped for Äspö Island. The CCDF for the fractures sets begin to depart from linearity for trace lengths at approximately 50 m. This implies that there is an under-representation of traces smaller than 50 m for the power law model fit to the multiscale data (see Section 3.1.1). To overcome this limitation, the dataset for the HRL was combined with that for Äspö Island by multiplying the number of fractures in the URL until the two CCDF curves aligned. The resulting CCDF is shown in Figure 3-4.

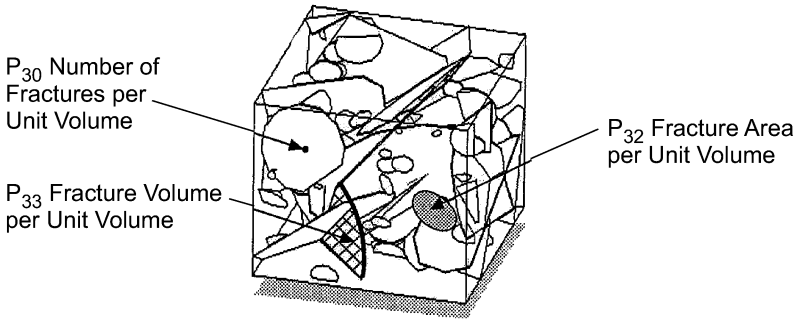

Three Dimensional Fracture Intensity Measures

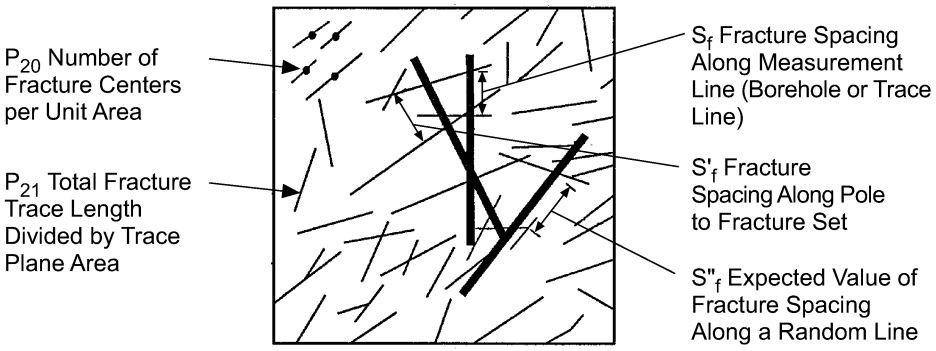

Two Dimensional Fracture Intensity Measures

FIGURE **3-7**
DEFINITION OF P_{32} AND P_{21} INTENSITY MEASURES

The procedure is to generate a DFN model based on all fractures using an arbitrary guess for P_{32}. A horizontal plane analogous to the surface of Äspö Island is inserted into the DFN model and intersections are computed. All traces less than 50 m are removed. The remaining P_{21} for this dataset is compared to the measured P_{21} (for which all traces less than 50 m have also been removed). P_{32} is adjusted automatically until the synthetic trace data P_{21} matches the measured trace data P_{21}. The computed value of P_{32} is 2.965.

A summary of the Aberg DFN model parameters are presented in Table 3-4.

Table 3-4. Summary of DFN Model Parameters for Aberg

Parameter	Value	Comments
Set 1		
Orientation (Mean pole trend, plunge, dispersion)	58.7, 1.8, κ = 13.37 Fisher model	From Follin and Hermanson (1996)
Intensity (P_{32})	1.4333	Derived in this study
Set 2		
Orientation (Mean pole trend, plunge, dispersion)	334.2, 5.6, κ = 7.82 Fisher model	From Follin and Hermanson (1996)
Intensity (P_{32})	0.7509	Derived in this study
Set 3		
Orientation (Mean pole trend, plunge, dispersion)	71.7, 85.5, κ = 11.92 Fisher model	From Follin and Hermanson (1996)
Intensity (P_{32})	0.7807	Derived in this study
All Sets		
Size	Power Law, D = 2.6 X_o = 0.1 m Min = 3 m, Max = 50 m	Derived in this study
Flow Properties	Ignored	
Spatial Model	Baecher	La Pointe and others (1995)

3.2 Beberg

3.2.1 Trace Length Analyses

For Beberg, trace length maps at three scales were analyzed. These maps are shown Figure 3-8 and the data sources are summarized in Table 3-5. The map scales vary from 1:400,000 for the Osthammar region (Bergman and others, 1996) down to 1:20,000 for a rock block map of the Finnsjön site (Ahlbom and Tirén, 1991). These maps are of topographic lineaments that are interpreted to be fractures and fracture zones. Because a change in fracture intensity is apparent to the eye in the 1:400,000 map, it was split into the east and west halves for analysis. The results from the west half are

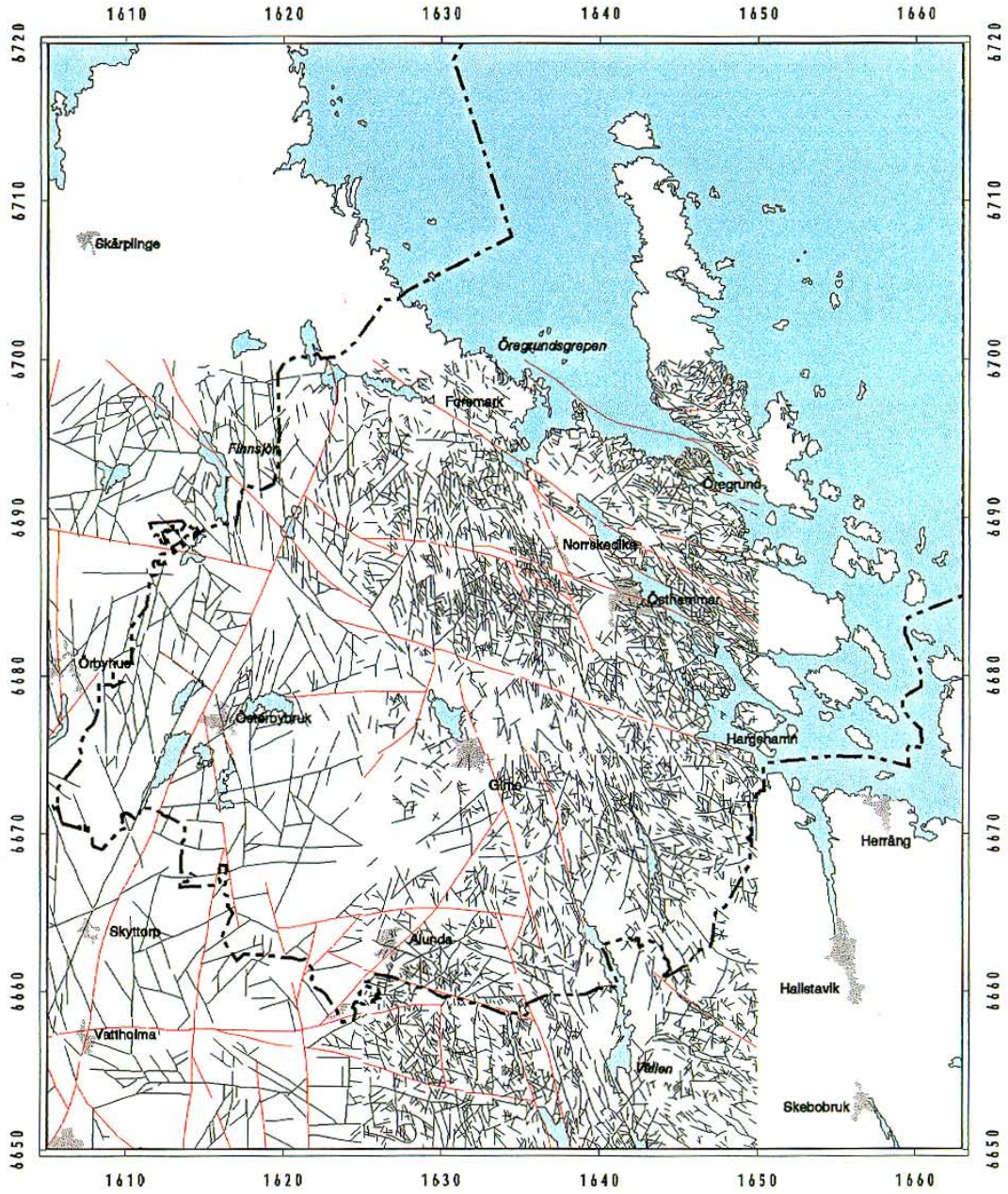

Fig. 7 –4 SGU/GeoVista AB

SKB DJUPFÖRVAR

Topografiska lineament tolkade från flygbilder, Östhammarsområdet. Lineament vilka finns markerade på de tryckta geologiska kartorna visas med röd färg

Förstudie Östhammar

0 20 km

Kommungräns

Vatten

Tätort

FIGURE **3-8a**
LINEAMENT MAP AT BEBERG (FINNSJÖN) AT A SCALE OF 1:400,000

After SKB PR D-96-016 (Bergman et al. 1996)

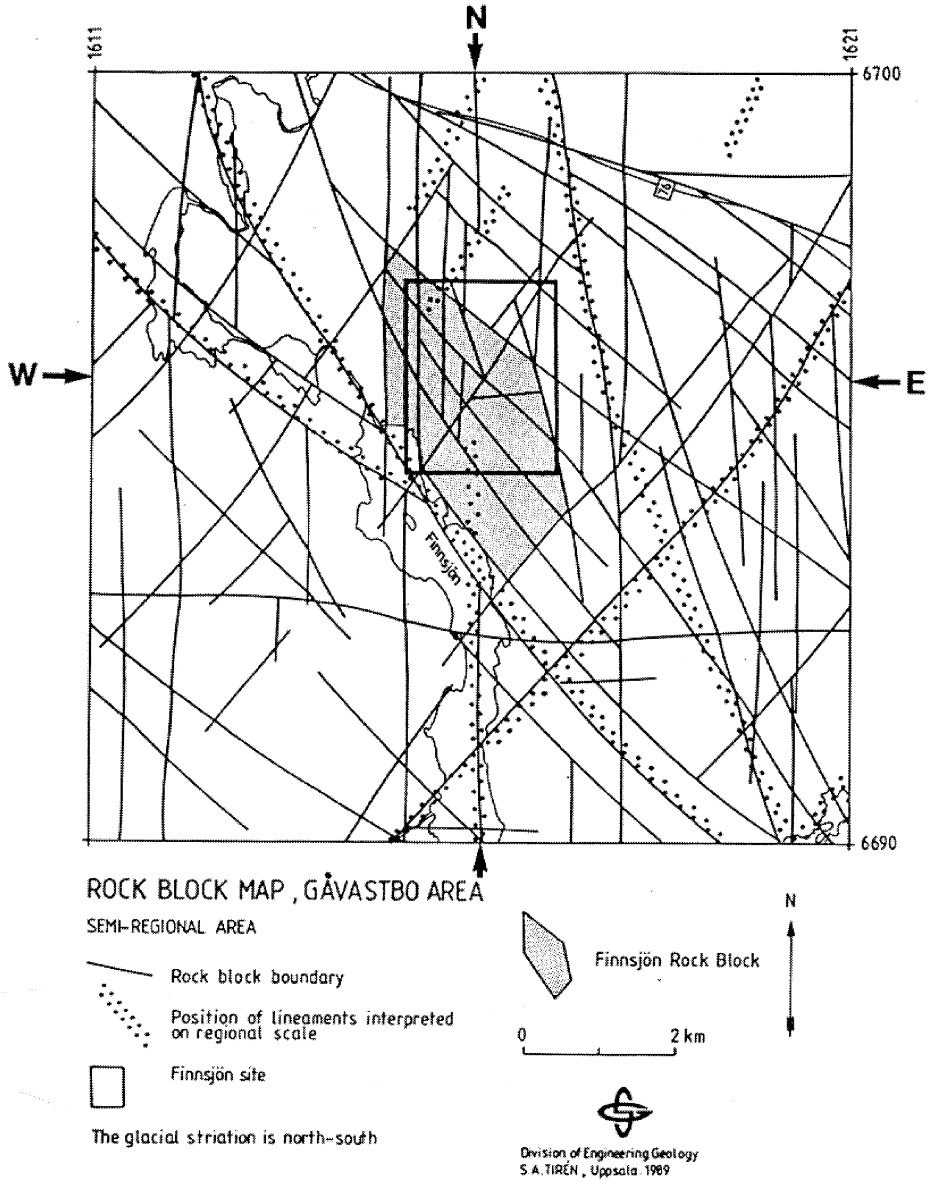

FIGURE **3-8b**
LINEAMENT MAP AT BEBERG (FINNSJÖN) AT A SCALE OF 1:87,000

After SKBTR 91-08 (Ahlbom and Tirén 1991)

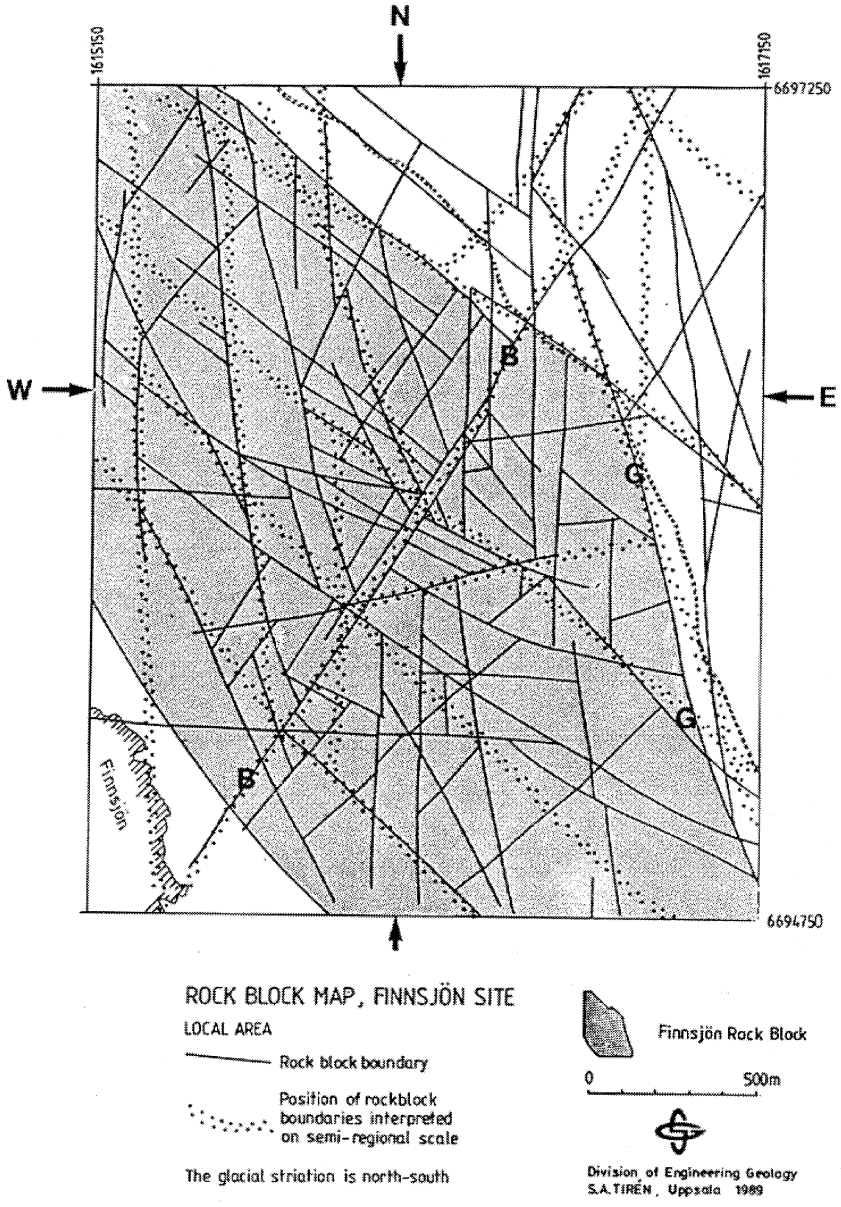

FIGURE **3-8c**
LINEAMENT MAP AT BEBERG (FINNSJÖN) AT A SCALE OF 1:20,000

After SKBTR 91-08 (Ahlbom and Tirén 1991)

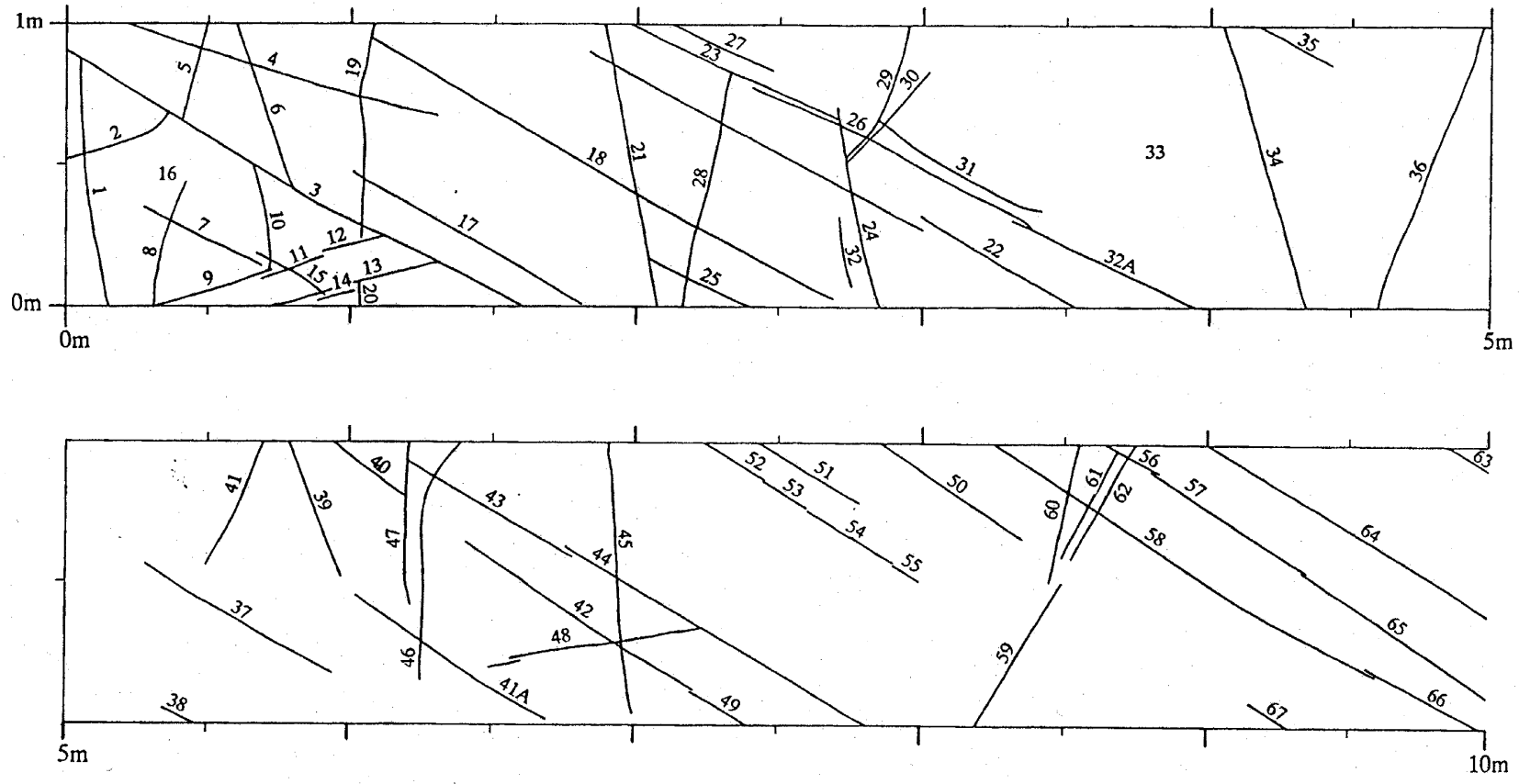

FIGURE **3-8d**
FRACTURE TRENCH MAP AT BEBERG (FINNSJÖN) AT A SCALE OF 1:20, FIRST 10M (OF 48M)

After SKB TR 91-24 (Andersson et al. 1991)

considered more relevant to the Finnsjön site, which is in the center of the west half of the map. In addition to the three trace maps, a 1:20 scale map of fractures on a trench wall at the Brandan Area (Andersson and others, 1991) was analyzed.

Table 3-5. Beberg (Finnsjön) Data Sources

Source	Fig. #	Scale
PR D96-016 (Bergman and others, 1996)	Fig. 7-4 west	1:400,000
PR D96-016	Fig. 7-4 east	1:400,000
TR 91-08 (Ahlbom and Tirén, 1991)	Fig. 10	1:87,000
TR 91-08	Fig. 5	1:20,000
TR 91-24 (Andersson and others 1991)	A76-A80	1:20

Traces were divided into sets for each map. Division was based upon the rosettes shown in Figure 3-9. The azimuthal ranges used to define each set are given in Table 3-6. The trace length CCDF was calculated for each set separately. The 1:87,000 map was digitized and initially included in the analysis; however, once censored fractures (those truncated by the edge of the map) were removed, only 32 fracture traces remained. This was deemed too few data points to be of use (particularly when divided into orientation sets); so the dataset was dropped. The results for the other three maps (Figure 3-10 and Table 3-7) show that the CCDF's for all eight of the data sets have approximately linear portions that extend over a wide range of scales. While, the fractures on the east half of the 1:400,000 map have a fractal dimension of 1.85, the trace lengths on the other three maps have a fractal dimension of 1.7-1.8. Because the Beberg site is on the west half of the 1:400,000 map, we find the lower value to be the most significant for this study. Another important observation is that the slopes of the linear portions do not show marked differences among the different fracture orientation sets at each scale. This implies that the sets on the west half of the 1:400,000 map and the 1:20,000 map scale in approximately the same way at a given scale of observation. Because trace lengths scale over all of the sizes of interest for earthquake modeling, a single power-law size model can be used for each fracture set for the Beberg study. Figure 3-11 shows the combined data set.

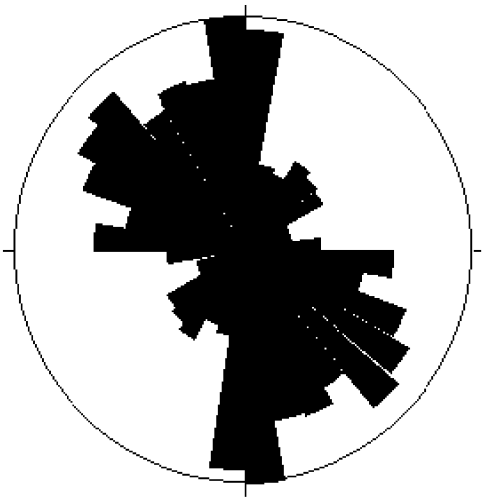

a. 1:400,000 Map, East Half

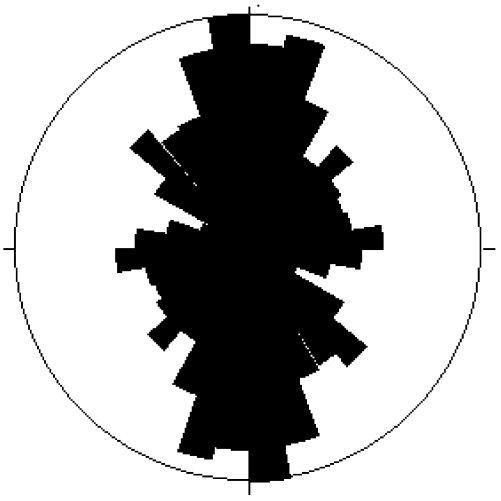

b. 1:400,000 Map, West Half

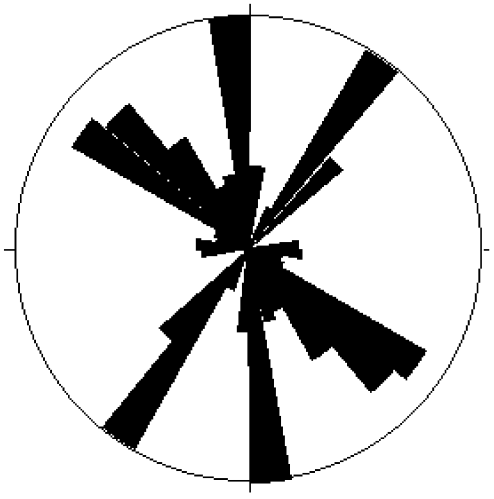

c. 1:87,000 Map

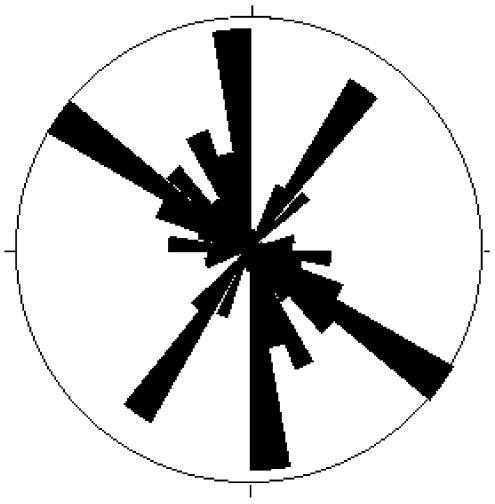

d. 1:20,000 Map

FIGURE **3-9**
ROSE DIAGRAMS OF FRACTURE STRIKES FOR BEBERG

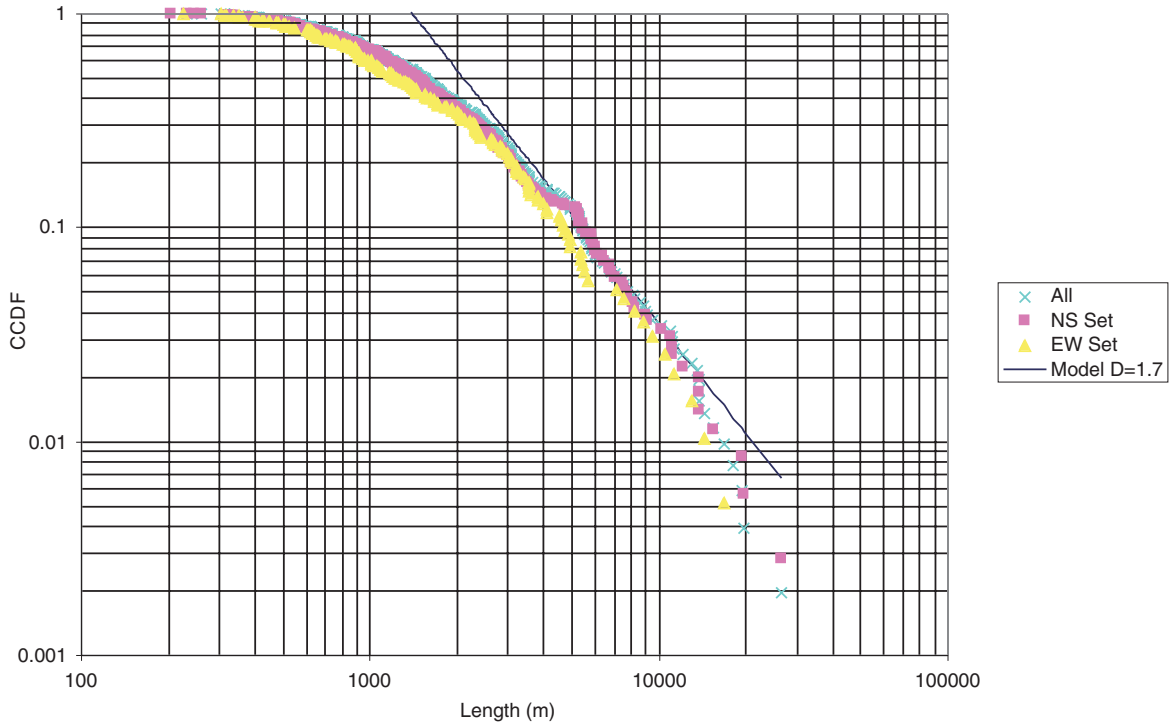

West Part of 1:4,000,000 Map

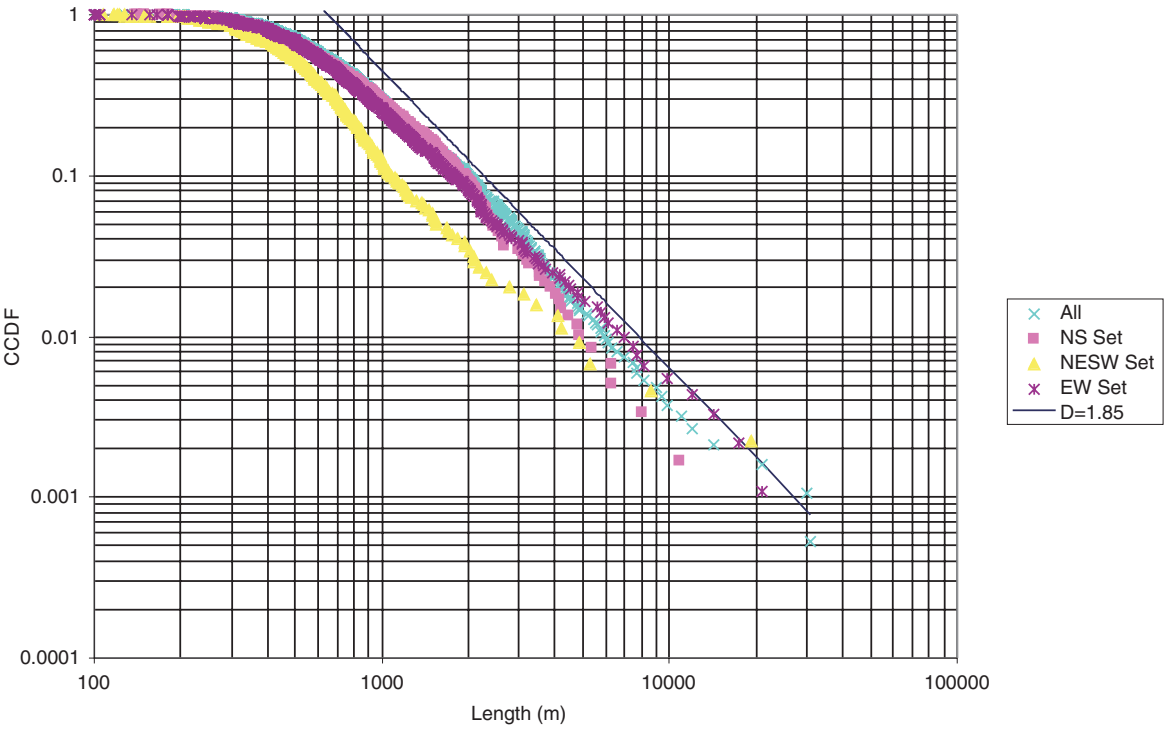

East Part of 1:400,000 Map

FIGURE **3-10a**
CUMULATIVE LENGTH DISTRIBUTIONS BY SETS, BEBERG (FINNSJÖN)

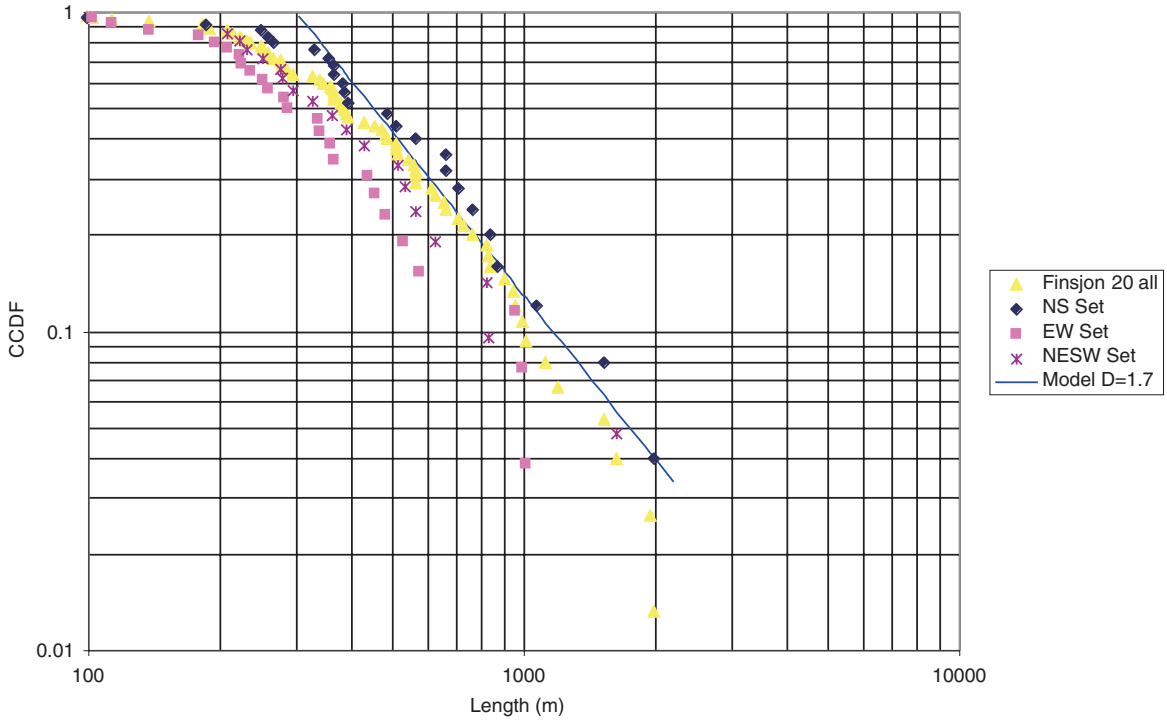

1:20,000 Lineament Map

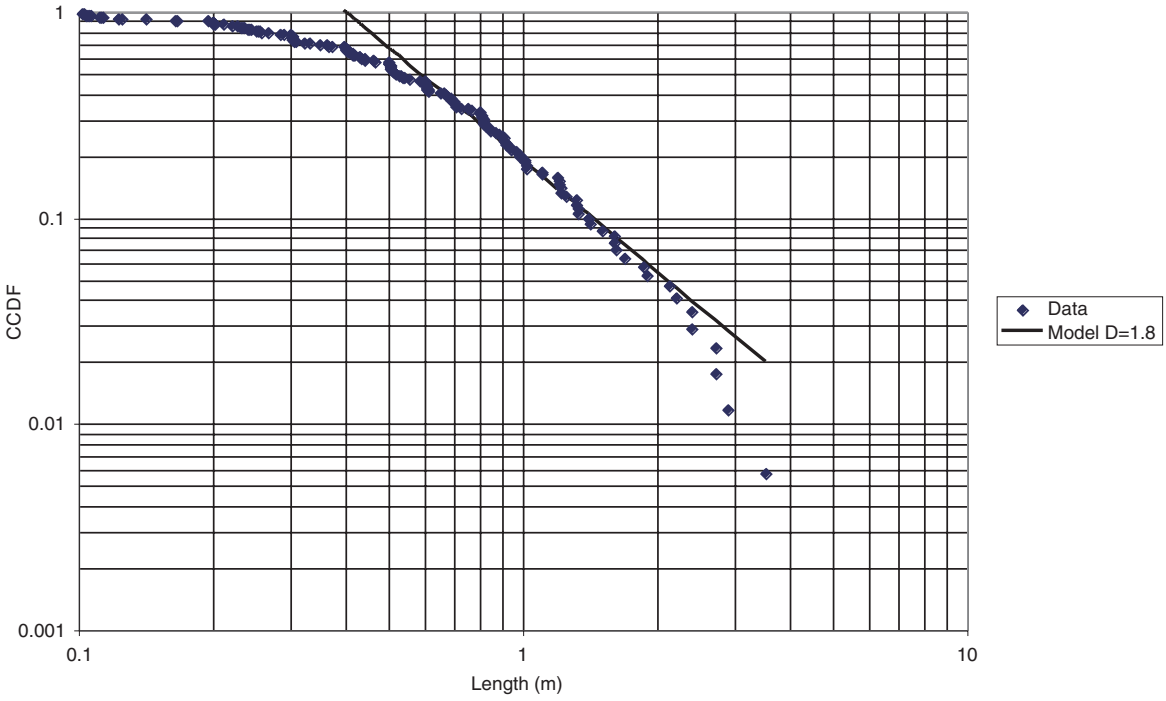

1:20 Lineament Map of Trench

FIGURE **3-10b**
CUMULATIVE LENGTH DISTRIBUTIONS BY SETS, BEBERG (FINNSJÖN)

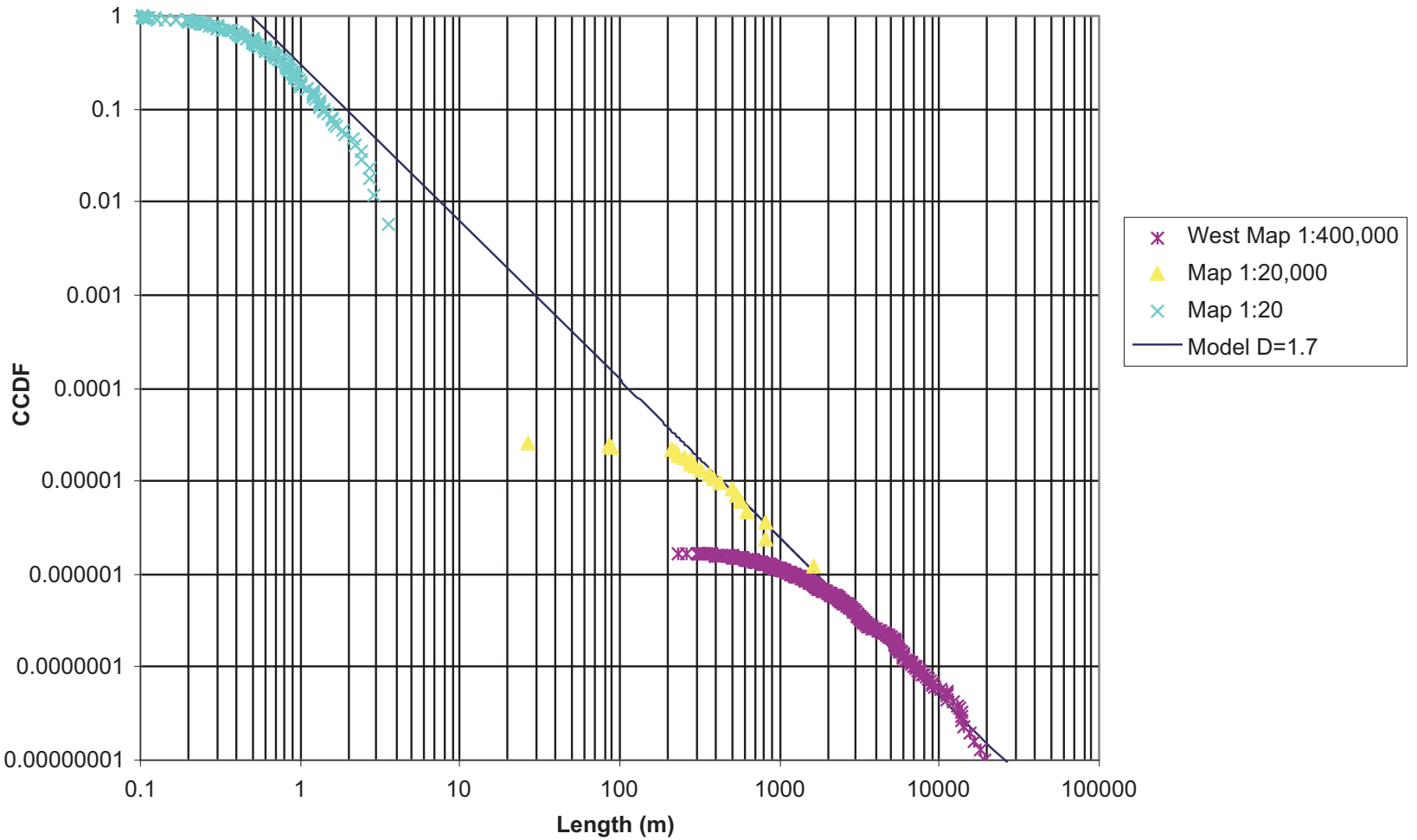

FIGURE **3-11**
CUMULATIVE LENGTH DISTRIBUTIONS OF COMBINED SCALES AND SET, BEBERG (FINNSJÖN)

Table 3-6. Trace Set Definitions for Beberg

Map Scale	Set Name	Azimuthal Range
1:400,000 West	N	120-220º
1:400,000 West	ENE	40-120º
1:400,000 East	N	160-220º
1:400,000 East	NE	20-80º
1:400,000 East	WNW	80-150º
1:20,000	NNE	10-70º
1:20,000	NW	110-150º
1:20,000	NNW	150-190º

Table 3-7. Beberg Results

Map	# sets	set orients	D, tracelength	D, box
1:400,000 west	2	N, ENE	D=1.7	D_b=1.8
1:400,000 east	3	N, NE, WNW	D=1.85	D_b=1.8
1:87,000	3	NNE, NW, NNW	too few data points	D_b=1.8
1:20,000	3	NNE, NW, NNW	D=1.7	D_b=1.8
1:20	1	- -	D=1.8	D_b=1.25

3.2.2 Box Dimension Calculations

The four sets of traces mapped on in the Finnsjön region show consistent box fractal dimensions (Figure 3-12 and Table 3-7). As with the box dimensions analysis of Aberg, each curve plotted in the figure can be broken into two linear segments. The more shallowly-dipping portion has a slope of approximately 1.0, and is an artifact of allowing box sizes to become too small (Barton, 1995). The steeper portion of each curve is not biased by box size and represents the true box dimension of the data. The more steeply-dipping portion of each curve yields box dimensions of ~1.8 for all the trace maps. The trench wall map has a much lower dimension of 1.25. The different box dimensions between the 1:20 scale cross-section and the larger scale map views could be due to either the orientation of the sample or the scale. We believe the 1.8 Box dimension to be more diagnostic of the fracturing at Beberg. A dimension near 2.0 suggests that the fracture spacing is nearly Poissonian. The various trace maps shown in Figure 3-8 show a densely fractured rock mass with many blocks of nearly the same size, a pattern consistent with a box dimension near 2.0.

The consequence of the Box dimension analysis is that it supports a DFN model that scales over a large scale range in a predictable manner. The analyses suggest that fracture locations determined by a Poissonian process is appropriate for generating the stochastic component of the DFN model for Beberg.

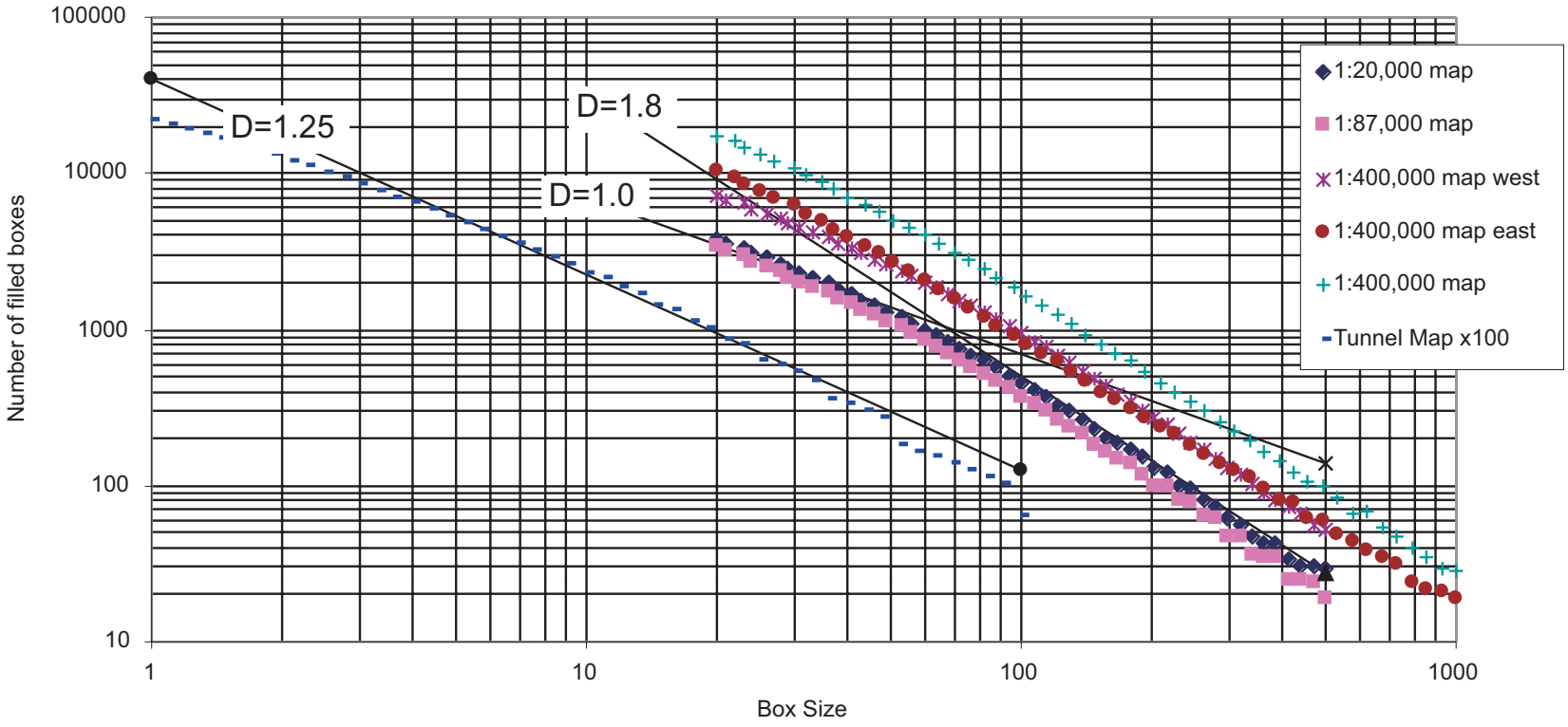

FIGURE **3-12**
BEBERG BOX DIMENSIONS

3.2.3 DFN Model Parameters

The strategy for estimating P_{32} for Beberg was similar to that used for Aberg. The CCDF for fractures on the 1:20,000 map (Figure 3-10b) begins to depart from linearity for trace lengths less than 300 m. If all traces shorter than 300 m are removed from the 1:20,000 trace map, a trace length intensity (P_{21}) of 0.007 m^{-1} is calculated. Forward trial-and-error modeling indicated that a fracture area per volume intensity (P_{32}) of 0.1 m^{-1} corresponds to P_{21} = 0.007 m^{-1} in the 2 km (the maximum trace length on the map) to 300 m size range. The fracture intensity is partitioned to the three sets identified in the rosette diagrams.

Because canisters in Block 9 are separated from the other blocks by a large distance (Figure 5-1b), two fracture generation regions were defined for Beberg. Region 1 generates the fractures in Block 9 and Region 2 generates the fractures in the remaining blocks.

A summary of the Beberg DFN model parameters all of which were derived in this study are presented in Table 3-8.

Table 3-8. Summary of DFN Model Parameters for Beberg

Parameter	Value*
Set 1	
Orientation (mean pole trend, plunge, dispersion	125.0, 0.0, κ=75
Intensity (P_{32})	0.02
Set 2	
Orientation (mean pole trend, plunge, dispersion	215.0, 0.0, κ=50
Intensity (P_{32})	0.04
Set 3	
Orientation (mean pole trend, plunge, dispersion	85.0, 0.0, κ=30
Intensity (P_{32})	0.04
All Sets	
Size	Power Law, D=2.7, x_0=10m
Flow Properties	Ignored
Spatial Model	Baecher

*Note: All parameters derived in this study

3.3 Ceberg

3.3.1 Trace Length Analyses

For Ceberg, trace length maps at two scales were analyzed (Hermanson and others, 1997). These maps are shown Figure 3-13 and the data sources are summarized in Table 3-9. The 1:200,000 map is based upon fracture mapping and the 1:20,000 maps based upon interpretation of seismic velocity and resistivity surveys.

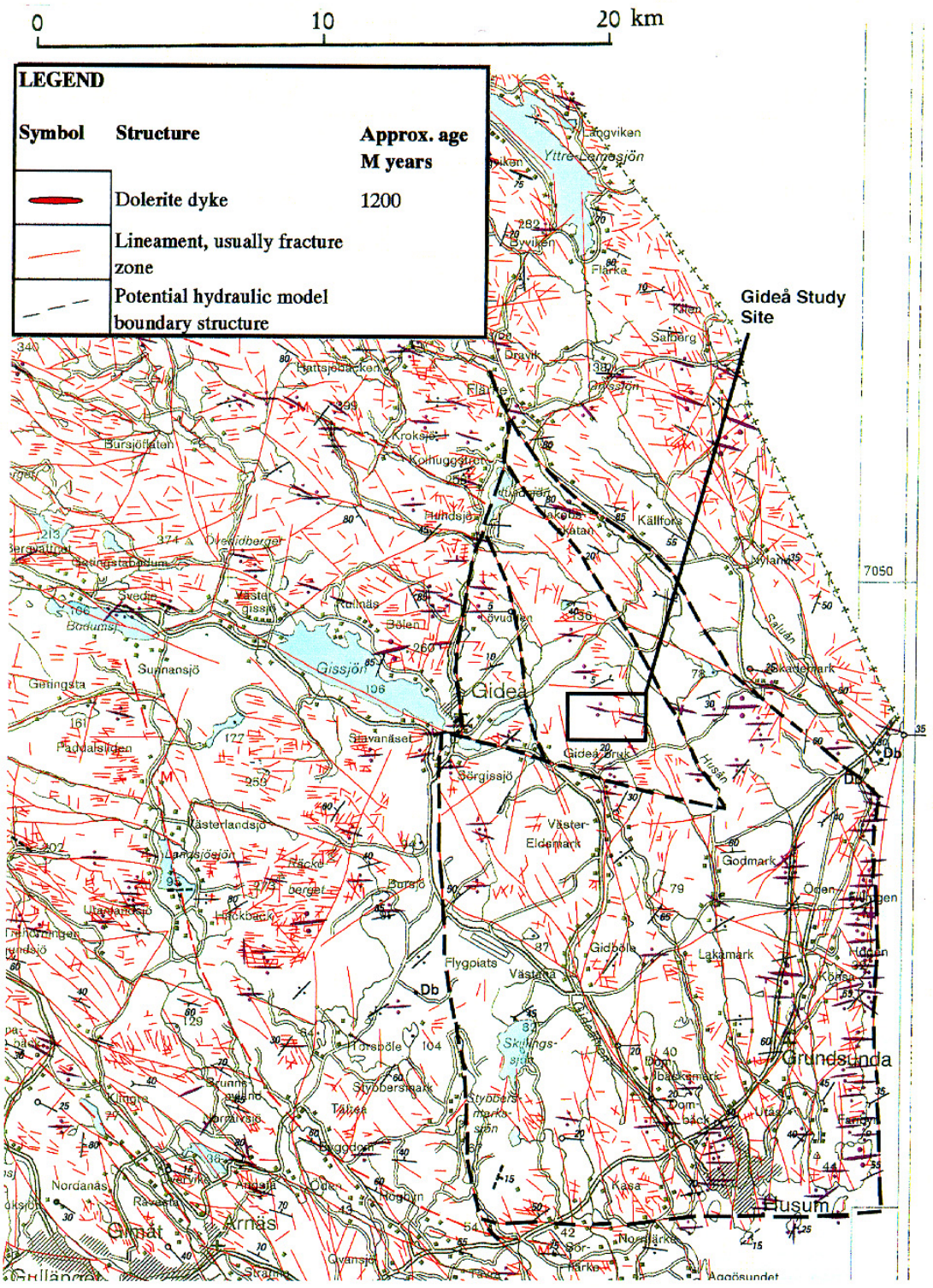

FIGURE **3-13a**
LINEAMENT MAP AT CEBERG (GIDEA) AT A SCALE OF 1:200,000

After SKB R-97-05 (Hermanson et al. 1996)

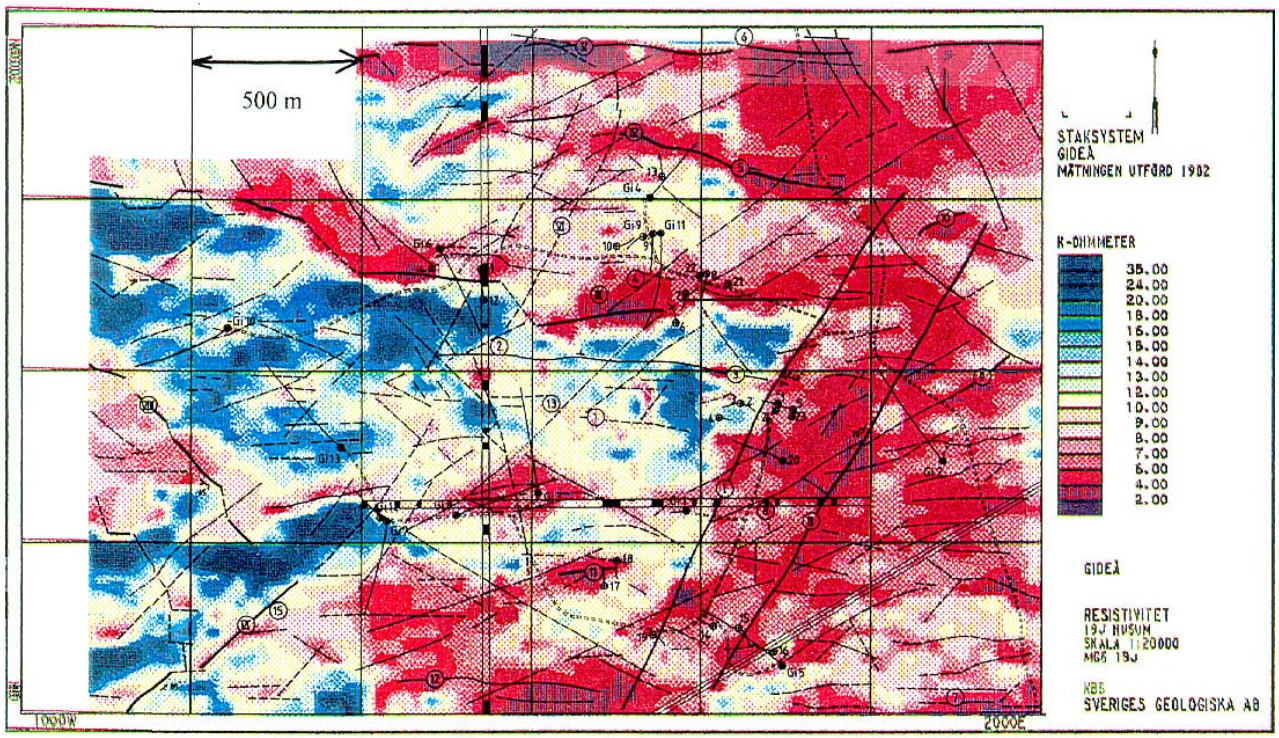

LEGEND

Electric lineaments		– – –	Weak
———	Strong		Weak resistivity lineament
———	Distinct		Interpreted extent
	Seismic refraction survey line with low velocity zones		
Gi 11 ●	Core drilling	11 ○	Percussion drilling

FIGURE **3-13b**
LINEAMENTS INTERPRETED FROM GEOPHYSICS AT CEBERG (GIDEÅ) AT A SCALE OF 1:200,000

After SKB R-97-05 (Hermanson et al. 1996)

Table 3-9. Ceberg (Gidea) Data Sources

Source	Fig. #	Scale
R97-05 (Hermanson et al., 1997)	Fig. 2-3	1:200,000
R97-05	Fig. 3-4	1:20,000

Traces were divided into sets for each map. Division was based upon the rosettes shown in Figure 3-14. The azimuthal ranges used to define each set are given in Table 3-10. The trace length CCDF was calculated for each set separately. The results (Figure 3-15 and Table 3-11) show that the CCDF's for all four data sets have approximately linear portions that extend over a wide range of scales. The slopes of these linear portions do show some differences among the different fracture orientations sets and at each scale. The NS orientation set on the 1:20,000 map contains too few trace lengths to find a valid fractal dimension. The other three sets have dimensions from 1.85 to 1.95. Because trace lengths scale over all of the sizes of interest for earthquake modeling, a single power-law size model can be used for each fracture set for the Ceberg study. Figure 3-16 shows the combined dataset.

Table 3-10. Trace set Definitions for Ceberg

Map Scale	Set Name	Azimuthal Range
1:200,000	NS	130-230º
1:200,000	EW	50-130º
1:20,000	NE-SW	0-70º
1:20,000	EW	70-140º

Table 3-11. Ceberg Results

Map	# sets	set orients	D, tracelength	D, box
1:200,000	2	NS, EW	D=1.85	D=1.7
1:20,000	2	EW, NESW	D=1.95	D=1.7

3.3.2 Box Dimension Calculations

The four sets of traces mapped in the Gidea region show consistent box fractal dimensions (Figure 3-17 and Table 3-11). As with the Box dimension analysis of Aberg, each curve plotted in the figure can be broken into two linear segments. The more steeply-dipping portion of each curve yields box dimensions of ~1.7 for all the trace maps. A dimension near 2.0 suggests that the fracture spacing is nearly Poissonian. The analyses suggest that fracture locations can be determined by a Poissonian process is appropriate for generating the stochastic component of the DFN model for Ceberg.

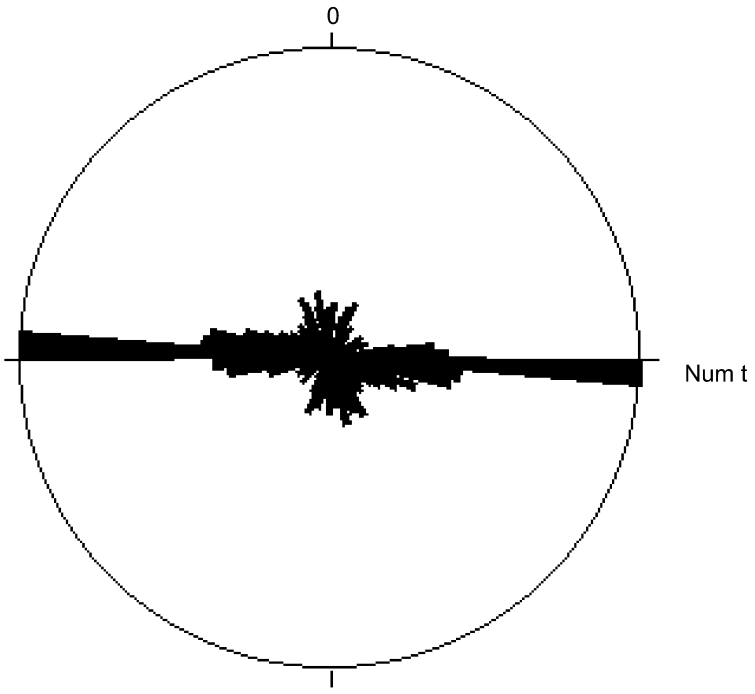

a. 1:200,000 Map

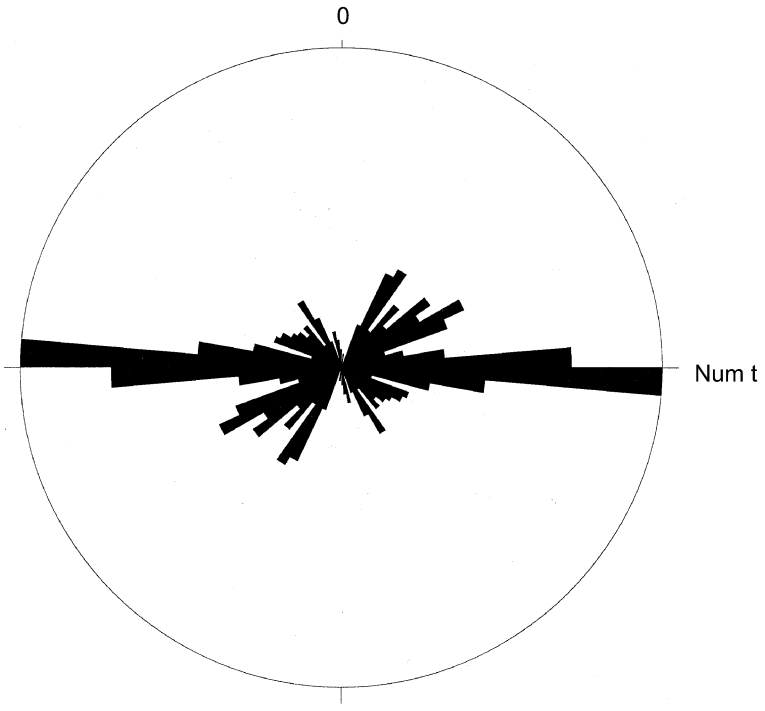

b. 1:20,000 Map

FIGURE **3-14**
ROSE DIAGRAMS OF FRACTURE STRIKES FOR CEBERG

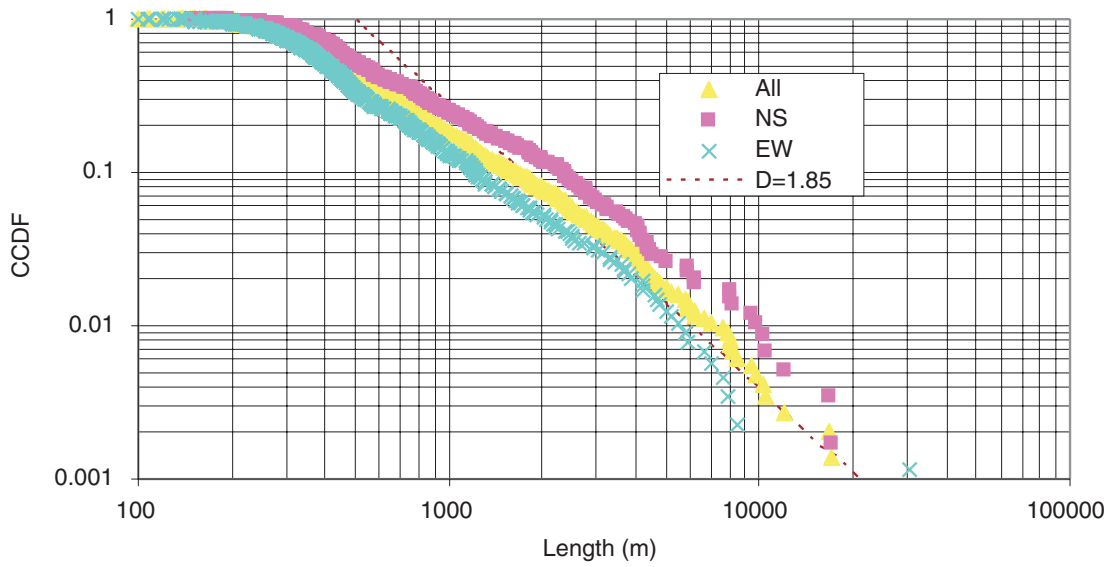

a. Tracelengths by Set, 1:200,00 Ceberg Map

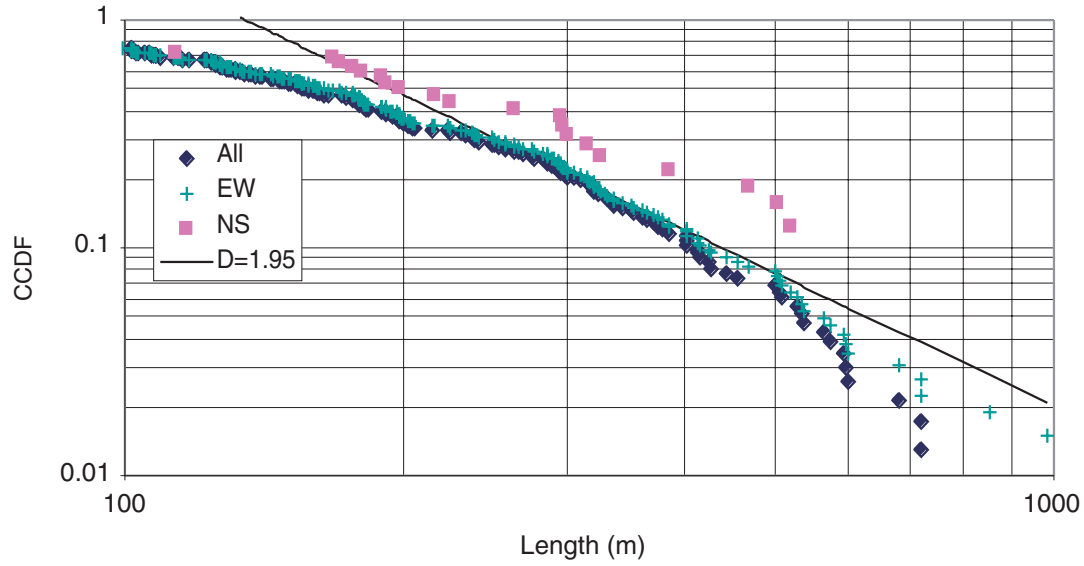

b. Tracelengths by Set, 1:20,00 Ceberg Map

FIGURE **3-15**
TRACELENGTHS BY SET

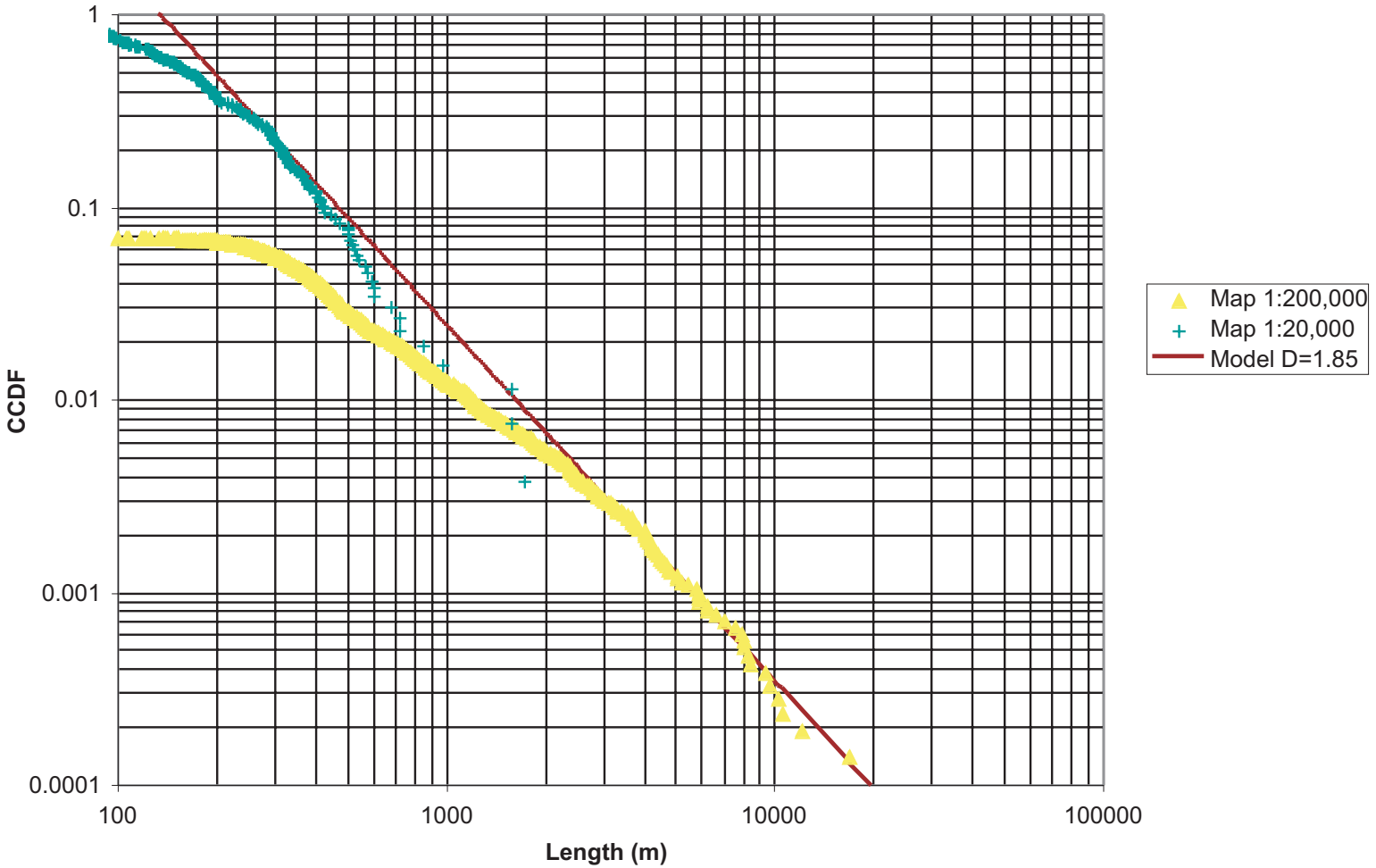

FIGURE **3-16**
COMBINED CUMULATIVE LENGTH DISTRIBUTION, CEBERG (GIDEÅ)

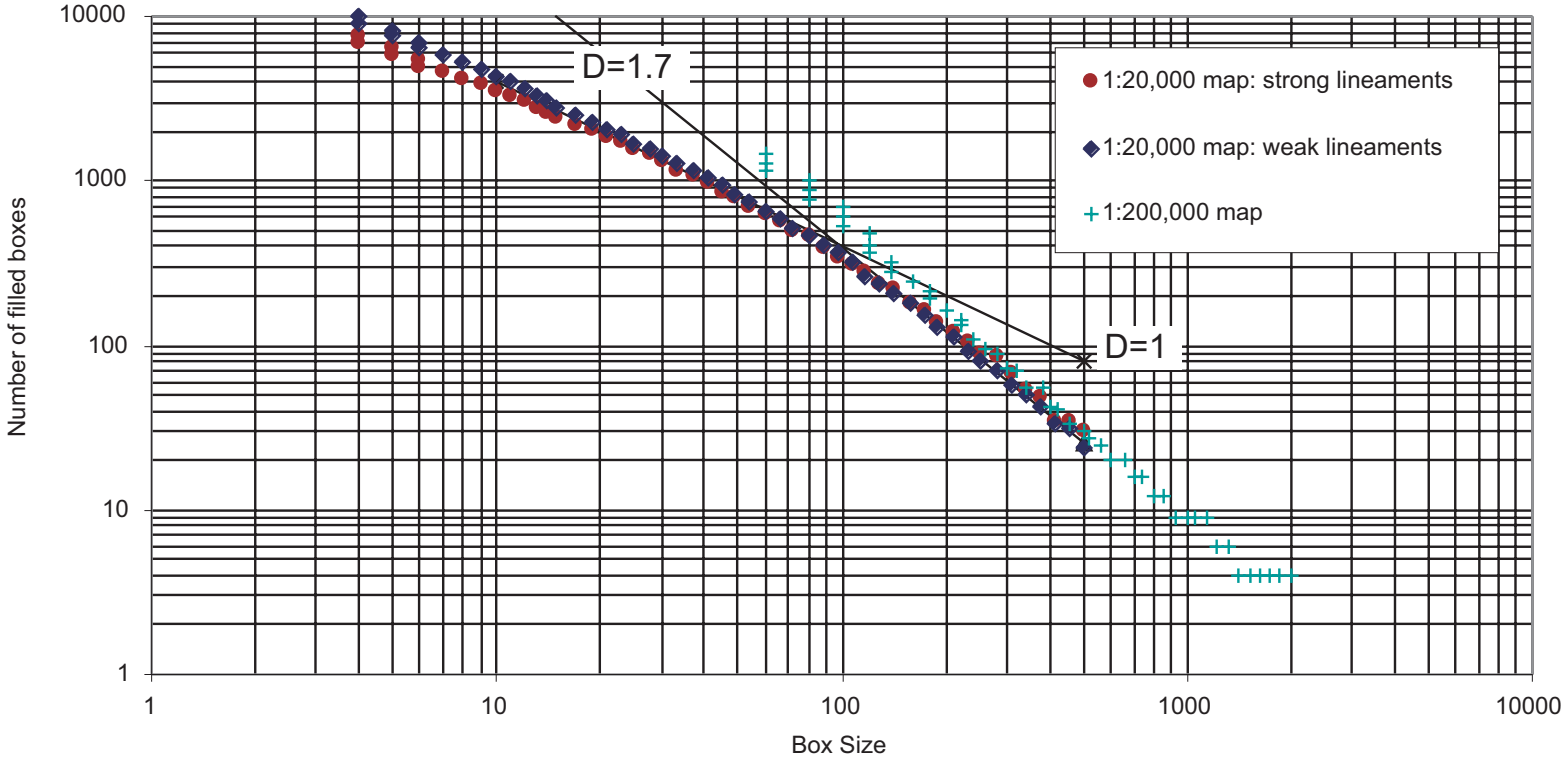

FIGURE **3-17**
CEBERG BOX DIMENSIONS

3.3.3 DFN Model Parameters

The strategy for estimating P_{32} for Ceberg was the same as that used for Aberg and Beberg. The CCDF for fractures on the 1:20,000 map (Figure 3-13b) begins to depart from linearity for trace lengths less than 300 m. If all traces shorter than 300 m are removed from the 1:20,000 trace map, a trace length intensity (P_{21}) of 0.0033 m^{-1} is calculated. Forward trial-and-error modeling indicated that a fracture area per volume intensity (P_{32}) of 0.12 m^{-1} corresponds to P_{21} = 0.0033 m^{-1} in the 2 km (the maximum trace length on the map) to 300 m size range. The fracture intensity is partitioned to the three sets identified in the rosette diagrams.

A summary of the Ceberg DFN model parameters all derived in this study are presented in Table 3-12.

Table 3-12. Summary of DFN Model Parameters for Ceberg

Parameter	Value*
Set 1	
Orientation (mean pole trend, plunge, dispersion	175.0, 0.0, κ=50
Intensity (P_{32})	0.08
Set 2	
Orientation (mean pole trend, plunge, dispersion	135.0, 0.0, κ=50
Intensity (P_{32})	0.04
All Sets	
Size	Power Law, D=2.85, x_0=10m
Flow Properties	Ignored
Spatial Model	Baecher

*Note: All parameters derived in this study

4. CALCULATION OF EARTHQUAKE PARAMETERS

The modeling process requires data for two aspects of future earthquakes:

1) What is the likely frequency of earthquakes that might affect each site over the next 100,000 years as a function of their magnitude?

2) For each earthquake, how large a fault would be required to produce it, and what would be the displacement on the fault?

The first question is important since individual earthquakes might not cause unacceptable slippage on fractures intersecting canisters, but hundreds or thousand of earthquakes over 100,000 years might cause *cumulative* displacements that could affect the canister. Section 4.1 describes the magnitude/frequency relations used to forecast future tectonic earthquakes.

The second question has to do with obtaining parameters for the numerical modeling. In order to simulate an earthquake, it is necessary to know the rupture area and the displacement that is typical of an earthquake of that magnitude. Moreover, it is necessary to select a candidate lineament that has a surface rupture length of sufficient length to accommodate the earthquake. Section 4.2 describes how surface rupture length, subsurface displacement and rupture width (depth) are estimated from earthquake magnitude.

4.1 Forecasting the Frequency and Magnitude of Future Earthquakes in Sweden

4.1.1 Issues

It is necessary to know how many earthquakes might occur and what their magnitudes might be for the next 100,000 years in order to assess canister performance at each generic site. The standard way to estimate earthquake risk to structures such as power plants is to extrapolate from instrumental and historical earthquakes. This presents two problems for the current study, one geological and the other statistical, due to the much greater time in the future over which earthquakes need to be forecast:

1) There exists a geological controversy as to whether present-day earthquakes are tectonic or glacial-rebound in origin. Slunga (1991), for example, presents evidence for purely tectonic causes due to ridge-push, while Muir-Wood (1993) presents evidence for glacial rebound. Another issue is post-glacial faulting. These earthquakes may have occurred as tectonic strain accumulated beneath the ice. Deglaciation

served as a trigger for the earthquakes. The post-glacial earthquakes may have been much larger in magnitude (Johnston, 1993, 1996) because of this trapped energy or due to the rebound, although there is also controversy as to whether some of the large scarps actually constitute single rupture events (Adams, 1993, Muir-Wood, 1993). These large scarps are important, for if they represent single rupture events, they are the only evidence for large earthquakes in Sweden. If current earthquakes are tectonic, then their size-frequency relations may not be relevant for estimating the size-frequency relations of earthquakes due to rebound or a combination of de-glaciation and tectonics.

2) There are also statistical problems. Sweden has low levels of seismicity, so that the historical and instrumental record of earthquakes is relatively small and confined to earthquakes of magnitude 5 or less. Extrapolation to much larger earthquakes is consequently more uncertain.

The current study cannot resolve the first problem having to do with the causes of present-day and past earthquakes. However, the implications for each scenario can be addressed.

If current seismicity is dominated by rebound, and not tectonics, then extrapolation of recurrence rates into the future should overestimate the number of earthquakes, since rebound is decreasing and would continue to decrease until after the next glacial cycle. However, rates might increase immediately following the next future deglaciation as well, leading to underestimation during this period. However, the very large earthquakes inferred due to deglaciation would not have stored tectonic stress, which is the assumption of this scenario since tectonic forces are assumed to play no role even today. Thus, the larger earthquakes occurring during deglaciation would constitute the large size fraction of the overall earthquake catalog, occurring at the very early stages of de-glaciation when rebound was at a higher rate. According to this scenario, the current earthquake activity has diminished in frequency and magnitude as the rebound has slowed.

Another scenario is that current earthquakes are tectonic in origin, and that the large scarps found in northern Sweden may or may not represent single rupture events related to de-glaciation. If the scarps are not single rupture events, either because they are geomorphic features rather than seismic features, or are tectonic features not triggered by de-glaciation, then extrapolation of the current size/frequency data would not be missing a significant component of future earthquakes.

The final alternative is that the scarps do represent large rupture events in which tectonic strain accumulated under the ice and was released as fewer, larger earthquakes upon de-glaciation. In this case, there would be a discontinuity in the size/frequency relation between present-day earthquakes and those associated with post-glacial processes.

Fortunately, this is not as significant as it might seem for the modeling approach as long as most of the energy released due to ice unloading is derived from tectonic mechanisms like ridge-push. The reason that it is less important is that the total amount of slip induced on a fracture in a linearly elastic material is related to the total amount of energy applied to the system. In other words, one large earthquake on a particular fault would produce the same cumulative slip on a remote fracture as two earthquakes which each released half the energy of the single large earthquake. As long as the tectonic processes dominate the accumulation of energy on faults relative to glaciation, which is the assumption of this scenario, then it does not matter for the numerical calculation of cumulative induced displacement whether the energy is released in fewer, larger events, or in a greater number of smaller events. Within the linear elastic fracture mechanics formulation, events are linearly additive and will produce the same answer however they are added, so long as the total energy is the same and the location of energy release is the same. The main difference between the case where stress accumulates beneath the ice and the case where it does not is in the timing of the displacements induced on fractures intersecting canisters, and the magnitude of slip produced by individual earthquakes, but not in the net cumulative slip over a period of time that includes a complete glaciation/de-glaciation cycle. There are some differences that make a single large earthquake worse than several equivalent smaller earthquakes, as discussed at the end of the next section.

4.1.2 Magnitude/Frequency Relations for Future Earthquakes in Sweden

The record of earthquakes in Sweden comes from a variety of sources. Some of the events are sufficiently recent that they have been quantified using instruments. Other events were not measured using instruments, but accounts of the amount, type and location of damage produced was recorded. Not only are there different types of records (instrumental vs. historical), but there are also spatial and temporal gaps in these records as well. Kijko and others (1993) have discussed these and other problems in estimating the magnitude/frequency relations for earthquakes in Sweden.

The number of earthquakes as a function of magnitude for a specific region often conforms to the equation:

$$Log(\dot{N}) = -bm + Log(\dot{a}) \qquad 4\text{-}1$$

where $\dot{N}$ is the number of earthquakes per unit time have a magnitude greater than m, and b and $\dot{a}$ are constants. In many publications, the expression $Log(\dot{a})$ is written as $\dot{a}$.

This equation is often re-written as:

$$Log(N) = -bm + Log(a) \qquad 4\text{-}2$$

where N is the number of earthquakes greater than m occurring in a specified time interval, and a and b are constants. In many publications, the expression $Log(a)$ is written as a.

The constant b describes the relative proportion of large earthquakes to smaller earthquakes. As b increases, the proportion of large earthquakes decreases. As a increases, the number of earthquakes increases for earthquakes of all magnitudes.

Several distinct zones with characteristic a and b values have been recognized in Sweden (for example, Skordas and Kulhánek, 1992; Kijko and others, 1993). For the current study, the distinct zones and their parameter values identified by Kijko and others (1993) have been used.

They have divided Sweden into a northern portion north of 60° north latitude and a southern portion to the south (Figure 4-1). In addition, they have delineated two zones of enhanced seismic activity: the Lake Vänern region in western southern Sweden, and the Gulf of Bothnia along the east coast of northern Sweden. Their table of seismic hazard parameters is reproduced below as Table 4-1.

Table 4-1. Seismic Hazard Parameters

Area	b	$\lambda_{2.4}$	m_{max}	N
Southern Sweden	1.04 ± 0.05	1.8 ± 0.2	4.9 ± 0.5	135
Lake Vänern	0.98 ± 0.06	1.3 ± 0.2	4.9 ± 0.5	104
Northern Sweden	1.35 ± 0.06	3.7 ± 0.3	4.3 ± 0.5	241
Coast of Gulf of Bothnia	1.26 ± 0.06	2.4 ± 0.2	4.3 ± 0.5	164

In Table 4-1, $\lambda_{2.4}$ is the annual number of earthquakes with magnitude 2.4 or greater, m_{max} is the maximum expected magnitude during the time span equal to that of the catalog, and N is the total number of earthquakes above the threshold magnitude for the time period for the catalog time period.

The b values for the four regions suggest that the proportion of large earthquakes will be much smaller in northern Sweden in general, including the Gulf of Bothnia. As Skordas and Kulhánek (1992; pg 583) observe, "This area has a pronounced earthquake activity but practically all seismic energy there is released through a number of relatively weak shocks." The total number of earthquakes as a function of the magnitude expected over a 100,000 year time interval are shown in Table 4-2.

The number of earthquakes for each of these four regions cannot be directly compared from the values in Table 4-1 because the a or λ parameter is a function of the area of the region. When adjusted for a common area of 31,415 km^2 , which corresponds to a circle with radius equal to 100 km, the expected number of earthquakes over a period of 100,000 years greater than or equal to a magnitude m is shown in Figure 4-2 and Table 4-3.

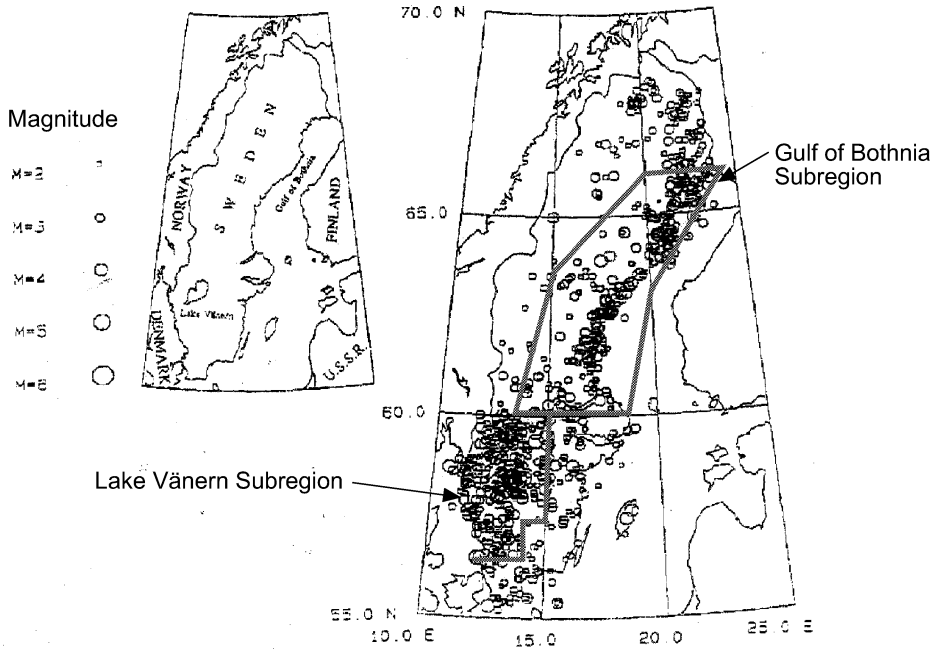

FIGURE **4-1**
EARTHQUAKE EPICENTER DISTRIBUTION IN SWEDEN FOR THE PERIOD 1375 TO 1989

From Kijko and others (1993)

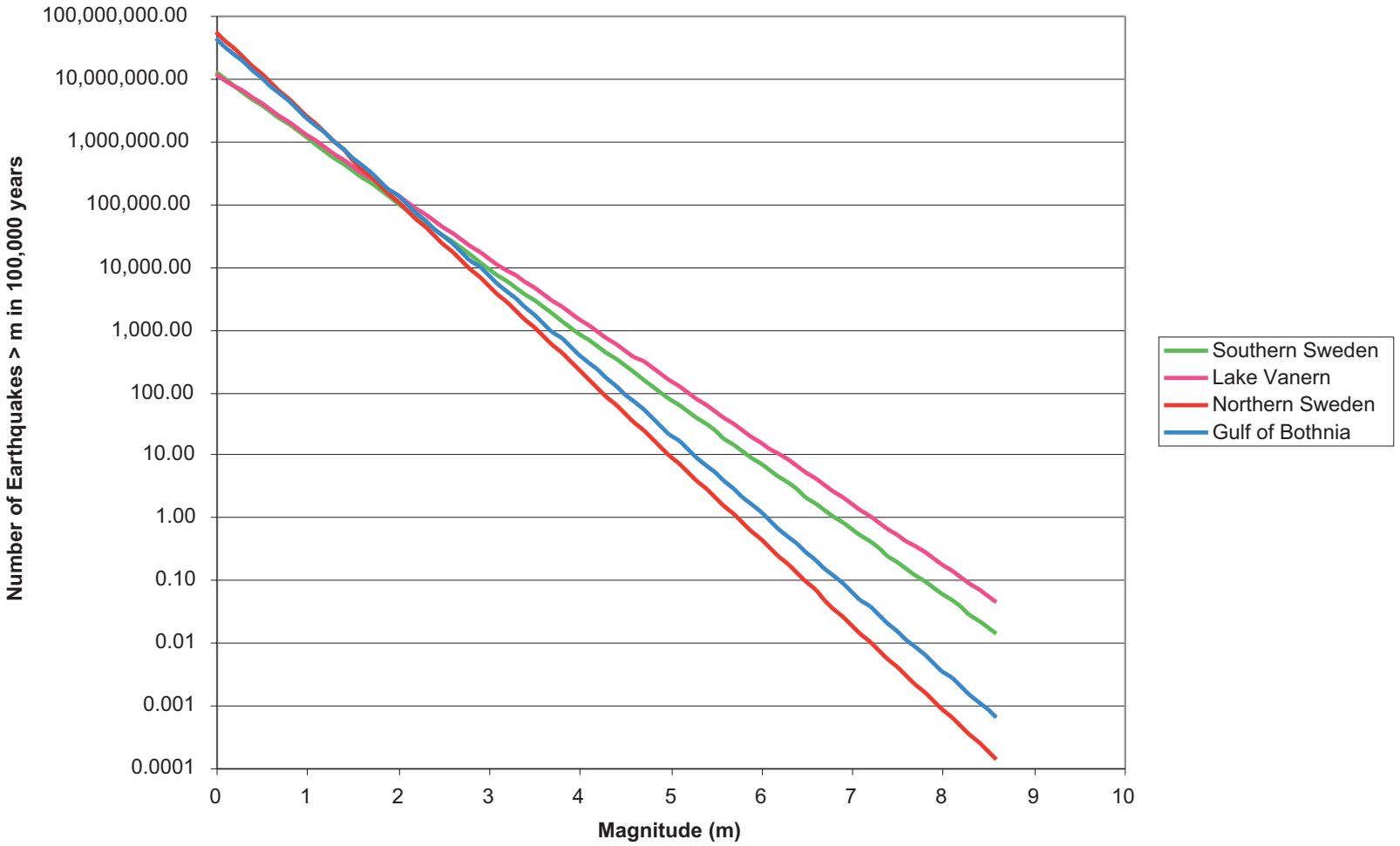

FIGURE **4-2**
COMPARISON OF EARTHQUAKE INTENSITY AMONG FOUR SEISMIC REGIONS IN SWEDEN

Table 4-2. Number of Earthquakes Expected in Different Seismic Zones in Sweden Over a 100,000-Year Interval

Magnitude Range	Southern Sweden	Lake Vanern	Gulf of Bothnia	Northern Sweden
< 0.5	39,366,874	19,776,572	194,178,073	507,091,855
0.5-1.0	11,888,606	6,399,573	45,519,783	107,173,308
1.0-1.5	3,590,302	2,070,861	10,670,879	22,650,961
1.5-2.0	1,084,254	670,118	2,501,498	4,787,256
2.0-2.5	327,439	216,846	586,408	1,011,781
2.5-3.0	98,885	70,170	137,468	213,839
3.0-3.5	29,863	22,707	32,226	45,195
3.5-4.0	9,018	7,348	7,554	9,552
4.0-4.5	2,724	2,378	1,771	2,019
4.5-5.0	822	769	415	427
5.0-5.5	248	249	97	90
5.5-6.0	75	81	23	19
6.0-6.5	23	26	5	4
6.5-7.0	7	8	1.25	0.85
7.0-7.5	2.07	2.73	0.29	0.18
7.5-8.0	0.62	0.88	0.07	0.04
> 8.0	0.19	0.29	0.02	0.01

Table 4-3. Number of Earthquakes Expected in Different Seismic Zones in Sweden Over a 100,000-Year Interval Normalized for an Area of 31,415 km^2

Magnitude Range	Southern Sweden	Lake Vanern	Gulf of Bothnia	Northern Sweden
< 0.5	8,535,705	8,033,455	32,695,974	42,833,261
0.5-1.0	2,577,742	2,599,575	7,664,684	9,052,763
1.0-1.5	778,466	841,206	1,796,777	1,913,291
1.5-2.0	235,093	272,209	421,206	404,372
2.0-2.5	70,997	88,085	98,740	85,464
2.5-3.0	21,441	28,504	23,147	18,063
3.0-3.5	6,475	9,224	5,426	3,818
3.5-4.0	1,955	2,985	1,272	807
4.0-4.5	591	966	298	171
4.5-5.0	178	313	70	36
5.0-5.5	54	101	16	7.62
5.5-6.0	16	33	3.84	1.61
6.0-6.5	5	11	0.90	0.34
6.5-7.0	1.48	3.43	0.21	0.07
7.0-7.5	0.45	1.11	0.05	0.015
7.5-8.0	0.14	0.36	0.012	0.003
> 8.0	0.04	0.12	0.003	0.001

Figure 4-2 shows that there will be more earthquakes per unit area in northern Sweden and the Gulf of Bothnia than in southern Sweden, but that this is due to a large number of earthquakes with magnitudes less than about

2. Both southern Sweden as a whole, and also the Lake Vänern subregion will have a larger number of medium and large magnitude earthquakes.

The total energy in the seismic waves generated by an earthquake, or the strain released by an earthquake is a semi-logarithmic function of magnitude, such that the log of the strain or energy is linearly proportional to magnitude. This implies that the relative area under each curve in Figure 4-2 is proportional to the relative total energy released by all of the earthquakes for the entire 100,000 year period for each region. For all magnitudes, more total energy would be released in northern Sweden. If earthquakes smaller than about magnitude 2 are neglected, then the total energy released will be much greater for southern Sweden.

The underlying temporal pattern of earthquakes is assumed to be Poissonian for the purposes of hazard assessment, a common assumption when estimating non-exceedance probabilities for power plants or other structures.

Figure 4-1 shows that the spatial distribution of seismicity in southern Sweden is not uniform. There has been much greater earthquake activity in the Lake Vänern subregion than elsewhere in southern Sweden, which is why Kijko and others (1993) estimated separate magnitude/frequency parameters for this region. However, Aberg and Beberg are situated outside of this subregion, and while seismic activity within the Lake Vänern subregion might effect these sites, it is far more likely that earthquake activity outside of the Lake Vänern subregion in southern Sweden will have the greatest impact. Using Kijko and others' (1993) *a* and *b* parameter values for southern Sweden probably overestimates the frequency of earthquakes that would effect Aberg and Beberg since these published parameter values also include the seismic activity in the more active Lake Vänern subregion. A more realistic estimate of future earthquake frequencies should in some way compensate for the fact the Aberg and Beberg will be less effected by activity in the Lake Vänern subregion than by seismicity outside of it and much closer to the sites.

Unfortunately, Kijko and others (1993) do not provide any parameters for southern Sweden that excludes the Lake Vänern subregion. The small number of earthquakes in southern Sweden outside of the Lake Vänern subregion in the earthquake catalog make it difficult to estimate reliable magnitude/frequency relations. Nor is it possible to compute the magnitude/frequency relation merely by subtracting the Lake Vänern earthquakes from the total southern Sweden earthquakes shown in the second and third columns of Table 4-2. For example, starting with earthquakes in the magnitude class 5.0 to 5.5, there are more earthquakes predicted for the local Lake Vänern subregion than for all of southern Sweden, which includes the Lake Vänern subregion. In other words, there would be a *negative number* of earthquakes in the region of southern Sweden outside of the Lake Vänern region! This apparent contradiction comes about as a result of the log-linear extrapolation of the magnitude/frequency relations and the uncertainty in the estimates of the *a* and *b* parameters for these two regions. The black line in Figure 4-3 illustrates the number of earthquakes predicted to occur for the next 100,000

years obtained by substracting the earthquakes predicted using the local Lake Vänern parameters from the earthquakes predicted using the parameters for all of southern Sweden. The magnitude at which the curve becomes negative is between magnitudes 4.7 and 4.8.

It may be possible to obtain a better estimate of the magnitude and frequency of earthquakes outside of Lake Vänern by extrapolating the results from the portion of the black line in Figure 4-3 that corresponds to the small magnitude earthquakes only. Since this is the portion where there is measured data, the resulting *a* and *b* parameters might more accurately predict the future magnitude/frequency. Moreover, as Figure 4-3 shows, the extrapolation (red line) predicts far more moderate and large magnitude earthquakes than the simple subtraction (black line), and is thus more conservative than the simple subtraction.

Table 4-4 summarizes the *a* and *b* parameters obtained through nonlinear regression of Equation 4-2 to the subtracted data (black line in Figure 4-3) and the $\lambda_{2.4}$ value calculated from them and the area of southern Sweden outside of the Lake Vänern subregion. Table 4-5 describes the number of earthquakes as a function of earthquake magnitude predicted over a 100,000 year interval normalized for an area of 31,415 km^2. These predicted number of earthquakes are comparable to the results shown in Table 4-3. A comparison of Table 4-3 with Table 4-4 shows that there should still be a higher proportion of large earthquakes to small earthquakes in southern Sweden than in northern Sweden or the Gulf of Bothnia, and a higher absolute number of larger and medium earthquakes and lower number of smaller earthquakes in southern Sweden, even after compensation for the Lake Vänern subregion.

The frequency/magnitude relations summarized in these Tables 4-3 and 4-4 are termed the *Adjusted Southern Sweden* earthquake scenario in the remainder of this report.

Table 4-4. Possible Seismic Hazard Parameters for Southern Sweden Excluding the Lake Vänern Region

Area	*a*	*b*	$\lambda_{2.4}$
Adjusted Southern Sweden (Southern Sweden excluding the Lake Vänern subregion)	271.83	1.113	0.58

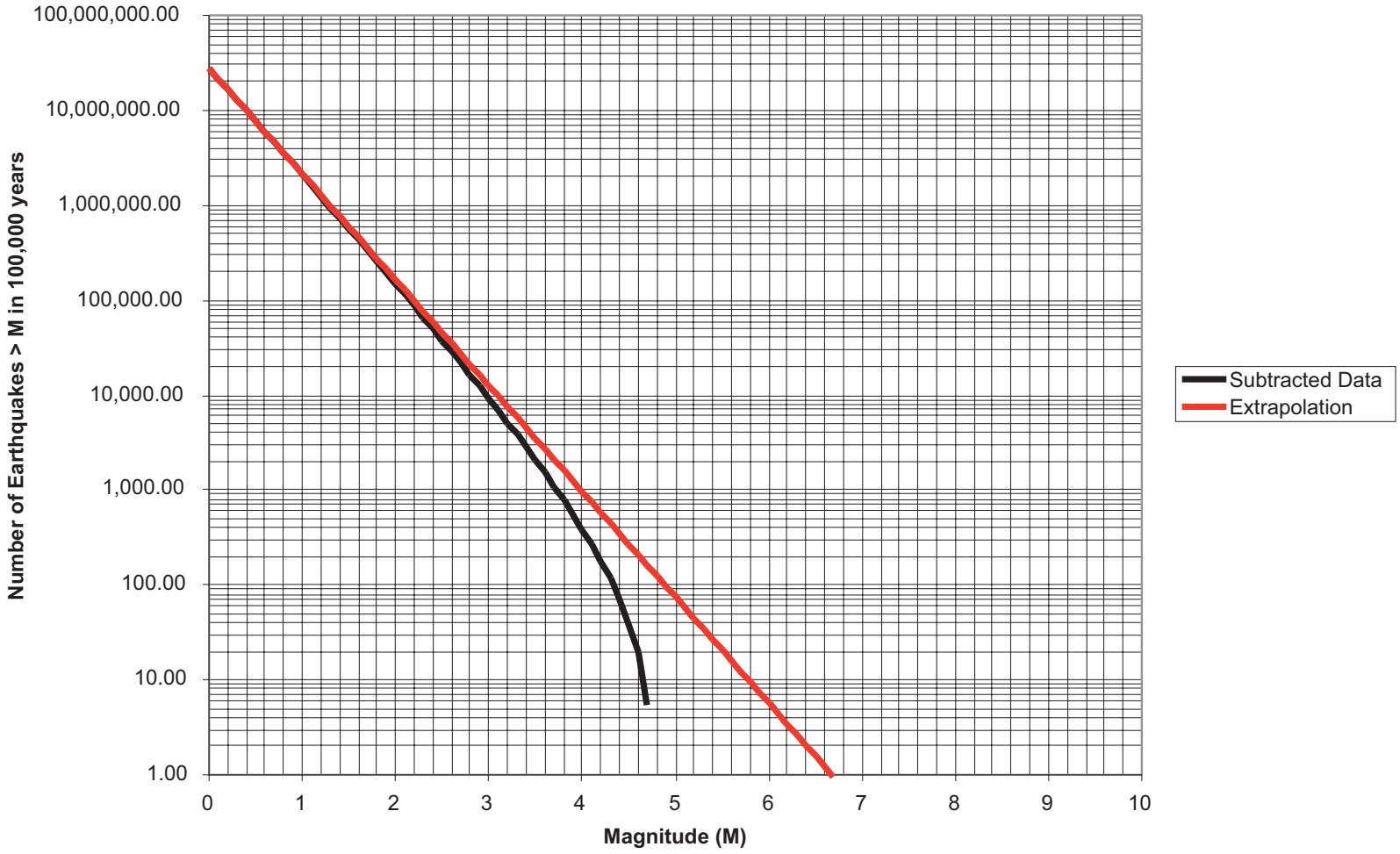

FIGURE **4-3**
NUMBER OF EARTHQUAKES IN SOUTHERN SWEDEN EXCLUDING THE LAKE VANERN REGION

Table 4-5. Possible Number of Earthquakes Expected for Southern Sweden Excluding the Lake Vänern Region Normalized for an Area of 31,415 km^2

Magnitude Range	Expected Number
< 0.5	9,139,436
0.5-1.0	2,537,971
1.0-1.5	704,781
1.5-2.0	195,714
2.0-2.5	54,349
2.5-3.0	15,092
3.0-3.5	4,191
3.5-4.0	1,164
4.0-4.5	323
4.5-5.0	90
5.0-5.5	25
5.5-6.0	7
6.0-6.5	2
6.5-7.0	0.53
7.0-7.5	0.15
7.5-8.0	0.04
> 8.0	0.01

4.1.3 Implications for Seismic Risk to Canisters

Previous work (La Pointe and others, 1997) showed that individual small earthquakes had an exceedingly low probability of producing slip greater than 0.1 m on fractures intersecting canisters unless they were on the order of meters away or less. Only the very large earthquakes, on the order of magnitude 6.5 or greater, could produce slips greater than 0.1 m from an individual event.

Although the cumulative energy release of many small earthquakes might exceed that of a few large events, all at the same distance from the repository, the impact on the repository could be less for the myriad of small earthquakes. Since the small events would not individually cause slip to exceed 0.1 m threshold, and because there would be many of them widely located throughout the region, they might tend to cancel out each other's slip. This is directly analogous to a random walk in which each successive step is of the same size and whose direction is completely random. In a random walk with constant increments, the expected net distance from the starting points increases proportionally to the square root of the number of steps. Since "steps" or induced displacements are not constant, the actual expected net displacement may follow another relation. Nonetheless, the consecutive displacements will still partially offset one another so that cumulative earthquake effects may have a much smaller impact on canister safety than single earthquakes. However, individual large magnitude events could produce single steps that exceed the displacement threshold, so that it does not matter that a large number of them would tend to cancel each other out. If the individual displacements are sufficiently large that a few of them would produce net cumulative slip greater than a threshold, there ought to be a higher probability that the canister will fail. This would imply that the

seismic hazard to canisters in southern Sweden is greater than in northern Sweden, even using the parameters for the Adjusted Southern Sweden scenario.

4.2 Relations Between Earthquake Magnitude, Slip and Rupture Geometry

The modeling approach, as elaborated in Section 1, requires simulating the number and magnitude of earthquakes expected to occur over the next 100,000 years for the various regions of Sweden relevant to assessing potential hazard at the three generic sites. The relations described in Section 4.1.2 only provide magnitude information. In order to carry out the numerical simulations, it is necessary to relate magnitude to a rupture area in order to construct a dislocation of the correct surface area in the numerical model, and also to specify a dislocation magnitude. This is because the magnitude is a function of the earthquake moment, which in turn is equal to the product of the rupture area, the displacement across the rupture, and the shear stiffness of the rock. Moreover, in order to spatially locate the dislocation in the numerical model, at least for the larger earthquakes, it is necessary to identify a lineament trace that is sufficiently large enough to have a rupture area consistent with the magnitude of the earthquake. Thus, it is necessary to know the relations between these parameters in order to carry out the modeling.

It is possible to infer these values from a comprehensive database of earthquake source parameters assembled by Wells and Coppersmith (1994). This database gives values for rupture area, moment magnitude, average surface displacement, maximum surface displacement and surface rupture length, among other parameters. It is possible to compute the subsurface displacement from these parameters.

The data is separated into three groups based upon fault type. The fault types consist of normal, reverse and strike-slip faults. The relations among some of the parameters differ based upon fault type.

The values of fault depth and subsurface displacement were estimated from regressions between surface rupture length (SRL) and the parameters subsurface displacement (SD) and fault depth (RW). The regressions of SRL and RW for each fault type are shown in Figure 4-4. Each plot shows the raw data, the best-fit regression line, and the 5% and 95% confidence bounds. Figure 4-5 shows the analogous relations between SRL and SD. These relations are superimposed in Figure 4-6.

Figures 4-6 shows that the relations between surface rupture length and subsurface displacement differ as a function of fault type. For smaller faults (those less than about 40 km, or with magnitudes less than 7, since magnitude is very strongly correlated with surface rupture length and independent of fault type, Wells and Coppersmith, 1994), reverse fault exhibit the greatest displacements for a given surface rupture length or specified magnitude. For traces greater than 40 km, corresponding to magnitudes greater than 7, strike-slip faults have the greatest displacements.

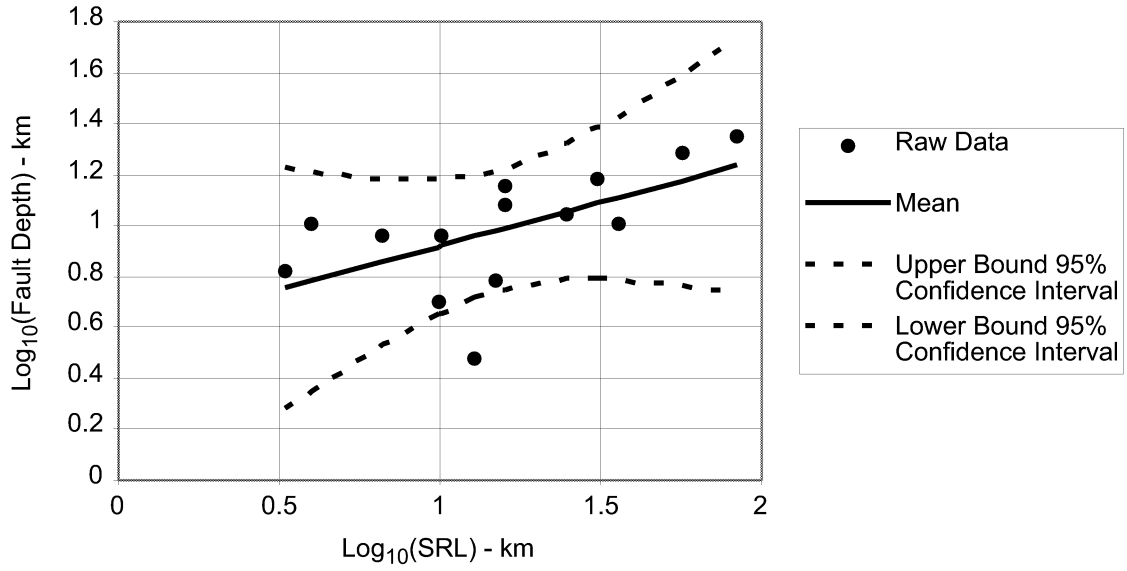

a. Reverse Faults

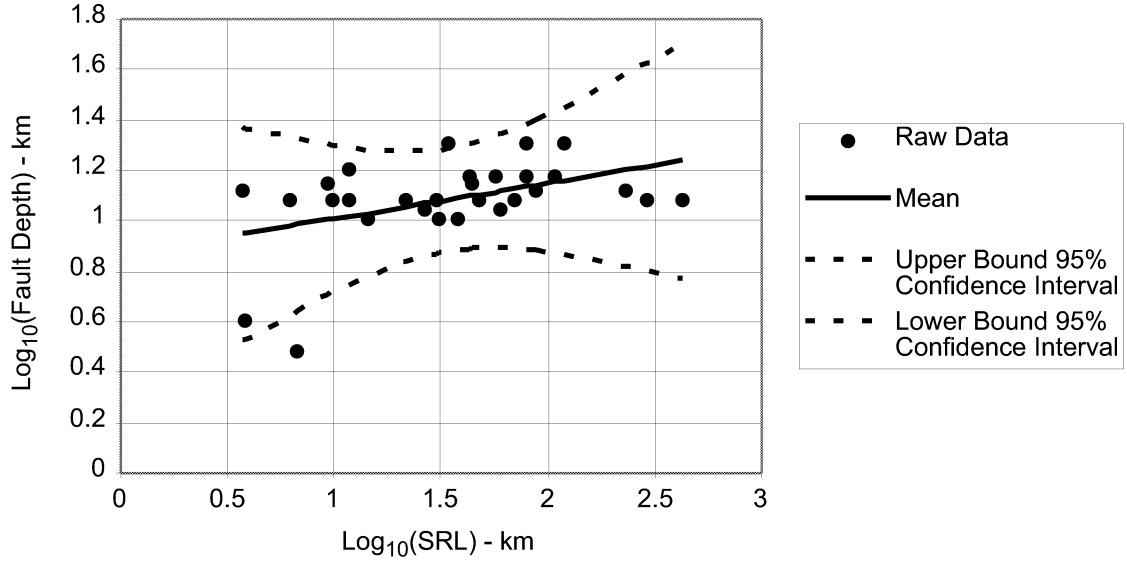

b. Strike-Slip Faults

FIGURE **4-4**
REGRESSION RELATIONS BETWEEN SRL AND RW (FAULT DEPTH)

Data from Wells and Coppersmith (1994)

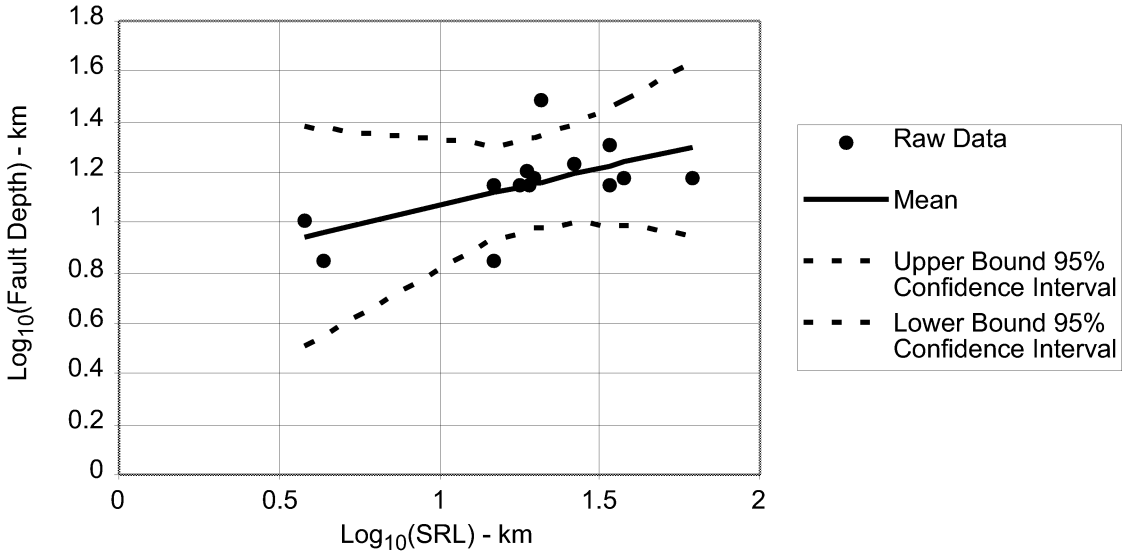

c. Normal Faults

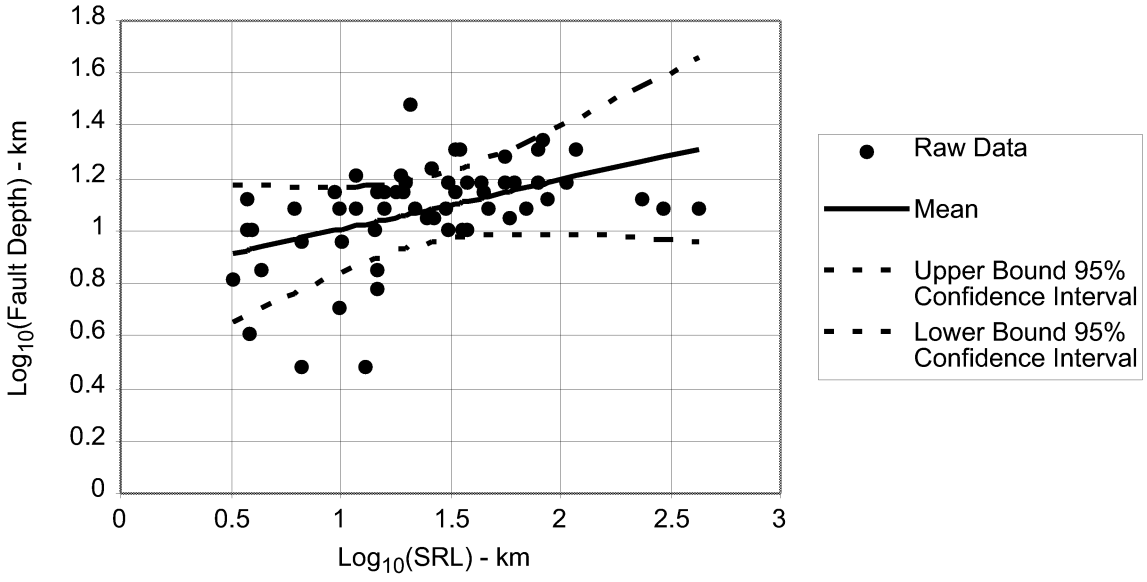

d. All Data

FIGURE **4-4**
(CONTINUED)

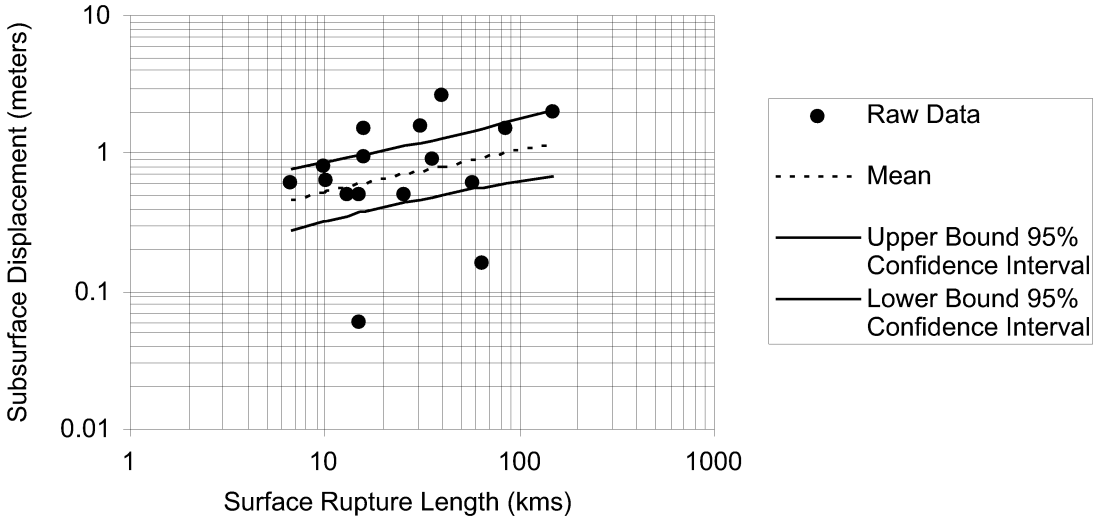

a. Reverse Faults

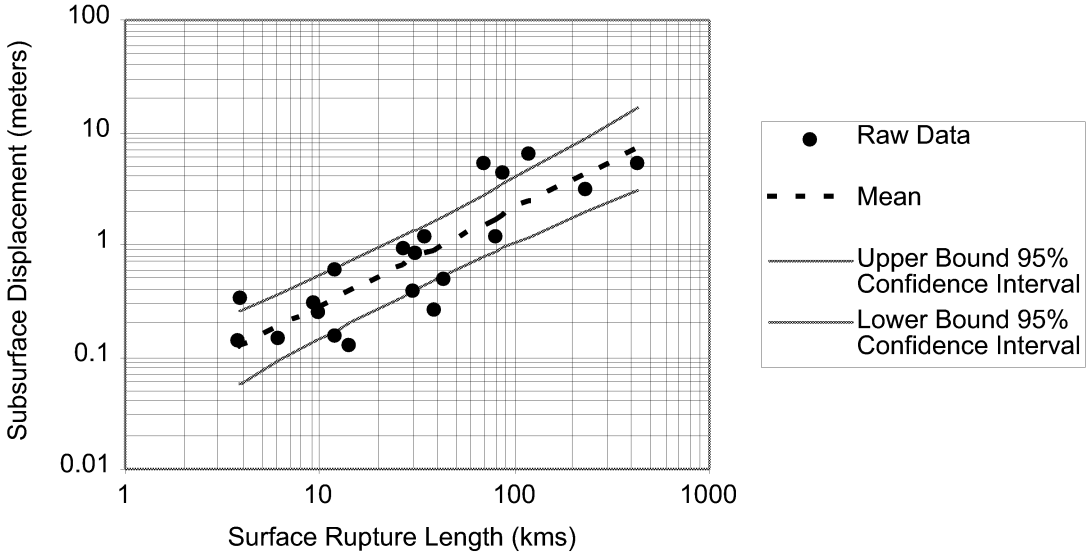

b. Strike-Slip Faults

FIGURE **4-5**
REGRESSION RELATIONS BETWEEN SRL AND SD

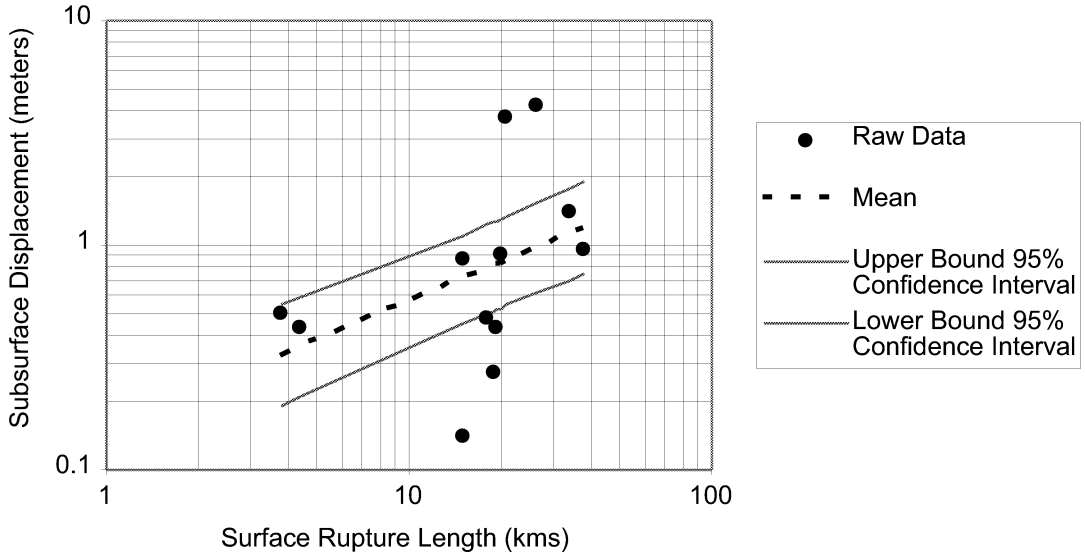

c. Normal Faults

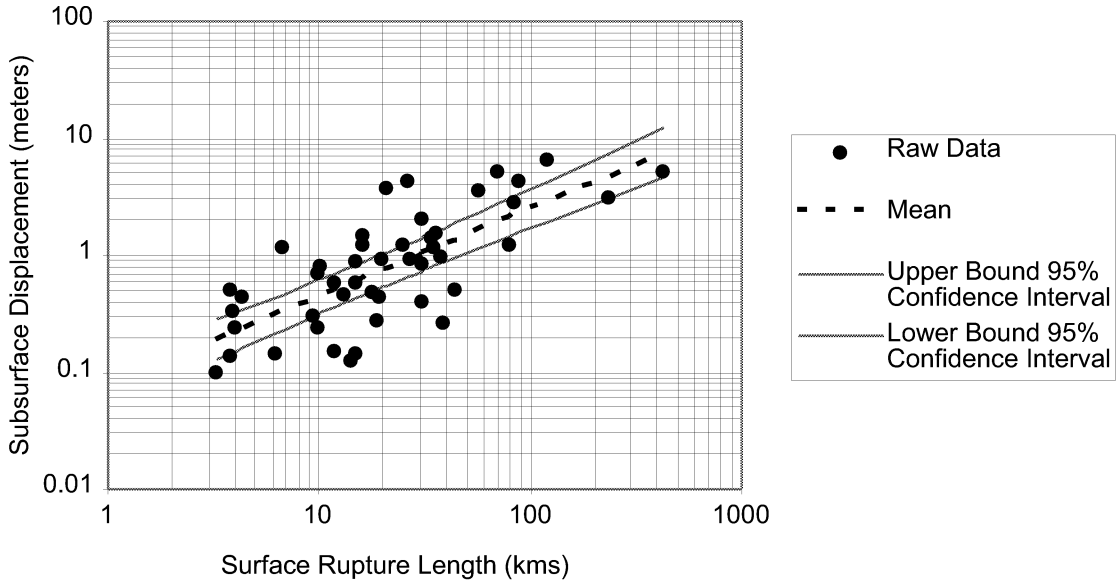

d. All Data

FIGURE **4-5**
(CONTINUED)

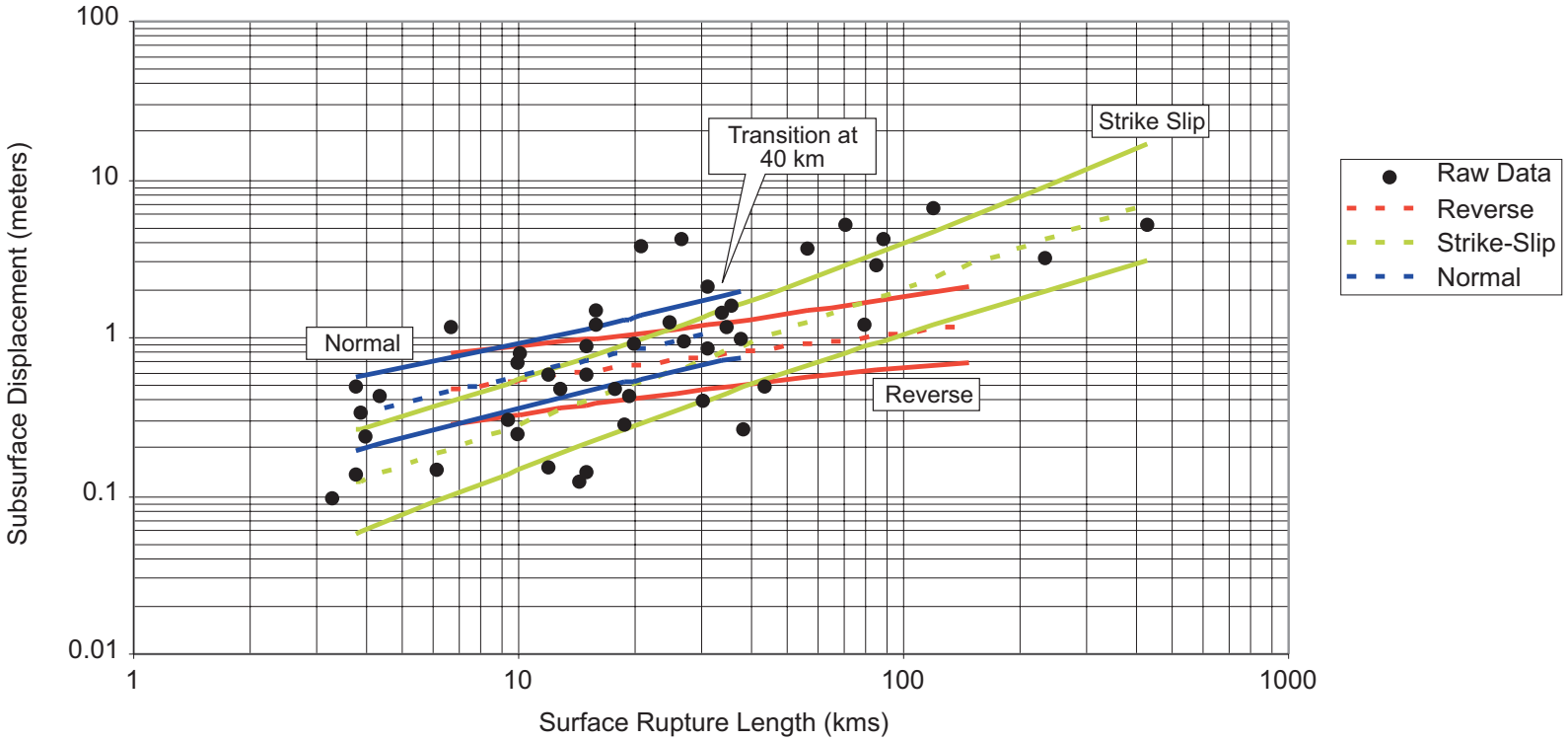

FIGURE **4-6**
COMPOSITE OF ALL 95% CONFIDENCE INTERVALS

It is not possible to predict whether any given fault lineament will reactivate as a normal, reverse or strike-slip fault during some future earthquake event. A conservative approach would be to select the worst-case parameters for any fault trace. This was accomplished by selecting displacements and depths based upon the regressions for reverse faults if the surface rupture length is less than 40 km or the magnitude is less than 7, and selecting displacements and depths from the strike-slip regressions for faults greater than 40 km or magnitudes greater than 7.

The procedure for assigning a depth and a displacement to each fault was to make a random draw from the regressions for SRL vs. SD and SRL vs. RW. The possible values were based upon the surface rupture length.

5. CALCULATED SECONDARY DISPLACEMENTS

5.1 Simulation Procedures

5.1.1 Generation of DFN models

For each site, 100 realizations of the stochastic portion of the DFN models were generated. The stochastic portion represented fractures covering the smallest size scale, which varied for each site as described in Section 3. This number of realizations is usually sufficient to accurately compute 90% to 95% confidence intervals under Monte Carlo sampling. If greater accuracy is desired for future site assessment, additional realizations could easily be generated.

5.1.2 Computation of Canister Intersections

Ideally, all possible intersections between fractures and canisters would be computed for an actual candidate site. This calculation would involve determining which of tens or hundreds of thousands of fractures in the repository rock mass intersect with any of the thousands of canister holes. This calculation is both numerically challenging and also not required to develop robust statistics for earthquake analysis. The previous work by La Pointe and others (1997) showed that three parameters governed the ultimate canister safety statistics: earthquake magnitude; distance between the earthquake and the fracture intersecting a canister hole; and the size of the fracture intersecting the canister hole. For an earthquake occurring on a particular fault outside the repository, the major factor is the size of fractures intersecting the canister holes. The distance between the fault on which the earthquake occurs and the fractures intersecting canisters probably does not vary more than 10% among the fractures. The earthquake may be 4.5 km away from one canister, and 4.6 km away from another. The magnitude for a particular earthquake is the same for all of the fractures intersecting canisters. However, fracture sizes may vary over several orders of magnitude, and displacements will vary approximately linearly with fracture size (La Pointe and others, 1997). Thus, a representative sample of the affects of a single earthquake on all of the fractures intersecting all of the canisters can be obtained if the sample has the same fracture size statistics. Through empirical simulation of canister intersections, it was found that the mean, median, 5^{th} and 95^{th} percentiles were approximately equal to the entire population if the canister subset intersected from 100 to 200 fractures. The analyses showed that the values for these four parameters stabilize between 100 and 200 fractures.

Figure 5-1 shows all canister positions (>4000) for all three sites. For Aberg, 970 canisters were selected at random and for Beberg and Ceberg, 700 canisters were selected at random. On the order of 500 to 600 fractures were intersected by the 970 canisters at Aberg, and about 300 to 400 were intersected at Beberg and Ceberg. These fractures intersecting the randomly-selected canister holes was retained for each of the 100 DFN realizations for the numerical earthquake modeling.

The random selection of canisters produces some numerical effects whose magnitude can be assessed. The canister spacing along a drift that has been used for these simulations is 6 m, and the canister holes are approximately 7.8 m high. Since there are fractures in the simulation large enough to intersect more than one canister, should this fracture experience slip greater than 0.1 m, it is possible that two canisters could fail rather than just one. Since many of the neighboring canister positions are not included in the simulations, the impact of one fracture producing unacceptable displacements on more than one canister is reduced. Some simple calculations suggest that the reduction is very slight.

The spacing and height of canister holes implies by simple trigonometry that a fracture must dip less than 53 degrees for it to intersect more than one canister hole. This indicates that none of the subvertical sets which comprise most of the fracture intensity in the DFN models are likely to intersect more than one canister even if all of the canister holes were included.

Another calculation can be used to estimate the effect for subhorizontal fractures. The minimum average radius of a circular fracture that could intersect canisters 6 m apart can be calculated by assuming that the canisters would intersect the fracture at two random locations. The mean and median distance between two randomly selected points in a circle is equal to the radius of the circle. This implies that fractures with radii less than 6 m are unlikely to intersect more than one canister. Using the size statistics for the subhorizontal fracture set at Aberg, less than 17% of the fractures simulated have radii greater than 6 m, 10% of the fractures have radii greater than 7.3 m, and fewer than 5% have radii greater than 9.5 m. Since the subhorizontal set represents about one-fourth of all of the fractures, not all of the fractures that intersect canisters will belong to this set, so the actual number could be somewhat less than 17%. Moreover, displacements vary over the fracture surface from a maximum at the center to zero at the edges. Thus, the fact that the displacement at one canister location is greater than a threshold value does not guarantee that it will also be over that value at a different location where another canister intersects the fracture. These two observations suggest that the actual increase in failure percentage would be much less than 17%, maybe on the order of 5%. For a repository with 5000 canisters, this would increase the number of failed canisters by a maximum of one canister for the least favorable of all of the three generic sites and sets of seismic scenarios (Table 5-1), and would not increase it for all other sites and scenarios.

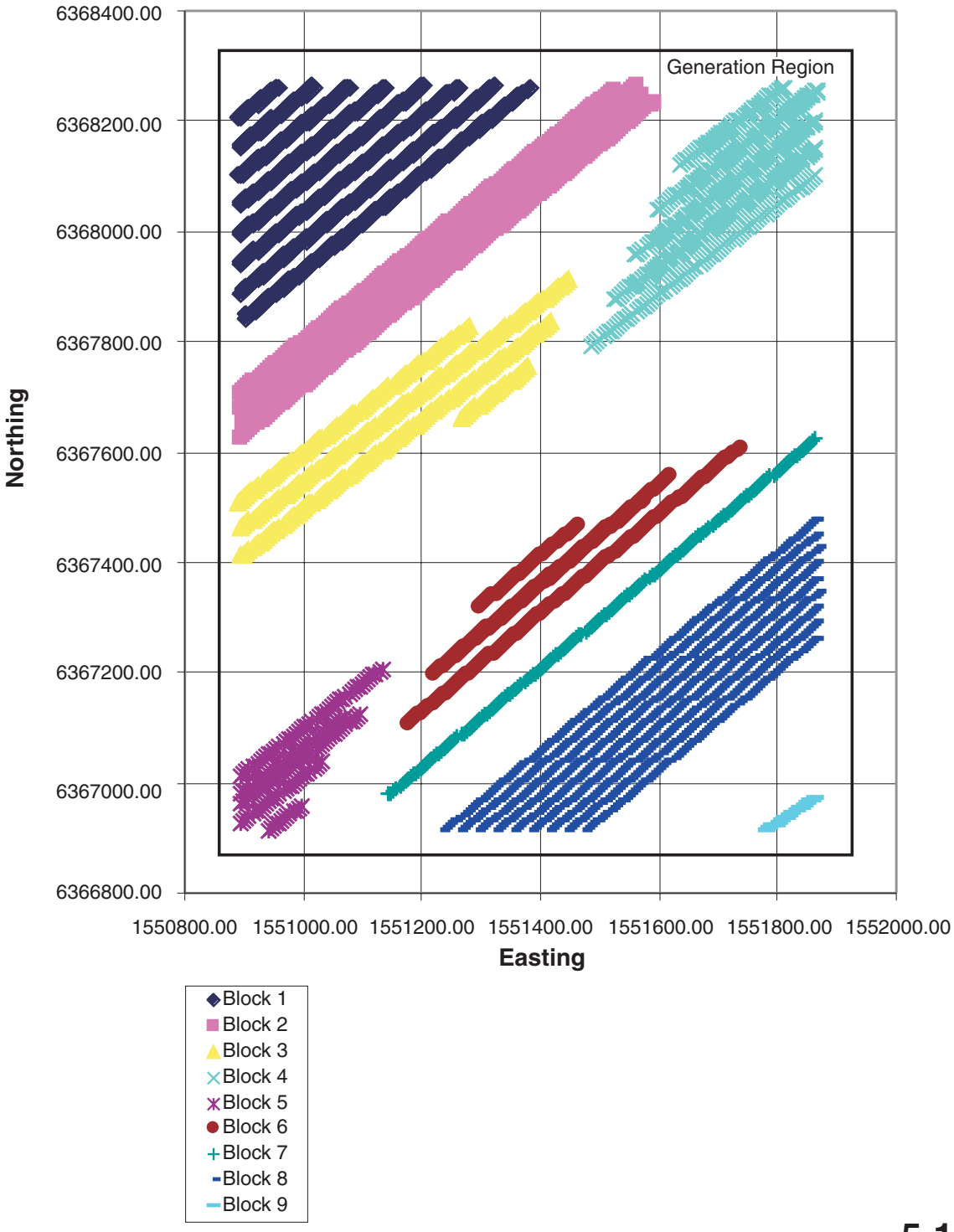

FIGURE **5-1a**
ABERG CANISTER LOCATIONS AND FRACTURE GENERATION REGIONS

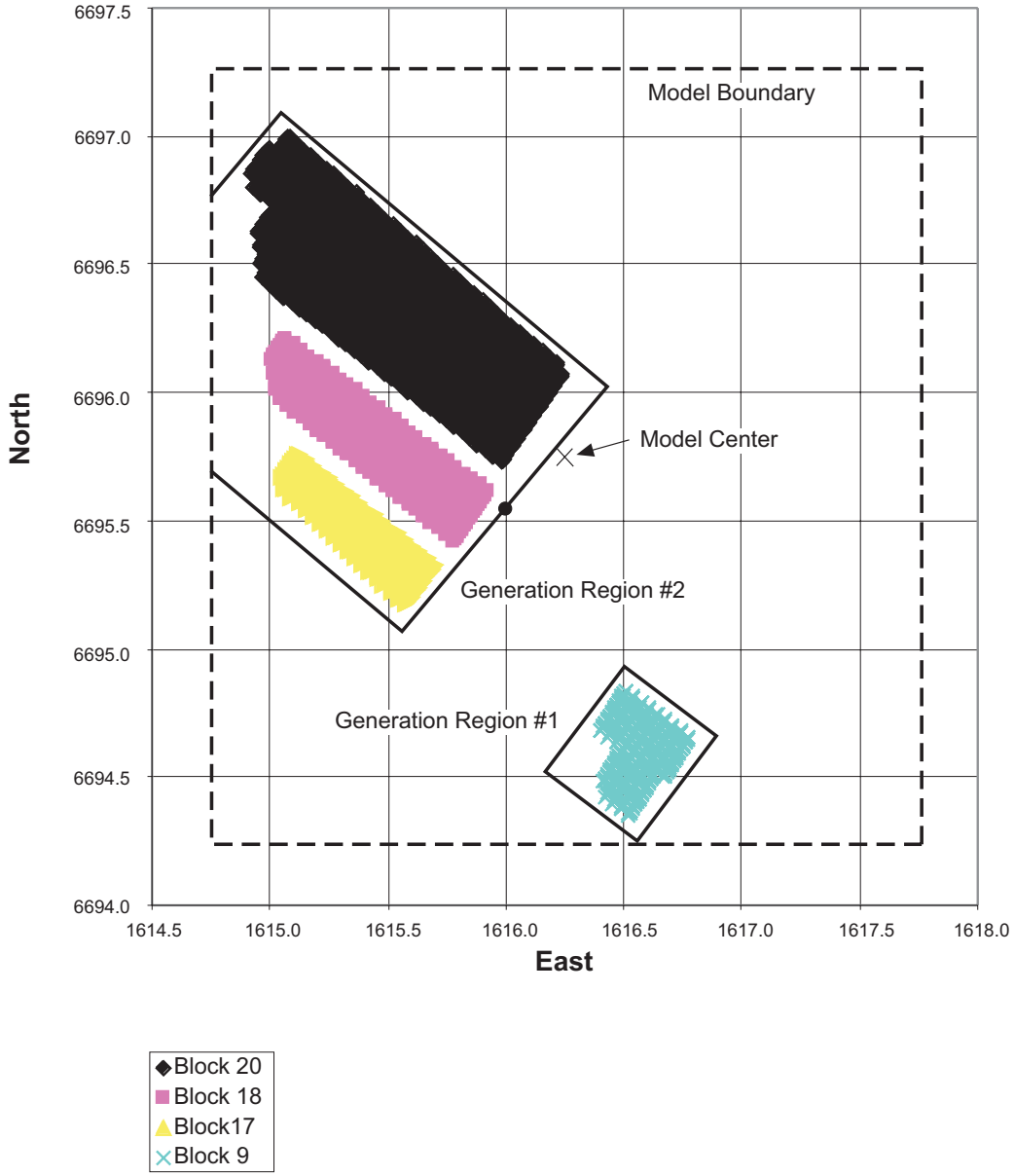

FIGURE **5-1b**
BEBERG CANISTER LOCATIONS, MODEL REGION, AND FRACTURE GENERATION REGIONS

After SKB R-97-05 (Hermanson et al. 1996)

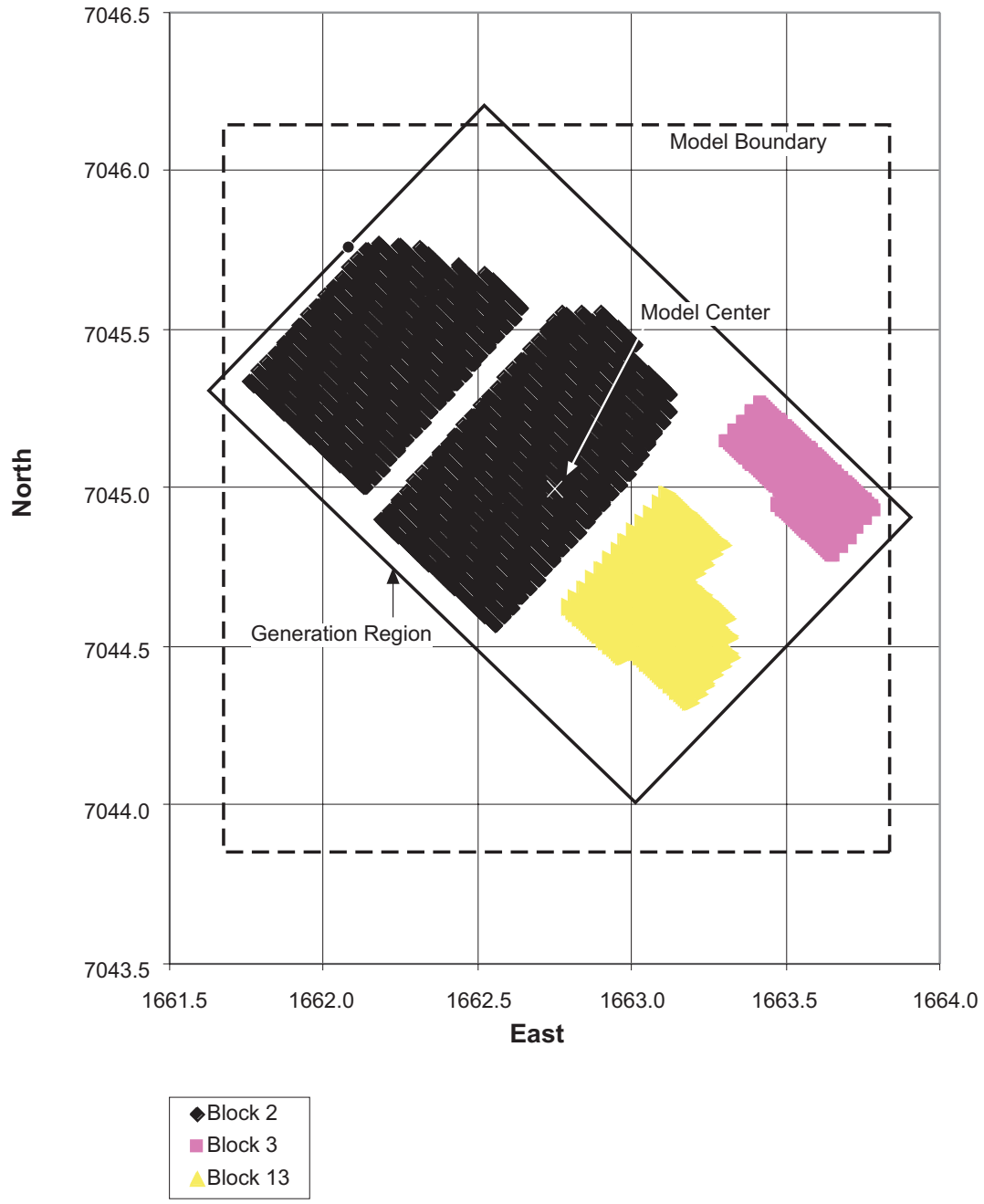

FIGURE **5-1c**
CEBERG CANISTER LAYOUT, MODEL REGION, AND FRACTURE GENERATION REGIONS

After SKB R-97-05 (Hermanson et al. 1996)

The calculated displacements are also adjusted to reflect the fact that canisters do not necessarily intersect the fracture at the fracture centerpoint. The numerical code Poly3D used to estimate induced slippage (Thomas, 1993) calculates displacements at the centers of fractures only. According to linear elastic fracture mechanics theory (Pollard and Segall, 1987), the induced slip displacement will be the greatest at the center of the fracture and decrease to zero at the crack tip or edges. However, canisters that intersect fractures in the numerical simulations intersect fractures at many different locations other than the center. Thus, the calculated displacements, which represent maximum centerpoint displacements, need to be adjusted for their actual locations. This adjustment is carried out as follows.

The displacement on a crack as a function of crack half-length, stress and rock properties is given by the following equation (Pollard and Segall, 1987):

$$\begin{Bmatrix} \Delta u_I \\ \Delta u_{II} \\ \Delta u_{III} \end{Bmatrix} = \begin{Bmatrix} \Delta\sigma_I \\ \Delta\sigma_{II} \\ \dfrac{\Delta\sigma_{III}}{1-\upsilon} \end{Bmatrix} \frac{2(1-\upsilon)}{\mu} (R^2 - x_2{}^2)^{\frac{1}{2}} \qquad 4\text{-}3$$

where $\begin{Bmatrix} \Delta u_I \\ \Delta u_{II} \\ \Delta u_{III} \end{Bmatrix}$ represents the displacements parallel and perpendicular to the fracture,

$\begin{Bmatrix} \Delta\sigma_I \\ \Delta\sigma_{II} \\ \Delta\sigma_{III} \end{Bmatrix}$ represents the stresses on the fracture,

μ and ν are elastic moduli,
R is the fracture radius, and
x_2 is the distance from the fracture center to the fracture tip.

This equation shows that the maximum displacement occurs at the fracture center, and decreases to zero at the fracture tip. It also shows that if the displacements are known at the fracture center, and the fracture radius is known, then it is possible to calculate the reduced displacement as a function of the distance from the fracture center.

This procedure was incorporated to adjust the displacements calculated by Poly3D to better reflect the actual intersection locations between the fractures and the canisters.

5.1.3 Combining the Stochastic DFN Model with the Trace Maps

A final series of models were prepared for the earthquake simulations. Each model represented the combination of one of the 100 realizations of the DFN model and a randomly selected fault from the lineament maps. The selected fault was assumed to be vertical. The depth of the fault and the displacement assigned to the fault were drawn from the regression relations shown in Figure 4-4 and Figure 4-6

However, this procedure was only followed for larger and medium sized earthquakes. For smaller earthquakes, the location is chosen at random, but the surface rupture length and width of the fault are still based on the correlation between magnitude and rupture geometry, as in the case for larger magnitude earthquakes.

5.2 Displacement Statistics and Canister Failure Probabilities

Performance assessment requires predicting the affects of all potential future earthquakes within a specified time period, which for this study is 100,000 years. Each earthquake during this performance period may produce displacement on fractures intersecting canister holes. The displacement is a vector, having both magnitude and direction. Canister failure occurs when the net cumulative displacement exceeds 0.1 m, whether this occurs as a result of the first earthquake or any subsequent earthquake.

Multiple stochastic realizations of the earthquake frequency/magnitude parameters were run for each DFN realization. Fifty realizations of the seismic parameters were run for each DFN realization, although the variability in results turned out to be sufficiently small that many fewer seismic parameter realization could have been run.

While Aberg is clearly within the southern Sweden seismic zone, Beberg and Ceberg could be placed within more than one zone. For example, Beberg could be affected by earthquakes in southern Sweden, northern Sweden and the Gulf of Bothnia zones. Ceberg could be affected by earthquakes in the northern Sweden and Gulf of Bothnia zones.

In order to evaluate the effects that these different sets of seismic parameters might have, a complete series of simulations were run for each site using set of seismic parameters. For example, this means that the stability of Beberg was evaluated three times, using the parameters for southern Sweden, northern Sweden and the Gulf of Bothnia for a series of successive simulations.

Figures 5-2 through 5-4 and Table 5-1 summarize the probability of the percent of canisters that might fail during a 100,000-year period for Aberg, Beberg and Ceberg under alternative earthquake magnitude/frequency scenarios. The failure percent represents the fraction of canisters that are estimated to experience slip greater than 0.1 m sometime during the 100,000 years. Canisters may fail during a single earthquake, or due to the cumulative effects of multiple smaller earthquakes. Failure percentages due to both single earthquake events and to the cumulative effects of multiple earthquakes are combined in Figure 5-2. Figure 5-3 shows only the failure percentage probabilities for cumulative displacements from multiple earthquakes, while Figure 5-4 shows the failure percentage probabilities for failures caused by single large earthquakes.

Figures 5-2a and b show that the majority of simulations led to no canister failures, either due to single large earthquakes or to the cumulative effects of multiple smaller earthquakes. Approximately 79% of all simulations for Aberg using the parameters for all of southern Sweden (including the Lake Vänern subregion) produced no canister failures. This represented the least favorable scenario. In the other scenarios considered, 90% to 95% of the simulations produced no canister failures. When the adjusted southern Sweden earthquake scenario was applied to Aberg and Beberg, approximately 96% of all of the simulations produced no canister failures. Table 5-1 shows that mean failure rates vary from a high of 0.65% for Aberg to a low of 0.037% for Ceberg. For reference, 0.02% failure percentage for a 5000-canister layout represents the failure of a single canister. Median canister failure percentages are all zero. In general, Ceberg has the lowest failure percentages while Aberg has the highest. If the adjusted southern Sweden seismic parameters are used, then the failure percentages for Aberg and for Beberg are considerably reduced relative to the normal southern Sweden seismic parameters (0.65% reduced to 0.077% for Aberg; 0.15% reduced to 0.045% for Beberg).

Table 5-1 also shows that most failures occur due to single earthquake events, rather than to the cumulative effects of multiple smaller earthquakes. The ratio of failures due to multiple events vs. single events is greatest for Beberg, regardless of the seismic parameter scenario considered, although single events are still the most numerous cause of canister failures.

Table 5-1. Statistical Summary of Canister Failures as a Function of Different Seismic Hazard Scenarios

	Aberg – Southern Sweden	Beberg – Southern Sweden	Beberg – Northern Sweden	Beberg – Gulf of Bothnia	Ceberg – Northern Sweden	Ceberg – Gulf of Bothnia	Aberg – Adjusted Southern Sweden	Beberg – Adjusted Southern Sweden
All Canister Failures (includes failure due to single events and multiple events)								
Mean	0.6471%	0.1521%	0.1210%	0.1227%	0.0373%	0.0373%	0.0773%	0.0452%
Median	0.0000%	0.0000%	0.0000%	0.0000%	0.0000%	0.0000%	0.0000%	0.0000%
Standard Deviation	2.6018%	0.6417%	0.6112%	0.6166%	0.1771%	0.1825%	1.0058%	0.3411%
Percent Failures Due to Multiple Earthquakes								
Mean	0.0564%	0.0426%	0.0406%	0.0363%	0.0038%	0.0046%	0.0003%	0.0023%
Median	0.0000%	0.0000%	0.0000%	0.0000%	0.0000%	0.0000%	0.0000%	0.0000%
Standard Deviation	0.2185%	0.1884%	0.1864%	0.1823%	0.0265%	0.0276%	0.0146%	0.0323%
Percent Failures Due to Single Earthquakes								
Mean	0.5907%	0.1095%	0.0804%	0.0864%	0.0335%	0.0327%	0.0770%	0.0429%
Median	0.0000%	0.0000%	0.0000%	0.0000%	0.0000%	0.0000%	0.0000%	0.0000%
Standard Deviation	2.5469%	0.4847%	0.4446%	0.4576%	0.1730%	0.1770%	1.0054%	0.3235%

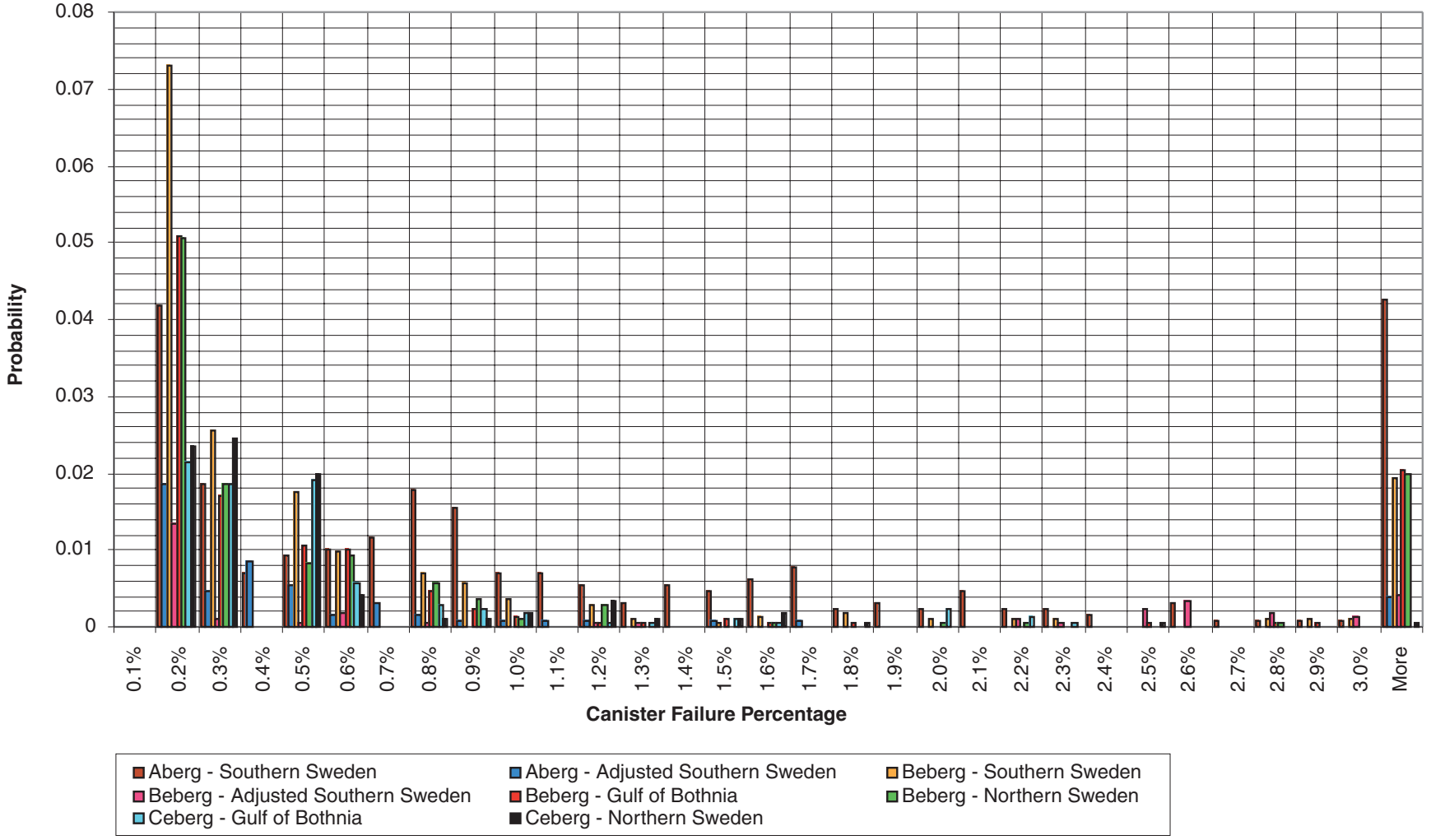

FIGURE **5-2a**
CANISTER FAILURE PROBABILITY DUE TO SINGLE AND MULTIPLE EVENTS

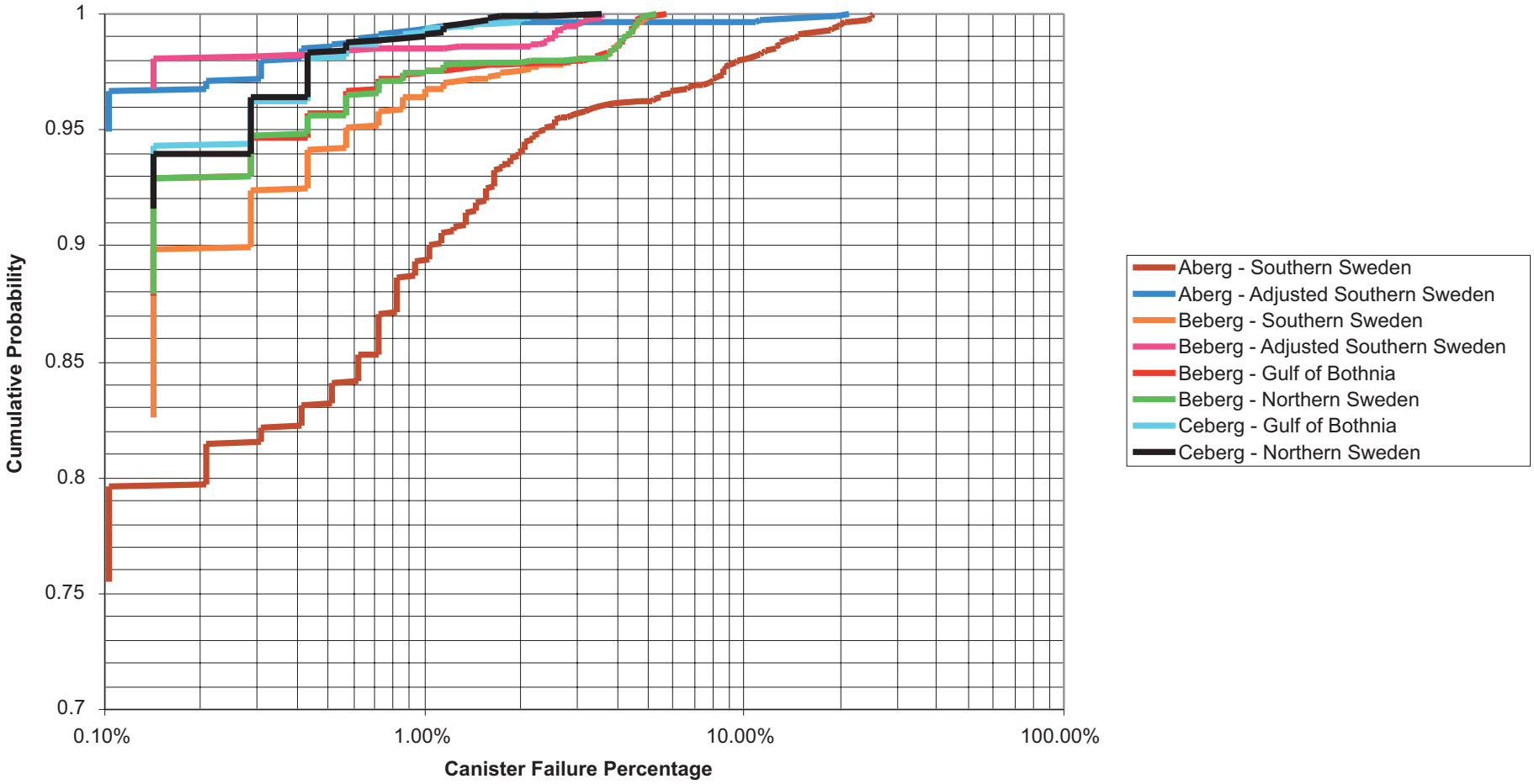

FIGURE **5-2b**
CUMULATIVE PROBABILITY OF CANISTER FAILURE DUE TO SINGLE AND MULTIPLE EVENTS

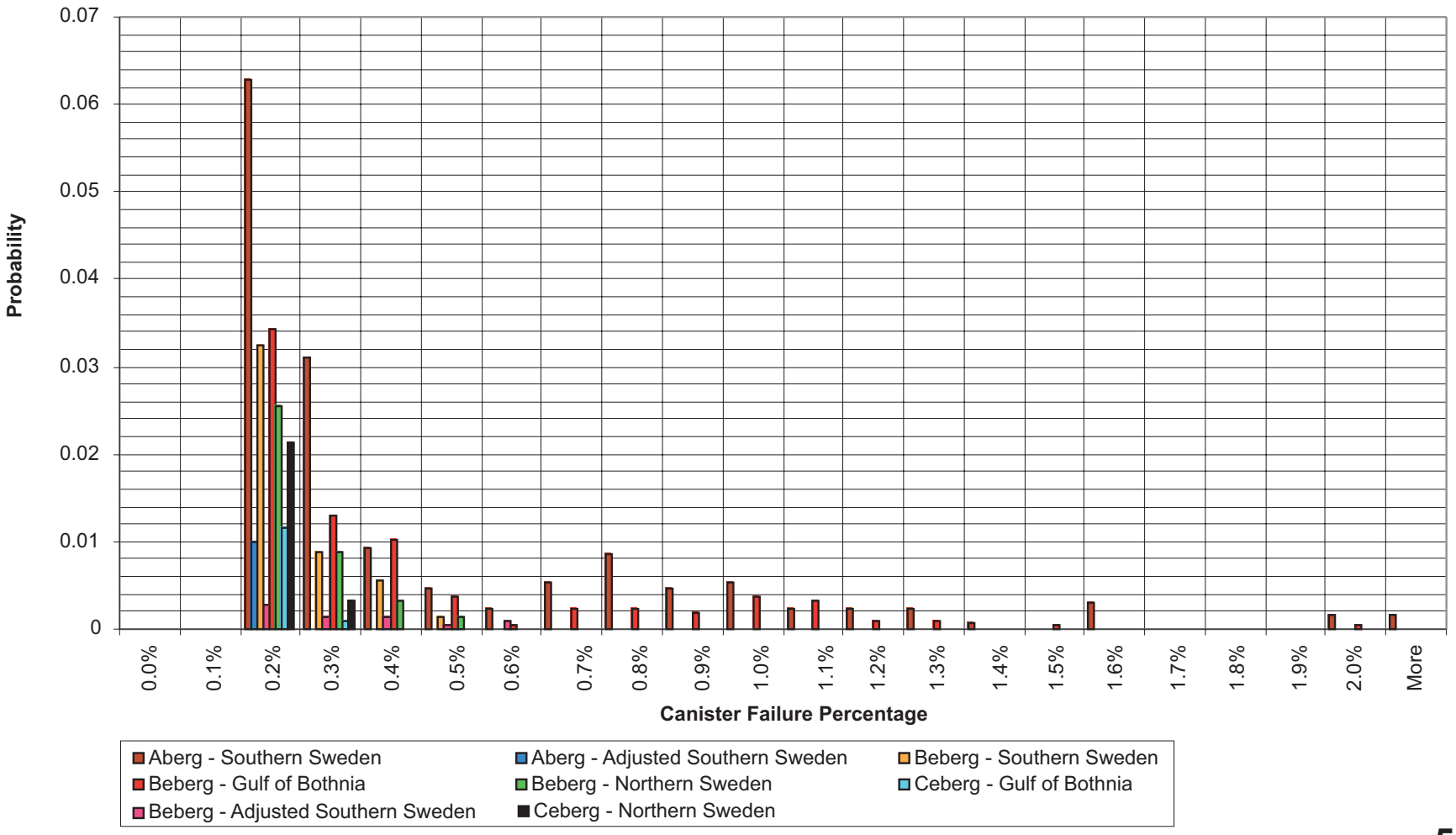

FIGURE **5-3a**
CANISTER FAILURE PROBABILITY DUE TO MULTIPLE EVENTS

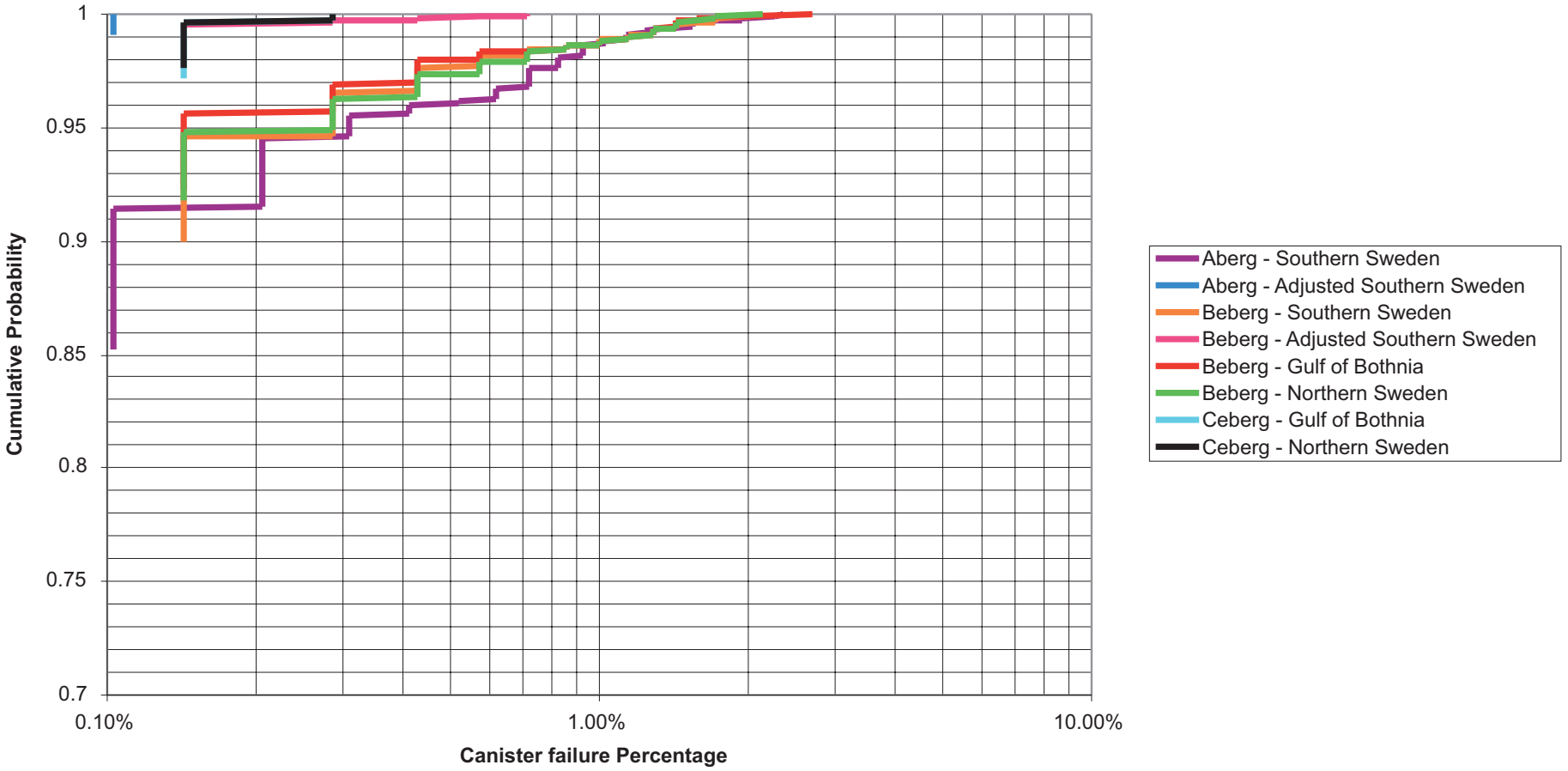

FIGURE **5-3b**
CUMULATIVE PROBABILITY OF CANISTER FAILURE DUE TO MULTIPLE EVENTS

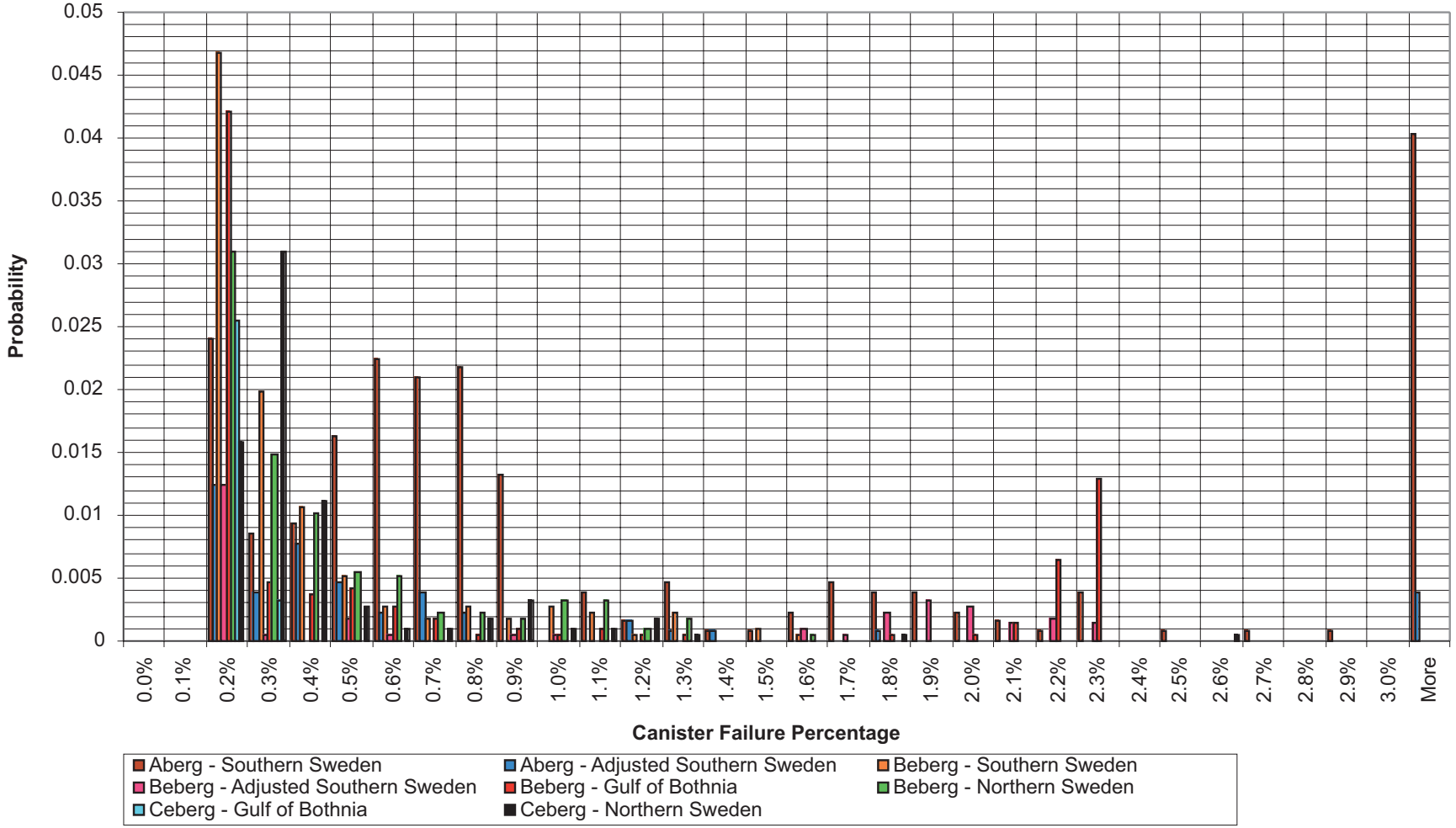

FIGURE **5-4a**
CANISTER FAILURE PROBABILITY DUE TO SINGLE EVENTS

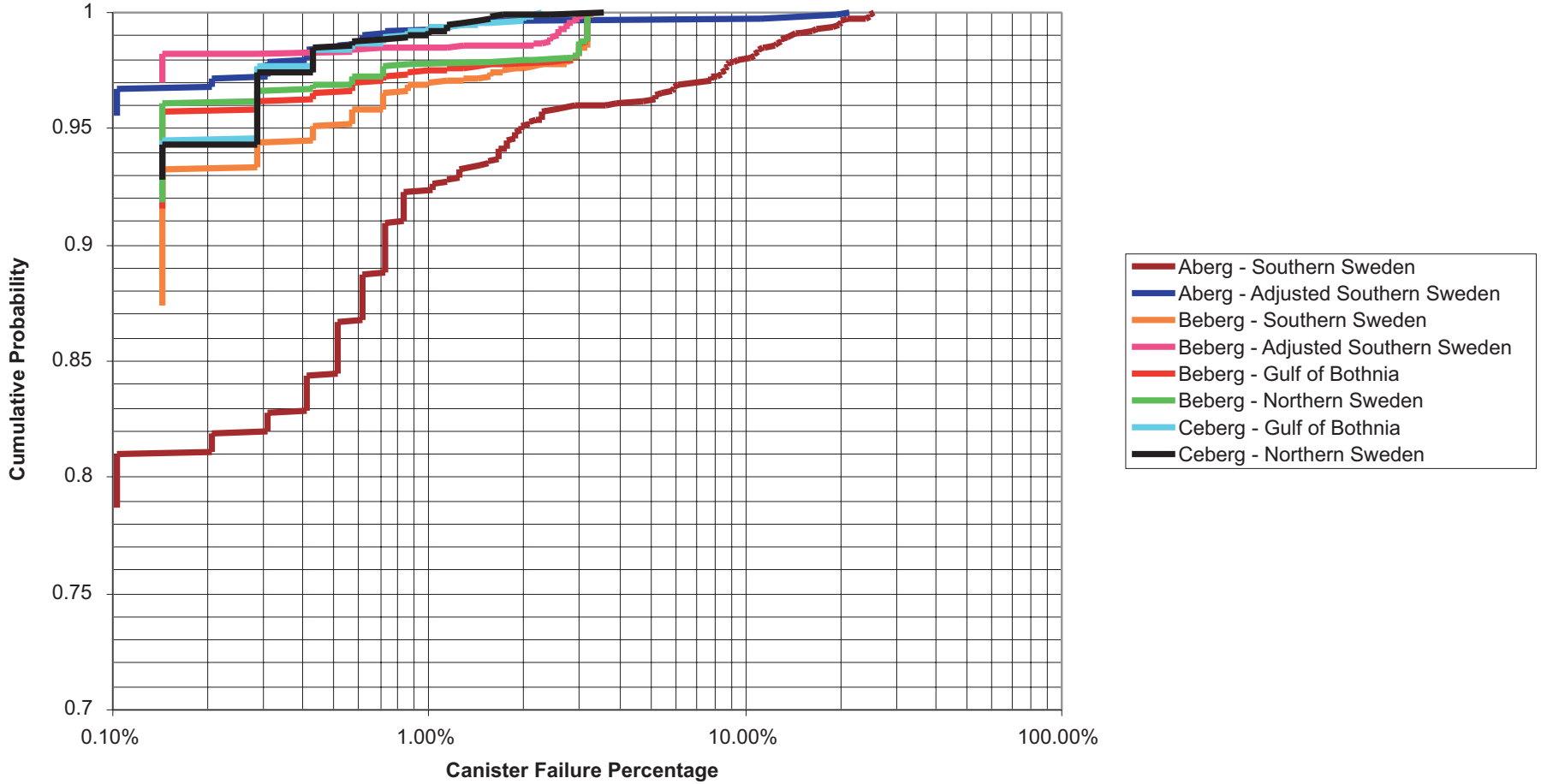

FIGURE **5-4b**
CUMULATIVE PROBABILITY OF CANISTER FAILURE DUE TO SINGLE EVENTS

Additional investigation of the single earthquakes that cause unacceptable slippage suggests that their probability of occurrence over a 100,000 year time period is very low (Figure 5-5 and Table 5-2), but that their consequences are more severe in that they tend to damage multiple canisters (Figure 5-6 and Table 5-3). The probability of an earthquake occurring that damages one or more canisters varies from 0.32 for Aberg to a low of 0.07 for Ceberg. Figure 5-5 shows that the predicted number of damaging single earthquakes at a single location such as Beberg or Ceberg is greatest the southern Sweden parameters, followed by the Gulf of Bothnia parameters and least for the northern Sweden parameters. This is consistent with the *b* values reported in Table 4-1. As predicted, the greatest number of damaging earthquakes correlates with the smallest *b* values, and the fewest damaging earthquakes correlate with the largest *b* values. Once again, compensation for the higher seismic activity in the Lake Vänern region in southern Sweden may reduce the probability for Aberg to a value near 0.05.

Table 5-2. Statistical Summary of the Number of Damaging Earthquakes Expected to Occur Within a 100,000-Year Time Period as a Function of Different Seismic Hazard Scenarios

Site & Seismicity Scenario	Mean	Median	Standard Deviation	Maximum
Aberg - Southern Sweden	0.325	0.00	0.745	5
Aberg - Adjusted Southern Sweden	0.054	0.00	0.243	2
Beberg - Southern Sweden	0.176	0.00	0.543	5
Beberg - Adjusted Southern Sweden	0.038	0.00	0.225	3
Beberg - Gulf of Bothnia	0.125	0.00	0.480	5
Beberg - Northern Sweden	0.129	0.00	0.521	5
Ceberg - Gulf of Bothnia	0.071	0.00	0.276	2
Ceberg - Northern Sweden	0.076	0.00	0.277	2

Table 5-3. Statistical Summary of the Percentage of Canister Failures Due to a Single Damaging Earthquake as a Function of Different Seismic Hazard Scenarios

Site & Seismicity Scenario	Mean	Median	Standard Deviation	Maximum
Aberg - Southern Sweden	1.82%	0.31%	4.09%	25.36%
Aberg - Adjusted Southern Sweden	1.41%	0.31%	4.11%	21.34%
Beberg - Southern Sweden	0.62%	0.14%	0.84%	3.00%
Beberg - Adjusted Southern Sweden	1.13%	0.57%	1.12%	3.14%
Beberg - Gulf of Bothnia	0.69%	0.14%	0.92%	3.00%
Beberg - Northern Sweden	0.62%	0.14%	0.88%	3.00%
Ceberg - Gulf of Bothnia	0.46%	0.29%	0.49%	2.29%
Ceberg - Northern Sweden	0.44%	0.29%	0.46%	3.57%

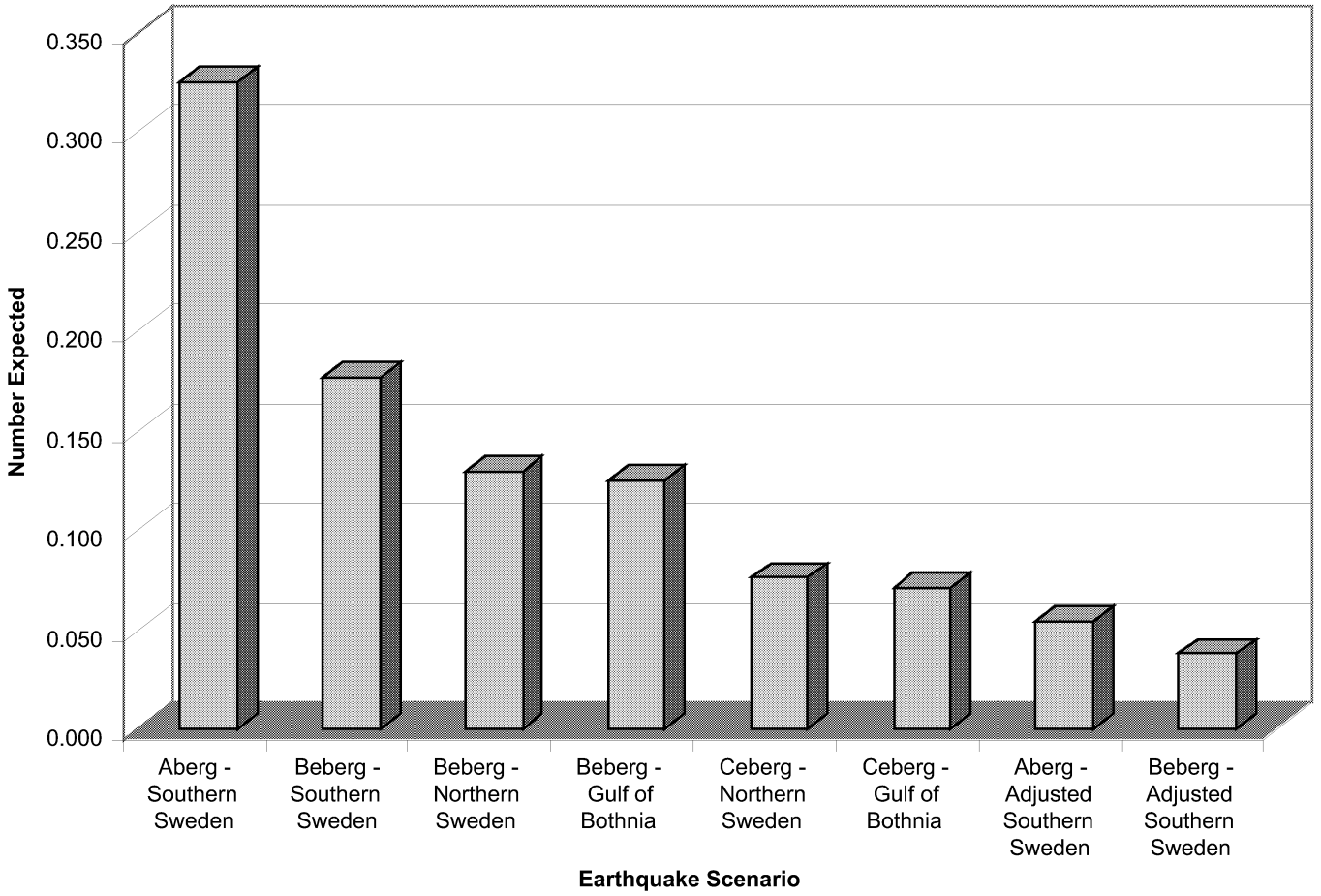

FIGURE **5-5**
NUMBER OF EXPECTED DAMAGING EARTHQUAKES IN 100,000 YEARS

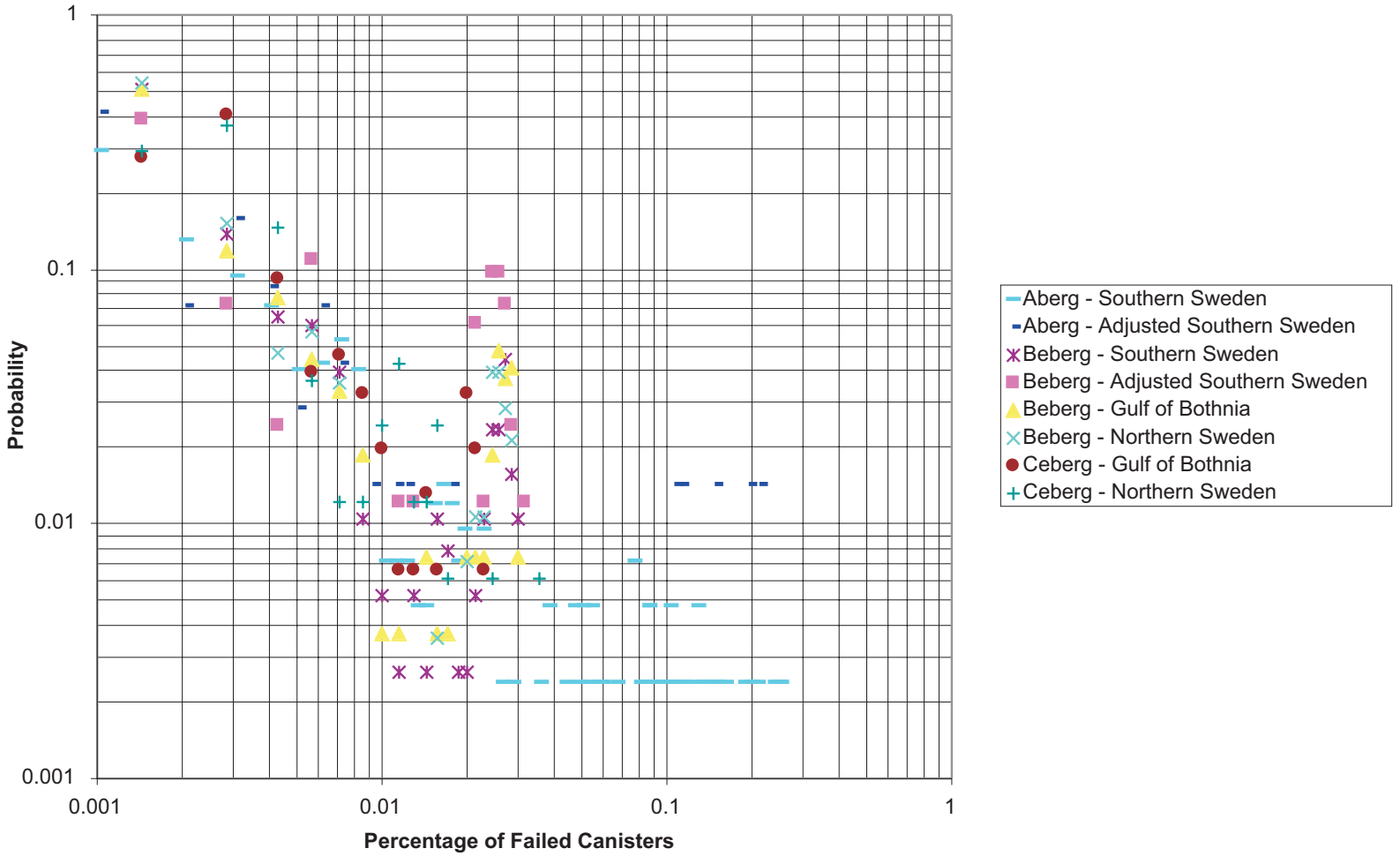

FIGURE **5-6a**
CONDITIONAL PROBABILITY OF CANISTER FAILURE FOR A SINGLE DAMAGING EARTHQUAKE

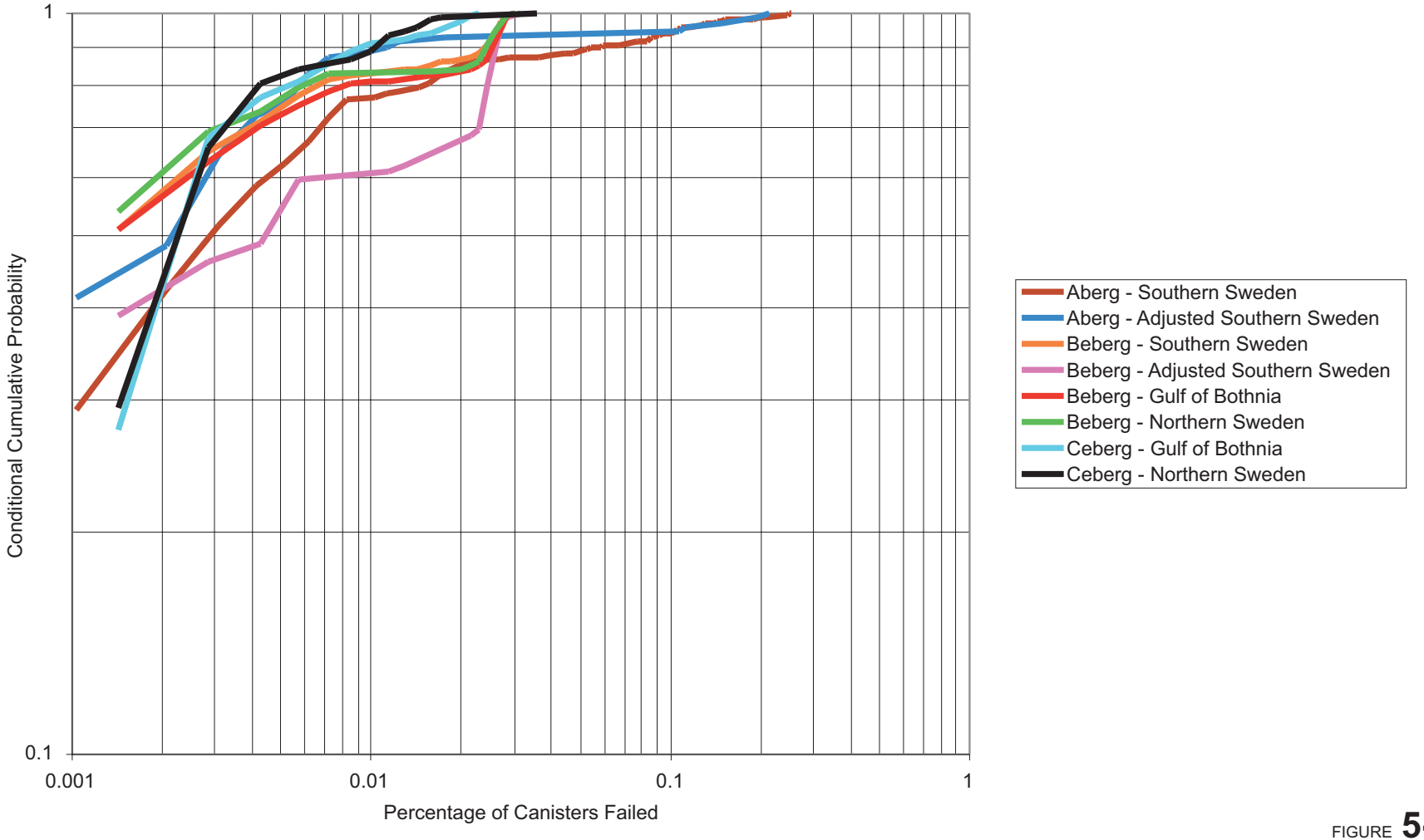

FIGURE **5-6b**
CUMULATIVE CONDITIONAL PROBABILITY OF CANISTER FAILURE FOR DAMAGING EARTHQUAKES

When a damaging earthquake occurs, an average of from 0.4% to 1.8% of the canisters experience induced slips greater than 0.1m, the higher number representative of Aberg, and the lower value representative of Ceberg. These percentages do not reflect overall failures; they are *conditional failure percentages*. For example, if a repository contained 5000 canisters, then a 1.8% percent failure value would imply that 90 canisters failed due to a single, damaging earthquake. As explained previously, most (> 90%) simulations do not produce a single damaging earthquake in the 100,000 year time period considered. The 1.8% canister failure rate is *conditional* upon the fact that a single damaging earthquake has occurred. It suggests that when a large earthquake occurs, a number of canisters are affected. However, since the probability that even one damaging earthquake occurs is small, the overall expected failure percentages are reduced to the levels shown in Table 5-1. Compensation for the higher seismic activity in the Lake Vänern region in southern Sweden may reduce the mean failure percentage for Aberg to a value near 0.6%, making it comparable to Beberg and Ceberg.

Although earthquakes were simulated at distances over 100 km from the canister positions, single earthquakes that produced displacements greater than 0.1 m were confined to the immediate vicinity of the repository. A histogram for the Ceberg simulations shows that over 95% of the single, damaging earthquakes are within 1 km of the canister that they damage, and 99% are with 2.5 km (Figure 5-7). The distance represented in this graph are the horizontal distances between the fault on which the earthquake occurs and the fracture intersecting the canister. The shape of the histogram shows the effects of two competing factors: the decrease in the impact of earthquakes with distance, and increase of earthquake epicenters with radial distance from a canister. The maximum distance for the simulations was approximately 31 km (Table 5-4). This suggests that the vast majority of faults that might potentially produce damaging earthquakes lie within a few kilometers of the repository. The simulations suggest that faults tens or hundreds of kilometers distant from the canisters are very unlikely to produce damage due to single earthquake events. In terms of site characterization, only the faults within a few kilometers or at most 50 km of the repository are likely to be sites of future damaging earthquakes. Moreover, seismic magnitude/frequency relations within a 50 km radius of the repository constitute the appropriate region for parameter values. This would suggest that the Lake Vänern seismicity should play no role in producing damaging earthquakes at Aberg or Beberg.

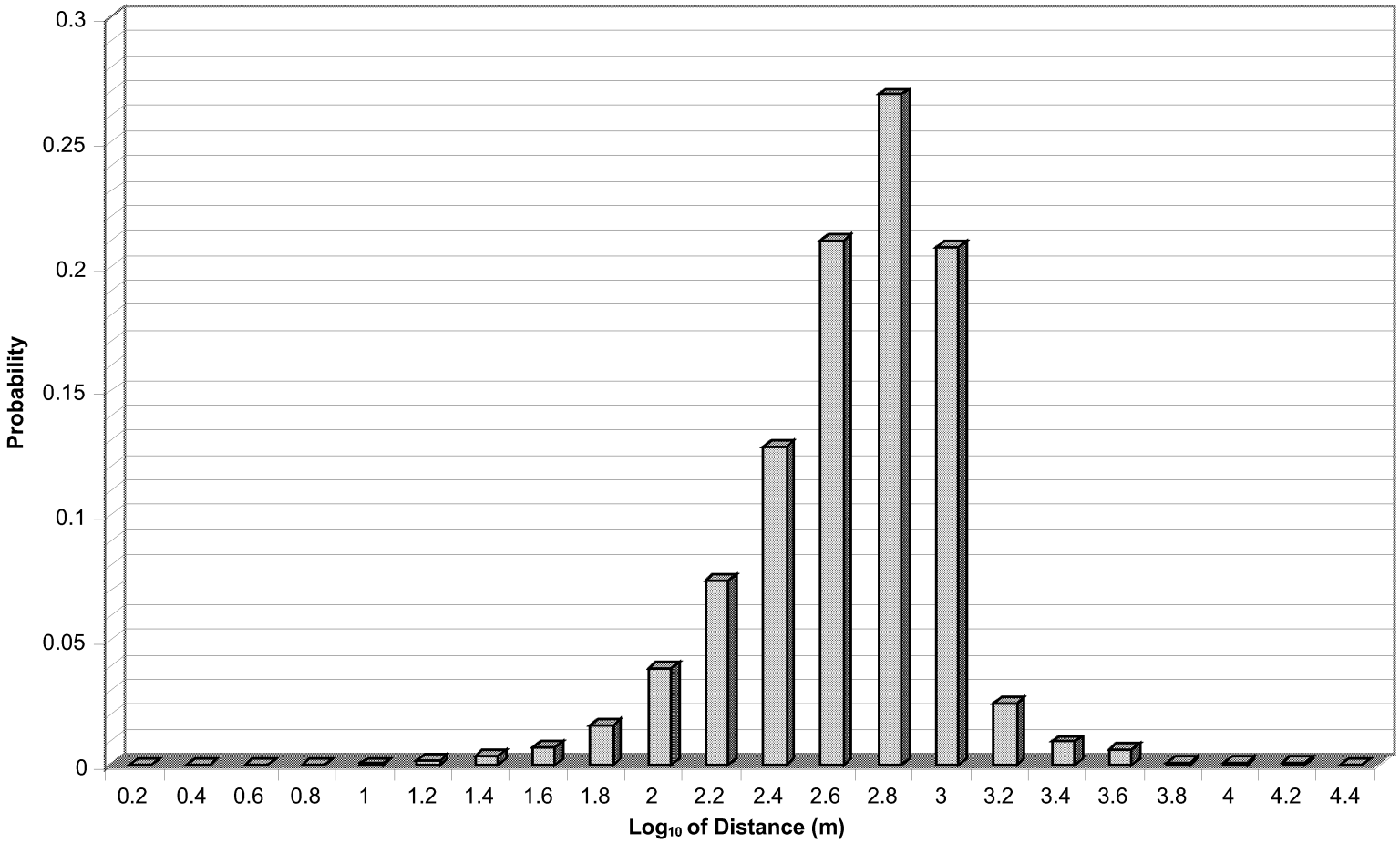

FIGURE **5-7**
HORIZONTAL DISTANCE BETWEEN EARTHQUAKE FAULTS AND CANISTERS EXPERIENCING DAMAGE DUE TO SINGLE EARTHQUAKE EVENTS – CEBERG EXAMPLE

Table 5-4. Statistical Summary of the Distance Between Damaging Earthquakes and Damaged Canisters-Ceberg Example

STATISTICAL PARAMETER	DISTANCE (meters)
Mean	504
Median	414
Standard Deviation	716
Maximum	31,269
PERCENTILES	
1%	33
5%	83
10%	126
25%	237
50%	414
75%	633
90%	836
95%	966
99%	2,426
99.9%	11,044

5.3 Primary Movement of Fractures Intersecting Canister Holes

The numerical earthquake simulations provide estimates of the canister failure percentage probabilities for slip induced by an earthquake occurring on a fault that does not intersect the canisters. However, during rebound or post-glacial faulting, it is possible that even small fractures intersecting the canister holes might slip as vertical loads decrease. The risk as a function of fracture size can be estimated using the data presented in Wells and Coppersmith (1994). The regression between the maximum subsurface displacement and surface rupture area for the three fault types and for all of the data without respect to fault type is given in Table 5-5 below. The regression coefficients are for the regression:

$$Log(RA) = a + bLog(MD) \qquad 5\text{-}1$$

where RA is the rupture area in km^2, MD is the maximum displacement in m, and a and b are constants.

Table 5-5. Regressions Results for Maximum Displacement vs. Surface Rupture Area

Fault Type	a	b	std error a	std error b	Area (km^2) for D =0.1 m	Radius (m)
Reverse	2.162	0.637	0.140	0.318	33.517	3266
Normal	2.626	0.373	0.050	0.066	179.355	7556
Strike Slip	2.818	0.751	0.068	0.089	116.686	6094
All	2.565	0.511	0.063	0.092	113.203	6003

Table 5-5 shows the dimension of the rupture area for a displacement of 0.1 m, and for the radius of a circle with the equivalent surface area. Note that for all fault types, the minimum rupture area is predicted to be from 33 to 179 km^2, or in terms of equivalent radius, from 3.3. km to 7.6 km.

These are large fractures, and would most likely be detected in any site reconnaissance program. It is highly unlikely that any canisters would be allowed to intersect fractures of this scale. Thus, primary slip on fractures intersecting canister holes due to tectonics, rebound or post-glacial faulting is of negligible concern unless a much smaller displacement threshold is applied.

6. CONCLUSIONS AND RECOMMENDATIONS

1. This study has greatly refined and elaborated the methodology developed in La Pointe and others (1997), and demonstrated it through application to the three generic sites Aberg, Beberg and Ceberg. In this approach, a three-dimensional model is constructed containing fractures at scales from meters to tens of kilometers based upon site-specific fracture data and more regional structural data derived from lineament maps at different scales. Proposed canister layouts are inserted into the fracture model to determine which canisters intersect fractures. Next, published earthquake magnitude/frequency relations are used to forecast the number and size of earthquakes that might occur within 100 km of the generic sites over a 100,000 year time period. The location of future earthquakes is determined in one of two ways: large earthquakes are located along randomly-selected lineaments within 100 km of the generic sites with the only constraint being that the lineaments are "long enough" to sustain an earthquake of the specified magnitude. The determination of length is based upon published world-wide regression relations between earthquake magnitude, rupture surface area and mapped surface rupture length. For smaller earthquakes, which are defined as those whose corresponding surface rupture length is less than the minimum trace length contained in the lineament maps, locations are selected at random within 100 km of the generic site. The size (length and width) of the rupture is based upon the same worldwide regression relations used to select lineament traces for large earthquakes. An instantaneous peak subsurface elastic displacement is assigned to the fault based upon published regressions between earthquake magnitude and fault displacement. Since all of these regressions contain variability, the selection is done through Monte Carlo sampling leading to a stochastic assignment of parameter values. Finally, the linear elastic fracture mechanics code Poly3d (Thomas, 1993) is used to compute the maximum elastic displacements on fractures that intersect canisters. This overall process contains many assumptions, but these assumptions tend to produce conservative (over-) estimates of induced displacements. The three-dimensional fracture model, the sequence of future earthquakes (which is treated as a Poisson process), and the regressions between various earthquake parameters are treated stochastically through Monte Carlo processes, leading to statistical distributions of canister failure percentages due to future earthquakes.

2. Aberg, Beberg and Ceberg differ in the failure percentage probabilities. Aberg has the highest percentages, while Ceberg has the lowest. The reason for this may be a function of the greater number of large earthquakes forecast for southern Sweden over a 100,000 year period, as

opposed to the Gulf of Bothnia and northern Sweden seismic zones, and to the greater overall fracture intensity and greater intensity of subhorizontal fractures at the Aberg site. Both Aberg and Beberg included a future seismic scenario based upon magnitude/frequency relations calculated for all of southern Sweden south of 60° north latitude. The Lake Vänern subregion, which is a region that has much higher seismicity than the rest of southern Sweden, is contained within this area. However, Aberg and Beberg are sufficiently far away from the Lake Vänern subregion that they may be much more affected by seismic activity outside of this subregion. New magnitude/frequency relations were calculated to try to compensate for this. When this future seismic scenario was applied to Aberg and Beberg, failure percentages dropped to the same levels as all of the other seismic scenarios applied to Beberg and Ceberg.

3. Although recent earthquakes are sparse outside of the Lake Vänern subregion, making estimation of magnitude/frequency relations statistically uncertain, it would be worthwhile to try to obtain more reliable estimates. The method used for compensation in this study provides only a qualitative impression of how much canister failures might decrease with better estimates.

4. The results show that upwards of 90% of the simulations for all sites and future earthquake scenarios produced no canister failures. When canister failures did occur in the simulations, they were more often the result of single, large earthquakes rather than due to the cumulative displacements produced by multiple earthquakes.

5. The single, large earthquakes that damage one or more canisters are termed "damaging earthquakes." The number of damaging earthquakes correlates well with the *b* values used to simulate future earthquakes. Large values of *b* indicate that the proportion of small earthquakes to large earthquakes will be greater than for small values of *b*. Since the majority of canister failures come about through damaging earthquakes, regions with small *b* values are less seismically favorable than regions with large *b* values, all other parameters being equal.

6. Fracture orientation, size and intensity also play a role in canister failure in terms of the percentage of canisters intersected by fractures. A higher the percentage of canisters intersected by fractures results in a greater percentage of canister failures during a large earthquake. Fractures oriented perpendicular to canisters have a higher probability of intersecting canisters than fractures that are inclined or subparallel to the canister axis. Larger fractures, regardless of orientation, have a higher probability of intersecting canisters than do small ones (which also will have less induced displacement due to an earthquake than a larger fracture, since induced displacement is proportional to fracture radius). A higher intensity of fracturing also increases the intersection probability. The major differences among the three generic sites in terms of fracturing have to do with intensity and orientation. The intensity is similar for Beberg and Ceberg, and much higher for Aberg. Likewise,

Aberg contains more subhorizontal fracturing. A comparison between the results for Aberg and Beberg under the southern Sweden seismic scenario shows that the predicted failure percentages are higher for Aberg than for Beberg. Since the seismic parameters are the same, the differences can only arise from differences in fracture geology at the site and in the lineament pattern within 100 km of each site. This suggests that it is important to accurately characterize fracture orientation, size and intensity for future site selection and characterization in terms of canister failure percentages. While failure percentages are low for the three generic sites in spite of fracturing differences, other sites may have much larger, more intense or less favorably oriented fracturing resulting in higher failure percentages.

7. Most canister failures in the numerical simulations occurred when the earthquake was within a few kilometers of the canister, and the most distant earthquake was on the order of a few tens of kilometers away. These results suggest that earthquakes hundreds of kilometers away are unlikely to cause any canisters to fail, regardless of their magnitude. The results also suggest that it is only the seismicity within a few tens of kilometers that needs to be considered, and it is the magnitude/frequency parameters for this local region which are relevant for calculations. Site investigations for future repository sites need only focus on the faulting within a few kilometers of the repository, and need not consider in as much detail faulting further away.

8. Perhaps the major uncertainty in this study concerns the mechanism of current and future earthquakes in Sweden. There exists disagreement in the scientific literature in two areas. The first area is whether current seismicity is due to purely tectonic causes, or to glacial rebound. The second debate concerns the role of post-glacial faulting in past and future earthquakes. The resolution of these issues governs how the seismic catalog for Sweden is extrapolated in both time and space over the next 100,000 years. The current results assume that current seismicity is dominated by tectonic ridge-push forces, and that the energy released by future post-glacial earthquakes is stored primarily by tectonic processes and is only triggered by glacial rebound.

9. Another uncertainty regarding future seismicity relates to the statistical uncertainty inherent in extrapolating the current earthquake catalog, which consists of only small and medium-magnitude earthquakes, to the much larger magnitude earthquakes that might occur in a longer time period. It might be possible to gain increased confidence in the extrapolation by comparing the relation between Swedish earthquake parameters to the relations published by Wells and Coppersmith (1994). This would require determining parameter values for rupture area, surface rupture length, earthquake magnitude and fault displacement for a statistically significant number of Swedish earthquakes. If the regession parameter values are consistent with those published by Wells and Coppersmith that were based on a world-wide database of large (> 5.5) magnitude earthquakes, then this would suggest the Swedish earthquakes are mechanically similar to most larger earthquakes

worldwide, and represent the small magnitude component of a single process. Moreover, since Wells and Coppersmiths' data is largely derived from tectonically-induced earthquakes, conformance or non-conformance of the Swedish earthquakes would provide additional evidence as to whether current Swedish seismicity is derived from tectonic processes or glacial rebound.

10. Risk from primary earthquakes, that is, an earthquake occurring on a fracture that intersects a canister, is likely to be insignificant for two reasons. First, the regression relations between fault size and peak displacement indicates that only fractures on the order of kilometers are large enough to have an earthquake that has a peak displacement greater than 0.1 m. Although faults of this scale occur at all three generic sites and may be common in other areas of Sweden, these large faults are reliably detected during site characterizations and it is unlikely that any canisters would be located by accident on or near one of these faults.

11. If future studies show that current seismicity relates to glacial rebound rather than tectonic processes, or that this scenario should be investigated as an alternative, then the approach described in this document could be adapted to model the rebound process. Current models for the future glaciation of Fennoscandia suggest that the pattern of ice loading will be similar to the loading pattern of the most recent previous glaciation. Rebound rates for the deglaciation have been estimated. One possible way to model the earthquakes generated due to rebound is to calculate the elastic strain energy released during rebound for the region within 100 km of a site and to assume that all of the energy is released through earthquakes. Since the strain energy released by an earthquake is proportional to the product of rupture area and displacement, and rupture area and displacement are correlated with surface rupture length (Wells and Coppersmith, 1993), it is possible to calculate the maximum amount of strain energy that any mapped lineament segment could accommodate during an earthquake. This energy would be assigned to existing lineaments or smaller stochastic faults such that the total strain energy available from the incremental rebound equals the strain energy released by the earthquakes, and that the magnitude/frequency conformed to the standard semi-log form of this relation.

12. In a similar manner, it may be possible to improve the estimate of post-glacial fault-related earthquakes. If it is assumed that most of the stored energy released during post-glacial faulting comes from tectonic processes although triggered by rebound, then it should be possible to estimate the total amount of strain energy stored from the velocities of the tectonic plates and their rheological properties, either analytically or through numerical models. If all of the stored energy is released as a series of earthquakes following deglaciation, then, as in the case of rebound, the total energy could be partitioned among mapped fault lineaments that would serve as the locations for future post-glacial faulting.

7. REFERENCES

Adams, J. (1993). Field visit to sites of post-glacial faulting in Sweden, June, 1991. *In* Post-glacial faulting in the Lansjärv area, northern Sweden: Comments from the expert group on a field visit at the Molberget post-glacial fault area, 1991, R. Stanfors and L. O. Ericsson, eds., SKB TR 93-11.

Ahlbom, K. and S. Tirén (1991). Overview of geologic and geohydrologic conditions at the Finnsjön site and its surroundings. SKB TR 91-08.

Andersson, J.E., R. Nordquist, G. Nyberg, J. Smellie, and S. Tirén (1991). Hydrogeological conditions in the Finnsjön area. Compilation of data and conceptual model. SKB-91-24.

Bak, P. and K. Chen (1995). Fractal dynamics of earthquakes. *In* Fractals in the Earth Sciences, C. C. Barton and P. R. La Pointe, eds., Plenum Press, New York. Chapter 11.

Barton, C. C. and P. R. La Pointe (1995). Fractals in the Earth Sciences. Plenum Press, New York.

Barton, C. C. (1995). Fractal analysis of scaling and spatial clustering of fractures. In Fractals in the Earth Sciences. C.C. Barton, and P.R. LaPointe, eds. Plenum Press, New York. Chapter 8.

Bäth, M. (1979). Seismic risk in Fennoscandia. Tectonophysics, Vol. 57, 285-295.

Bergman, S., H. Isaksson, R. Hohansson, A. Lindin, C. Persson, and M. Stephens (1996). Forstudie Östhimmar. SKB PR D-96-016.

Castaing, C., M.A. Halawani, F. Gervais, J.P. Chilès, A. Genter, B. Bourgine, G. Ouillon, J.M. Brosse, P. Martin, A. Genna, and D. Janjou (1996). Scaling relationships in intraplate fracture systems related to Red Sea rifting: Tectonophysics, Vol. 261, 291-314.

Dershowitz, W. S. and H. H. Herda (1992). Interpretation of fracture spacing and intensity. *In* Proceedings of the 33rd U. S. Symposium on Rock Mechanics, A. A. Balkema, Rotterdam, 757-766.

Draper, N. R. and H. Smith (1966). Applied Regression Analysis. John Wiley & Sons, New York. 407p.

Follin, S. and J. Hermanson (1996). A discrete fracture network model of the Äspö TBM tunnel rock mass. Report to SKB from Golder Associates AB, Stockholm. June 1996.

Gutenberg, B. and C. F. Richter (1954). Seismicity of the Earth and Associated Phenomenon, 2nd Edition, Princeton University Press, Princeton, New Jersey.

Hermanson, J., L.M. Hensen, and S. Follin (1997). Update of the geological models of the Gidea study site. SKB R-97-05.

Johnston, A. C. (1993). Post-glacial faults in northern Sweden: A post meeting assessment to SKB. *In* Post-glacial faulting in the Lansjärv area, northern Sweden: Comments from the expert group on a field visit at the Molberget post-glacial fault area, 1991, R. Stanfors and L. O. Ericsson, eds., SKB TR 93-11.

Johnston, A. C. (1996). A wave in the earth. Science, Vol. 274, p. 735.

Kijko, A., E. Skordas, R. Wahlström and P. Mäntyniemi (1993). Maximum likelihood estimation of seismic hazard for Sweden. Natural Hazards, Vol. 7, 41-57.

Knuepfer, P. L. K. (1989). Implications of the characteristics of end-points of historical surface fault ruptures for the nature of fault segmentation. Fault Segmentation and Controls of Rupture Initiation and Termination, Palm Springs, California. 1989, 193-228.

La Pointe, P. R. and J. A. Hudson (1985). Characterization and Interpretation of Rock Mass Joint Patterns. Geological Society of America Special Paper 199.

La Pointe, P. R., P. C. Wallmann, and S. Follin (1995). Estimation of effective block conductivities based on discrete network analyses using data from the Äspö site. SKB TR 95-15, 170 p.

La Pointe, P. R., P. C. Wallmann, A. L. Thomas and S. Follin (1997). A methodology to estimate earthquake effects on fractures intersecting canister holes. SKB TR 97-07.

Mandelbrot, B. B. (1983). The Fractal Geometry of Nature. W. H. Freeman, New York.

Muir-Wood, R. (1993). A review of the seismotectonics of Sweden. SKB TR 93-13, 225 p.

Nadeau, R.M. and T.V. McEvilly (1997). Seismological Studies at Parkfield V: Characteristic microearthquake sequences as fault-zone drilling targets, Bull. Seism. Soc. Am., 87.

Nisca, D. and C.A. Triumf (1989). Detailed geomagnetic and geoelectric mapping of Äspö. SKB PR 25-89-01.

Ouillon, G., C. Castaing and D. Sornette (1996). Hierarchical geometry of faulting. J. Geophysical Res., Vol. 101, No. B3, 5477-5487.

Pollard, D. D. and P. Segall (1987). Theoretical displacements and stresses near fractures in rock: with applications to faults, joints, veins, dikes, and solution surfaces, *Fracture Mechanics of Rock*. Academic Press Inc. Ltd., London, 1987.

Scholz, C. C. (1995). Fractal transitions on geological surfaces. *In* Fractals in the Earth Sciences, C. C. Barton and P. R. La Pointe, eds., Plenum Press, New York. Chapter 7.

Skordas, E. and O. Kulhánek (1992). Spatial and temporal variations of Fennoscandian seismicity, Geophys. J. Int., Vol 111, 577-588.

Slunga, R. (1985). The seismicity of southern Sweden 1979-1984, Final Report. FOA-Rapport C 20572-Tl (ISSN 0347-3694), Försvarets Forskningsanstalt (National Defense Research Institute), Stockholm, Sweden. 45p.

Slunga, R. (1991). The Baltic Shield earthquakes. Tectonophysics, Vol. 189, 323-331.

Thomas, A. L. (1993). Poly3D: A three-dimensional polygonal element displacement discontinuity boundary element computer program with applications to fractures, faults and cavities in the earth's crust. M. S. thesis, Stanford University, Stanford, CA, 221p.

Tirén, S., M. Beckholmen, H. Isaksson (1987). Structural analysis of digital terrain models, Simpevarp area, South-Eastern Sweden. SKB PR 25-87-21.

Tirén, S.A. & M. Beckholmen (1990). Rock block configuration in southern Sweden and crustal deformation. *Geologiska Föreningens i Stockholm Förhandlingar*, Vol. 112, Pt. 4, pp. 361-364. Stockholm.

Tirén, S.A. & M. Beckholmen (1992). Rock block map analysis of southern Sweden. *Geologiska Föreningens i Stockholm Förhandlingar*, Vol. 114, Pt. 3, pp. 253-269. Stockholm.

Turcotte, D. L. (1992). Fractals and chaos in geology and geophysics. Cambridge University Press, Great Britain, 1992.

Wahlström, R. (1998). Earthquakes in Fennoscandia: Spatial, temporal and size distributions, recurrence rates, fault mechanisms and seismogenic processes. Written communication 16th March, 1998 to L. Ericsson, SKB, and S. Follin, Golder Associates AB, Stockholm.

Wahlström, R. and T. Ahjos (1984). Magnitude determination of earthquakes in the Baltic Shield. Annales Geophysicae, Vol. 2, no. 5, 553-558.

Wells, D. L. and K. J. Coppersmith (1994). New empirical relationships among magnitude, rupture length, rupture width, rupture area, and surface displacement. *Bulletin of the Seismological Society of America*, 84(4), 974-1002.

ISSN 0284-3757
CM Gruppen AB, Bromma, 1999